CUKUROVA UNIVERSITY

INSTITUTE OF NATURAL AND APPLIED SCIENCES

MSc THESIS

Recovery of Antimony from a Smelter Slag

Ahmedaljaali Ibrahim Idrees IBRAHIM

Mining Engineering Department

June, 2024

CUKUROVA UNIVERSITY

INSTITUTE OF NATURAL AND APPLIED SCIENCES

MSc THESIS APPROVAL

Recovery of Antimony from a Smelter Slag

Ahmedaljaali Ibrahim Idrees IBRAHIM

Mining Engineering Department

This Master's Thesis was evaluated by the following Jury Members on 11/06/2024 and was approved by unanimity of votes.

Jury : Assoc. Prof. Dr. Mahmut ALTINER (Advisor) ……

: Prof. Dr. Oktay BAYAT ……

: Assoc. Prof. Dr. Sait KURŞUNOĞLU ……

This Thesis was written in the Department of Mining Engineering, Institute of Natural and Applied Sciences.

Thesis Number:

Prof. Dr. Sadık DİNÇER
Director
Institute of Natural and Applied Sciences

This work was supported by the Cukurova University Research Fund and the Scientific and Technological Research Council of Turkey (TUBITAK)
Project ID: Cukurova University (FYL-2022-15229) and TUBITAK (123M062)

CONTENTS

CUKUROVA UNIVERSITY
INSTITUTE OF NATURAL AND APPLIED SCIENCES

MSc THESIS

Recovery of Antimony from a Smelter Slag

Ahmedaljaali Ibrahim Idrees IBRAHIM

Advisor: Assoc. Prof. Dr. Mahmut ALTINER

Department of Mining Engineering

ABSTRACT

This thesis aimed to investigate the recovery of antimony (Sb) from slag generated in an antimony smelting plant using leaching followed by hydrolysis processes. The physicochemical properties of the slag were determined using various analytical techniques. The slag (4.12% Sb) was mainly composed of quartz and minor minerals phases, including microline, magnetite, hedenbergite, and stibiconite. The Sb types in the slag determined by XPS were found to be in the oxide form. The concentrations of rare earth elements (REEs-La, Y, Ce, and Nd) in the slag were 169.21 g/t. Preliminary leaching experiment results indicate that (i) HCl was selected rather than other acids due to its high extraction ability on the Sb from the slag, (ii) a sample with a d_{50} of <25 μm should be used, (iii) the slurry should be mixed at 300 rpm. In the following leaching tests, the effects of leaching parameters (acid concentration, amount of tartaric acid, solid-to-liquid ratio, reaction temperature, and time) on the extraction rates of Sb, impurities, and REEs were investigated based on the OFAT approach. At the best leaching conditions (HCl: 8 M, amount of tartaric acid: 1 g/L, stirring speed: 300 rpm, reaction temperature: 75 °C, and time: 180 min), the extraction rates of Sb from the slag were determined to be 91.19%, but the extraction rates of REEs were measured to be ≤50%. The activation energy (Ea) for Sb leaching was found to be 46.75 kJ/mol, indicating that the reaction was governed by the chemically controlled mechanism, one of the shrinking core models. In particular, it was understood from the additional experimental results that the leaching procedure should be carried out for 20 h to extract La with an extraction rate of >90%. However, the extraction rate of Sb was negligible in extended times. It was determined that using tartaric acid positively affected La's leaching mechanism, and the required leaching time for La decreased to 180 min from 20 h with the increase of tartaric acid from 1 g/L to 6 g/L. Hydrolysis tests were conducted using the Taguchi approach (L32, 2^1 4^3). The effects of the alkaline type (NH_4OH and NaOH), stirring speed (100, 200, 300, and 400 rpm), temperature (50, 60, 70, and 80 °C), and pH (1.5, 2, 2.5, and 3) on the precipitation of Sb from the pregnant leach solution (PLS) were investigated. NH_4OH was suggested for use in the hydrolysis test to obtain precipitates with higher purities. The product obtained under the optimal conditions comprised 81.43% Sb, 16.23% O, and 2.34% Fe. The product was identified as antimony oxide by X-ray diffraction analysis (XRD).

Keywords: Antimony, Slag, HCl leaching, Hydrolysis, Rare Earth Elements (REEs)

ÇUKUROVA ÜNİVERSİTESİ
FEN BİLİMLERİ ENSTİTÜSÜ

YÜKSEK LİSANS TEZİ

Izabe Tesisi Cürufundan Antimon Kazanımı

Ahmedaljaali Ibrahim Idrees IBRAHIM

Danışman: Doç. Dr. Mahmut ALTINER

Maden Mühendisliği Anabilim Dalı

ÖZ

Bu tez çalışmasında, liç ve hidroliz yöntemleri kullanılarak antimon izabe tesisinde açığa çıkan cüruftan Sb kazanımının araştırılması amaçlanmıştır. Farklı analiz teknikleri kullanılarak cürufun fizikokimyasal özellikleri belirlenmiştir. Cürufun (%4,13 Sb) bünyesinde ana hakim mineral olarak kuvars ile birlikte minör seviyede mikrolin, manyetit, hedenbergit ve stibikonit mineralleri belirlenmiştir. Cürufun içerdiği NTE (La, Y, Ce ve Nd) konsantrasyonu 169,21 g/t'dur. Ön liç deney sonuçları, (i) cüruftan Sb'nin yüksek çözündürme özelliği nedeniyle diğer inorganik asitler yerine HCl kullanılması, (ii) cürufun d_{50} değerinin <25 μm olması ve (iii) çözeltinin 300 dev/dk hızında karıştırılması gerektiğini işaret etmiştir. Takip eden liç deneylerinde; liç koşullarının (HCl asit konsantrasyonu, tartarik asit miktarı, katı-sıvı oranı, reaksiyon sıcaklığı ve süre) Sb, safsızlık ve NTE elementlerinin çözünme hızına olan etkisi OFAT yaklaşımı ile araştırılmıştır. En iyi liç koşullarında (HCl: 8 M, tartarik asit miktarı: 1 g/L, karıştırma hızı: 300 dev/dk, reaksiyon sıcaklığı ve süresi 75 °C ve 180 dk), cüruftan Sb çözünme hızı %91,19 olarak belirlenmiştir. Ancak, NTE elementlerinin çözünme hızı ≤%50 olarak belirlenmiştir. Sb çözünmesi için aktivasyon enerjisi (Ea) 46,75 kJ/mol olarak bulunmuş olup, bu değer reaksiyonun shrinking küçülen çekirdek modellerinden biri olan kimyasal kontrollü bir reaksiyon modeliyle açıklanabildiğine işaret etmektedir. Özellikle, yapılan yeni liç deneylerinde La çözünme oranının >%90 olabilmesi için gerekli liç süresinin 20 s olması gerektiği belirlenmiştir. Buna karşın, daha uzun reaksiyon sürelerindeki Sb çözünme hızındaki yükseliş gözardı edilebilir düzeydedir. Tartarik asit kullanımının La çözünmesine pozitif katkısı olduğu belirlenmiştir. Tartarik miktarının 1 g/L'den 6 g/L'e yükselmesi La çözünmesi için gerekli sürenin 20 s'den 180 dk'ya düşmesine neden olmuştur. Taguchi (L32, 2^1 4^3) yaklaşımına göre hidroliz testleri gerçekleştirilmiştir. Alkali türü (NH_4OH ve NaOH), karıştırma hızı (100, 200, 300 ve 400 dev/dk), sıcaklık (50, 60, 70 ve 80 °C) ve pH (1,50 – 2 – 2,50 – 3) yüklü liç çözeltisinden Sb'ın çöktürülmesine olan etkileri araştırılmıştır. Yüksek saflıkta çökelti elde edebilmek için NH_4OH kullanılması gerektiği belirlenmiştir. En iyi şartlarda elde edilen çökelti %81,43 Sb, %16,23 O ve %2,34 Fe içermektedir. XRD analizine göre de elde edilen çökelti antimon oksit olarak tanımlanmıştır.

Anahtar Kelimeler: Antimon, Cüruf, HCl Liçi, Hidroliz, Nadir Toprak Elementleri (NTE)

GENİŞLETİLMİŞ ÖZET

Antimon, 6,68 g/cm^3 özgül ağırlığa ve 630 °C erime noktasına sahip kırılgan, gümüş-beyaz, parlak ve günümüzde modern sanayileşmiş toplumlarda yaygın olarak kullanılan önemli bir metaldir. Antimon metali kendi başına kullanılamayacak kadar kolay kırılır ancak alaşımlara mukavemet, sertlik ve korozyona karşı direnç kazandırır (Miller, 1973). Kurşun asitli akümülatörler (otomobillerde yaygın olarak kullanılan türden) %4 – 6 oranında kurşunla alaşımlı antimon içerir ve antimonun korozyona karşı direnci, kurşun pil terminallerinin aslında kurşun-antimon alaşımından yapılmasının nedenidir. Çok yüksek saflıkta antimon metali (%99,99+ saf), yarı iletken endüstrisi tarafından ana bileşen olarak InSb, GaSb ve SbTe gibi bileşikler halinde silikon levhalarda kızılötesi dedektörler, diyotlar ve diğer cihazlar ve uygulamalar için kullanılmaktadır (Zhang ve ark., 2020).

Antimon trioksit (Sb_2O_3) formundaki antimon, esas olarak yapıştırıcılarda, boyalarda, kağıtlarda, plastiklerde ve sızdırmazlık maddelerinde alev geciktirici olarak kullanılmaktadır. Sb2O3 ayrıca tipik olarak brom veya klor bazlı halojenli bileşiklerle kauçuk ve tekstil döşemelerde yangın geciktirici bir destek olarak kullanılır (EFPA, 2004). Alev geciktiriciler için başlıca pazarlar arasında çocuk giyimi, uçak ve otomobil koltuk kılıfları ve yatak takımlarının yapımında kullanılan elektronikler, plastikler ve kumaşlar bulunur. Diğer antimon bileşikleri çeşitli kullanımlara sahiptir. Örneğin; cam, alaşım, fren balatası, Li ve Na-pil ve akü üretimi (Anderson, 2012; Mostashari ve Baie, 2008; Beutl ve ark., 2018; Öztürk ve ark., 2016).

Dünyada tanımlanmış antimon cevher yataklarının büyük bir kısmı Çin'de bulunmaktadır. Bunun yanı sıra Çin'e kıyasla az da olsa ABD, Bolivya, Kanada, Meksika, Rusya, Güney Afrika, Tacikistan ve Türkiye'de de antimon sahaları bulunmaktadır. Küresel ölçekte hazırlanan raporlar incelendiğinde antimon rezervlerinin büyük çoğunluğunun Çin'de bulunmasının ilerleyen yıllarda tedarik riski açısından ülkelerin problem yaşamasına neden olacağı görülmektedir. Araştırma ve endüstriyel sektörlerde birçok kullanım alanına sahip olan antimon, Dünyada farklı ülkeler (Avustralya, Güney Kore, Kanada, Amerika Birleşik Devletleri ve Japonya), ülke toplulukları (Avrupa Birliği, AB), araştırma kurumları (Britanya Jeolojik Araştırmalar Kurumu) ve Dünya Bankası tarafından son yıllarda yayımlanan kritik hammadde raporlarında yer almaktadır. Bu raporlar incelendiğinde, antimon (Sb) metalinin sekiz listenin yedisinde tedarik riski – ekonomik değer açısından oldukça "önemli kritik hammaddelerden" biri olarak nitelendirildiği görülmektedir (Uysal 2021).

Antimon, kükürt ve bakır, kurşun, altın, arsenik, civa ve gümüş gibi diğer metaller için güçlü afinitesi nedeniyle, doğal halde element olarak nadiren bulunur; tipik olarak sülfürlerde, sülfotuzlarda, oksitlerde, antimonatlarda ve antimonitlerde bulunur (Boyle ve Jonasson, 1984). En yaygın antimon cevheri minerali stibnittir (Sb_2S_3), ancak 100'den fazla diğer mineral de antimon içermektedir (Seal ve ark., 2017). Hali hazırda, hidrometalurjik ve pirometalurjik yöntemler uygulanarak cevherlerden antimon (Sb) metal\oksit üretimi sağlanmaktadır. Hidrometalurjik

yöntem; sırasıyla kimyasal liç, ayrıştırma/saflaştırma ve elektroliz aşamalarından oluşmaktadır. Bu yöntem ile kompleks antimon cevherlerinin işlenmesi mümkündür. Kullanılan çözücü türüne göre, asit veya alkali liç prosesleri uygulanmaktadır. Na_2S – NaOH karışımı hazırlanarak alkali ortamda stibnit cevherinden Sb'un çözünmesi oldukça yüksek verimde sağlanmaktadır (Yang ve ark., 2017). $FeCl_3$ – HCl, $SbCl_5$ – HCl, ozon-asit karışımları da çözücü kimyasallar olarak kullanılarak cevherden Sb'un çözündürülmesinde kullanılabilmektedir (Tian ve ark., 2016; Rodriguez ve ark., 2016; Ye ve ark., 2019). Ayrıca inorganik asitler ile birlikte tartarik asit kullanılarak liç işlemi sırasında antimonun antimonik asit olarak çökelmesi engellenmektedir (Groenewald, 1964; Rubešska ve ark., 1967; Chengzhi ve ark., 2011). $FeCl_3$ çözeltisi ile de stibnitten antimon %98,53 verimle kazanılabilmiştir (Ye ve ark., 2019). Hashimoto ve ark. (2003), Sb(III)-HCl–H_2O sisteminin kimyasal denge şartlarını belirlemiş ve sonrasında NaOH ilavesi ile değişik morfolojik özellikte Sb bileşiklerini çöktürme ile elde etmişlerdir. Sonrasında çözeltideki [SbOCl], $[(SbO)_2NO_3]$+, $[(SbO)_2SO_4]$ komplekslerinden elektroliz ile katodta antimon metali yüksek saflıkta toplanabilmektedir (Madkour ve Salem, 1996).

Yeryüzündeki antimon rezervlerinin, dünyadaki mevcut üretim hızının devam etmesi durumunda 2050 yılında tükeneceği ön görülmektedir (Zhong ve ark., 2018). Bu durum kaynakların sürdürülebilir kullanımı açısından antimonun cevherler dışında izabe cürufları gibi ikincil kaynaklardan kazanımını kaçınılmaz kılmaktadır. Antimon izabe tesisinde açığa çıkan cürufun etkin, ekonomik ve çevreye duyarlı bir şekilde değerlendirilmesi, bu tez çalışmasının en önemli hipotezidir.

Bu tez kapsamında kullanılacak olan cüruf numunesi Adana ilinde bulunan Anadolu Antimon Ltd. Şti'ne ait antimon izabe tesisinden temin edilmiştir. Tez kapsamında yapılacak çalışmalarda kullanılacak numunenin temsili alınması için; stok sahasının farklı bölgelerinden bir kepçe yardımı ile numuneler alınmıştır. Numune alma işlemine başlanmadan önce stok sahasının çevresi ve üzerinde numune alınacak yerler belirlenmiş ve etiket yerleştirme işlemleri gerçekleştirilmiştir. Kepçe yardımı ile işaretlenen noktalarda yarmalar açılmış olup toplam 3 ton malzeme alınmıştır. Harmanlama işlemini takiben numune azaltma yöntemlerinden olan konileme-dörtleme ile temsili bir şekilde numune alımı sağlanmıştır. Çalışma için alınan toplam numune miktarı 400 kg civarındadır. Cürufun özelliklerinin belirlenebilmesi amacıyla sırasıyla fiziko kimyasal analizler (görünüm/koku, pH, nem, organik madde miktarı), inorganik içerik analizi (XRD), toksik karakteristlik liç prosedürü (TCLP), sentetik çöktürme liç şartları (SPLP), radyoaktivite testleri uygulanmıştır.

XRD analizi sonuçları cüruf numunesinin ana hakim minerali olarak kuvars (SiO_2) mineralinden oluştuğu ve oldukça düşük miktarda stibikonit ($Sb_3O_6(OH)$) minerali içerdiğini işaret etmiştir. Rietveld metotuyla yapılan detaylı mineralojik analiz neticesinde; cüruf içerisinde mikrolin ($KAlSi_3O_8$), manyetit (Fe_3O_4, <%5) ve Hedenbergite ($CaFeSi_2O_6$) mineralleri tespit edilmiştir. SEM analizi ile cürufun elemental dağılımı da tespit edilmiştir. Aynı şekilde; cürufun içerdiği metallerin miktarları XRF, AAS ve ICP-OES&ICP-MS cihazları kullanılarak belirlenmiştir. XPS analizi ile

cürufun yüzey analizi yapılmıştır. Cürufun yüzeyinde tespit edilen S element miktarının çok az olması, S ile Sb arasında bir etkileşimin olduğu hakkında yorum yapılmasını mümkün kılmamıştır (Şekil 9.d). Sb_2O_3 (Sb^{+3}), Sb_2O_4 (Sb^{+4}) ve Sb_2O_5 (Sb^{+5}) olmak üzere üç farklı antimon oksit varlığı bilinmektedir. $Sb3d_{3/2}$ spektrumunun yalnızca bir pik ile ifade edilmesi, çalışmada kullanılan cüruf numunesinin içerdiği Sb elementinin Sb_2O_3 formunda bulunduğunu göstermektedir (Moulder ve ark., 1992; Wagner 2000). Numune üzerinde Sb metali veya başka bir Sb-oksit minerali varlığına dair herhangi bir sonuç elde edilememiştir.

Liç işlemlerinde araştırılacak parametreler ve kullanılacak asit türü belirlenmiştir. ön deneyler neticesinde çözücü asit olarak HCl'in kullanılmasına karar verilmiştir. Asit konsantrasyonu, reaksiyon süre gibi parametrelerin daha detaylı bir şekilde değerlendirilebilmesi için optimizasyon testlerinde bu parametrelerinde Sb çözünmesine olan etkinlikleri araştırılmıştır. Ön deneylerden de elde edilen sonuçlar ışığında; asit konsantrasyonu, tartarik asit miktarı, katı-sıvı oranı, süre ve sıcaklık parametrelerinin hedef metallerin (Sb ve NTE) ve safsızlık olarak nitelendirilebilecek (Al, K, Ca, Mg, Mn ve Si) elementlerin çözünme davranışlarına olan etkileri AAS ve ICP cihazları ile belirlenmiştir. OFAT (One Factor at a Time) analizi kullanılarak her parametrenin etkinliği diğer parametreler sabit tutularak belirlenmiştir. Belirlenen her optimum parametre sonrasında diğer parametre için işlemler tekrarlanmıştır.

Asit konsantrasyonun etkisinin belirlenmesinde yapılan deneylerde açık bir şekilde görüldüğü gibi; Sb çözünme veriminin artışı 6 M ve daha yüksek asit konsantrasyonlarında nispeten kayda değer bir farklılık öngörülememiştir. Literatürde yapılan bir çalışmada da HCl asit konsantrasyonunun Sb çözünmesi için yüksek olması gerektiği, aksi takdirde liç işleminin başında çözeltiye geçen Sb'un zamana bağlı olarak tekrar hidrolize olarak katılaştığı ve Sb çözünme veriminin düştüğü belirlenmiştir (Chae ve ark., 2020). Literatürde yapılan çalışmalar çözelti içinde Sb iyonlarının daha kararlı olması (tekrar hidrolize olmaması gibi) için belirli bir oranda tartarik asit ilave edilmesinin gerektiğini göstermekte ve bu şekilde doğru sonuçlar elde edileceğine işaret etmektedir (Küçükoğlu ve ark., 2022). Liç işlemi sırasında cüruf\cevher den çözünen antimon iyonlarının çözelti içinde kararlı olmadığı ve tekrar hidrolize olarak çökeldiği tespit edilmiştir (Groenewald, 1964; Moldan, 1966). Bu durumda gerçekleştirilen deneylerde liç işleminin veriminin dramatik bir şekilde etkilenmesi çalışmada hedeflenmeyen sonuçların elde edilmesine neden olabilecektir. Belirli bir oranda tartarik asit ilave edilmesi bu sorunun ortadan kaldırılmasını sağlamaktadır (Küçükoğlu, 2022). Yapılan önceki bir çalışmada çözelti içinde Sb ile tartarik asit arasında antimon tartarat şeklinde kompleks oluştuğu ve bu kompleksin hidrojen iyonlarından daha fazla negatif potansiyeli olduğu için çözelti içinde $SbCl_3$ iyonlarının hidrolize olmasını önlediği ortaya konmuştur (Uysal, 2019). Bu amaçla, liç işlemleri sırasında 0, 1, 2, 3, 5 ve 6 g/L tartarik asit ilaveleri gerçekleştirilmiştir. Tartarik asit miktarına bağlı olarak Sb çözünme hızı %19 ile %26

arasında değişiklik göstermiştir. Diğer safsızlıkların çözünmesine bir etkisi olmamıştır. Ancak, La elementinin çözünmesinde nispeten yüksek değerler elde edilmiştir.

Katı/sıvı oranı parametresinin HCl asit konsantrasyonu gibi etkin bir parametre olduğu, çözücü konsantrasyonu başına düşen numune miktarının azalmasının çözünme işlemini hızlandırmıştır. Katı/sıvı oranının 1/5'den 1/20'e yükselmesi ile birlikte sabit tutulan diğer deneysel şartlar altında Sb çözünme verimi %32'den %45 seviyelerine yükselmiştir. Cürufun içerdiği Fe'in çözünme hızı ise; Sb'ye göre daha hızlı olmuştur ve 1/20 katı/sıvı oranı şartlarında yapılan deneylerde cürufun içerdiği Fe'in neredeyse tamamı çözeltiye geçmiştir (çözünme verimi: >%99). Diğer safsızlıklar açısından da benzer durumlar söz konusu olmuş ve katı/sıvı oranının düşmesi (Mn ve Si hariç) safsızlıkların %100'e yakın çözünme verimi değerlerine ulaşmasına neden olmuştur. Beklendiği gibi katı/sıvı oranının düşüşü La'nın çözünme oranını da hızlandırmıştır. Ancak, Ce, Nd ve Y çözünme verimleri açısından bir farklılık gözlenmemiştir.

Sıcaklık ve sürenin etkisinin belirlenmesi çalışmalarında ise sabit tutulan parametreler HCl konsantrasyonu: 8 M, katı/sıvı oranı 1/10 ve karıştırma hızı: 300 dev/dk'dır. Görüldüğü gibi, oda sıcaklığında yapılan deneylerde çok düşük seviyelerde cüruftan Sb ve Fe çözünme değerleri (<%30) elde edilmiştir. Her ne kadar reaksiyon süresi 45 dk'dan 180 dk'ya artırılsa da oda sıcaklığında yapılan deneylerde çözünme verimleri açısından herhangi bir olumlu yönde bir etki görülmemiştir. Bu bulgular önceki bir çalışma ile uyumlu olmuştur. Guo ve ark. (2017) yaptıkları çalışmada oda sıcaklığında HCl ile liç deneylerinde asit konsantrasyonu ve karıştırma hızı dahi artırılmış olsa da elde ettikleri çözünme verimleri çok sınırlı olmuştur (Sb çözünme verimi: <%30). Yüksek verimde Sb çözünmesi için reaksiyon sıcaklığının yüksek olması rapor edilmiştir (Guo ve ark., 2017). Örneğin; 40℃'de gerçekleştirilen deneylerde reaksiyon süresi 45 dk olduğunda Sb çözünme verimi %40 civarında ölçülürken, reaksiyon süresinin artışına paralel olarak Sb çözünme verimi değerleri %40'dan %80'e doğru yükselme eğilimi göstermiştir. Bu deneylerde diğer safsızlıklarında çözünme verimlerinde süreye bağlı olarak artış eğilimi izlenmiştir. Aynı deneylerde NTE çözünme değerleri sınırlı seviyede olmuştur.

Sıcaklık 40℃'den 60℃'ye yükseltildiğinde cürufun içerdiği Fe'nin neredeyse tamamı 180. dk sonunda çözeltiye geçmiştir. Sıcaklığın artışı Sb çözünme veriminin 180 dk sonunda %80 civarında olmasına neden olmuştur. Palden ve ark. (2021) yaptıkları çalışmada da cüruftan Sb'un çözünmesinde sıcaklığın en az 50 °C olması gerektiğine işaret etmiştir. Bu açıdan bu çalışmada elde edilen Sb çözünme davranışlarının literatür ile uyumlu olduğu söylenebilir.

Literatürde bazı çalışmalar hem Sb hem de Fe liç davranışını incelemişlerdir. Bu çalışmalarda elde edilen sonuçlar Fe çözünme verimleri açısından bu çalışmadan farklılık göstermektedir. HCl kullanarak yüksek sıcaklıklarda yüksek Sb çözünme değeleri elde edilirken, Fe'nin çok düşük seviyelerde çözeltiye geçmelerini sağlamışlardır. Örneğin; stibnit cevherinin HCl ile çözeltiye alınması sırasında Sb çözünme verimi liç şartlarına bağlı olarak >%80 iken, Fe çözünme

verimi %10'dan düşük olmuştur (Tian ve ark., 2016). Bu farklılığın sebebinin Fe'in hammadde içerisinde bulunuş şekline (mineral kompozisyonuna) bağlı olduğu düşünülmektedir. Diğer bir ifadeyle mevcut çalışmada cüruf halinde ikincil Sb cevheri kullanılırken sözkonusu çalışmada doğal Sb mineralleri içeren cevherler kullanılmıştır.

Beklendiği gibi, bu çalışmada sıcaklığın artışına paralel cüruftan Sb hedeflenen seviyelerde çözeltiye geçmeye başlarken istenmeyen safsızlıkların da çözeltiye geçiş hızlarında artış olmuş ve neredeyse cürufun içerdiği K, Ca ve Mg'un tamamı çözünmüştür. Reaksiyon sıcaklığı 60℃ olduğunda 180 dk sonunda cüruftan La çözünme verimi değeri %50 civarında olmuştur. Ancak, Ce, Nd ve Y çözünme verimlerinde süreye bağlı olarak olumlu yönde bir artış gözlenmemiştir.

Yapılan deneyler neticesinde cürufun bünyesindeki Sb'un yüksek verimde çözeltiye alınabilmesi için atmosferik şartlarda uygulanması gereken liç parametreleri aşağıdaki gibi belirlenmiştir.

HCl konsantrasyonu: 8 M,

Katı/sıvı oranı: 1/10,

Karıştırma hızı: 300 dev/dk,

Tartarik asit miktarı: 1 g/L,

Reaksiyon sıcaklığı: 75 °C

Reaksiyon süresi: 180 dk

Optimum şartlarda yapılan ve farklı sıcaklıklarda yapılan liç deneyleri ile reaksiyonun hız sabiti, aktivasyon enerjisi (Ea) ve bu değere bağlı olarak reaksiyonun açıklanabildiği kimyasal kinetik model belirlenmiştir. Sb çözünmesi için reaksiyon hız sabiti değerleri sıcaklığa bağlı olarak $6{,}01 \times 10^{-5}$ dk^{-1} ile 107,84 $6{,}01 \times 10^{-5}$ dk^{-1} arasında yer almaktadır Gerçekleştirilen liç reaksiyonları Ea değerlerine göre farklı şekilde sınıflandırılmaktadır. Örneğin; Ea <20 kJ/mol ise; liç reaksiyonu difüzyon kontrollü bir mekanizmaya sahiptir. Eğer Ea > 42 kJ/mol ise, reaksiyon hız sabiti ile sıcaklık arasında üssel bir şekilde ilişki olduğu ve liç reaksiyonun kimyasal kontrollü bir mekanizmaya sahip olduğu anlaşılmaktadır (Kumari ve ark., 2018). Şekil 22'de verilen Arrhenius eğrisinin eğiminden yararlanılarak aktivasyon enerji (Ea) değeri 46,75 kJ/mol hesaplanmıştır.

Son aşamada ise gerçekleştirilen ilave liç deneylerinde ise tartarik miktarının NTE elementlerinin çözünmesine olan etkileri ortaya konmuştur. Liç işlemi sırasında ilave edilen tartarik asit yalnızca çözünen Sb iyonlarının hidrolize olmasını engellemekle kalmamış olup La çözünmesine de pozitif yönde katkı sağlamıştır. La çözünme verimi optimum şartlarda %50 civarında olmuştur. Bu deneylerde sabit tutulan parametreler sırasıyla: HCl konsantrasyonu: 8 M, katı/sıvı oranı: 1/10, karıştırma hızı: 300 dev/dk, tartarik asit miktarı: 1 g/L ve reaksiyon sıcaklığı: 60 °C'dir. Bu şartlar altında yapılan deneylerde cürufun içerdiği La'ın tamamın çözeltiye geçmesi için gerekli sürenin 20

saat olması gerektiği ortaya çıkmıştır. Aynı şartlarda diğer NTE elementlerinin de çözünme verimleri %25 - %40 aralığında olmuştur. La'ın tamamının çözünmesi için gerekli süre 20 saat olarak belirlenirken, tartarik asit miktarının 1 g/L'den 6 g/L'e çıkartılması La'ın yüksek verimde çözünmesi için gerekli sürenin 180 dk'ya inmesini sağlamıştır. Bu bulgular literatürde yapılan çalışma ile uyum göstermektedir. Liang ve ark. (2016) yaptıkları çalışmada tartarik asit kullanarak toprak numunesinin içerdiği La elementinin çözünmesini hızlandırmıştır. Yapılan çalışmada tartarik asit konsantrasyonuna bağlı olarak La çözünme veriminin de arttığı belirlenmiştir.

Uygulanan bu şartlar altında cüruf numunesinden Sb çözünme verimi %91,19 olarak belirlenmiştir. La çözünme verimi %97 civarındayken diğer NTE'lerin (Y, Ce, Nd) çözünme verimleri ≤%50 olarak ölçülmüştür.

Taguchi (L32, 2^1 4^3) yaklaşımına göre hidroliz testleri gerçekleştirilmiştir. Alkaline türü (NH4OH ve NaOH), karıştırma hızı (100, 200, 300 ve 400 dev/dk), sıcaklık (50, 60, 70 ve 80 °C) ve pH (1,50 – 2 – 2,50 – 3) yüklü liç çözeltisinden Sb'ın çöktürülmesine olan etkileri araştırılmıştır. Yüksek saflıkta çökelti elde edebilmek için NH_4OH kullanılması gerektiği belirlenmiştir. En iyi şartlarda elde edilen çökelti %47,13 Sb, %10,23 O ve %2,51 Fe içermektedir. XRD analizine göre de elde edilen çökelti antimon oksit olarak tanımlanmıştır.

ACKNOWLEDGEMENTS

I would like to extend my deepest gratitude to my Assoc Prof. Dr. Mahmut ALTINER, my esteemed advisor, for all the guidance, support, time, effort, and understanding in helping me and the instruction he provided me throughout my Master's research and writing process, I would like also to thank Assist. Prof. Dr. Abdulkadir ÜRÜNVEREN for his technical assistance throughout my research.

Moreover, expressing my gratitude to the head of the department and everyone in the Department of Mining Engineering for providing the necessary resources and facilities where much of my work was conducted made this thesis possible. Thanks to their generosity and encouragement, my time spent studying at Cukurova University has been truly rewarding. I would like to thank Allah, my family, especially my mother for her endless love, support, and encouragement, and my colleagues (Kartal Kaan SOYLU, Zayanou Idrisse HAMIDINE, and Muhammed ABOELGAMEL). It would have been impossible to finish my studies without their unwavering support over the past few years.

This study was supported by the Scientific and Technological Research Council of Turkey (TUBITAK) under Grant Number 123M062. The author thanks TUBITAK for their support. Also, the author would like to thank Cukurova University Research Fund for financial support (FYL-2022-15229).

LIST OF TABLES

LIST OF FIGURES

SYMBOLS AND ABBREVIATIONS

AAS: Atomic Absorption Spectrometer

Al: Aluminum

ALS: Private Laboratory

Au: Gold

Ca: Calcium

CUMERLAB: Cukurova University Central Research Laboratory

E_a: Activation Energy

EU: European Union

Fe: Iron

HCl: Hydrochloric Acid

ICP MS: Inductively Coupled Plasma Mass Spectrometry

ICP OES: Inductively Coupled Plasma-Optical Emission Spectrometry

K: Potassium

M: Molar

Mg: Magnesium

Min: Minutes

MLA: Mineral Liberation Analysis

MTA: General Directorate of Mineral Research and Exploration

Na_2CO_3: Sodium Carbonate

NaOH: Sodium Hydroxide

NH_4OH: Ammonium Hydroxide

HNO_3: Nitric Acid

$H2SO_4$: Sulfuric Acid

OFAT: One Factor at a Time

PLS: Pregnant Leachate Solution

REEs: Rare Earth Elements

S/N: Signal to Noise

Sb: Antimony

Si: Silicon

SPLP: Synthetic Precipitation Leaching Conditions

TCLP: Toxic Characteristic Leaching Procedure

XRD: X-ray Diffraction

XRF: X-Ray Fluorescence

1. INTRODUCTION

Antimony (Sb) is a brittle, silver-white, shiny, and important metal with a specific gravity of 6.68 g/cm^3 and a melting point of 630 °C, which is widely used in modern industrialized societies today. Sb metal breaks too easily to be used on its own, but it gives strength, hardness, and resistance to corrosion to alloys (Miller, 1973). The physicochemical and mechanical properties of Sb are listed in Table 1.1.

Table 1.1. General properties of antimony

Properties/Characteristics	**Value**	**Unit**
Atomic number	51	N/A
Atomic weight	121.76	u
Melting point	630.5	◦C
Boiling point (at 101.3 kPa)	1325	◦C
Density (at 20 ◦C)	6.688	g/cm^3
Tensile strength	10.8	N/mm^2
Mohs hardness	3.0-3.5	N/A
Modulus of elasticity	566	N/mm^2
Surface tension of solid (at 432 ◦C)	317.2	mN/m
Surface tension of a liquid (at 1200 ◦C)	255	mN/m
Crystal structure	Rhombohedral	N/A
Lattice constant	a = 0.437, c = 1.1273	nm
Latent heat of fusion	10.49	kJ/mol
Latent heat of evaporation	195.10	kJ/mol
Coefficient of linear expansion (at 20 ◦C)	8-11	µm/m-◦C
Electrical resistivity (at 0 ◦C)	37	µΩ.cm
Molar heat capacity of solid (at 630.5 ◦C)	30.446	J/mol-K
Molar heat capacity of liquid (at 630.5 ◦C)	31.401	J/mol-K
Thermal conductivity (at 0 ◦C)	25.9	W/m-K

There are many reports published in recent years by different countries around the world (Australia, South Korea, Canada, The United States of America, and Japan), country communities (European Union, EU), research institutions (British Geological Survey), and the World Bank (AG, 2024). When these reports are examined, it is seen that antimony (Sb) metal is considered as one of

the “most important critical raw materials” in terms of supply risk and economic value in seven of the eight lists. For example, the classification in the report prepared by the EU (2023) is shown in Figure 1.1. Antimony is not only present in the 2023 report also have been in the critical raw materials reports published in 2011, 2014, 2017, and 2023 (EU, 2023).

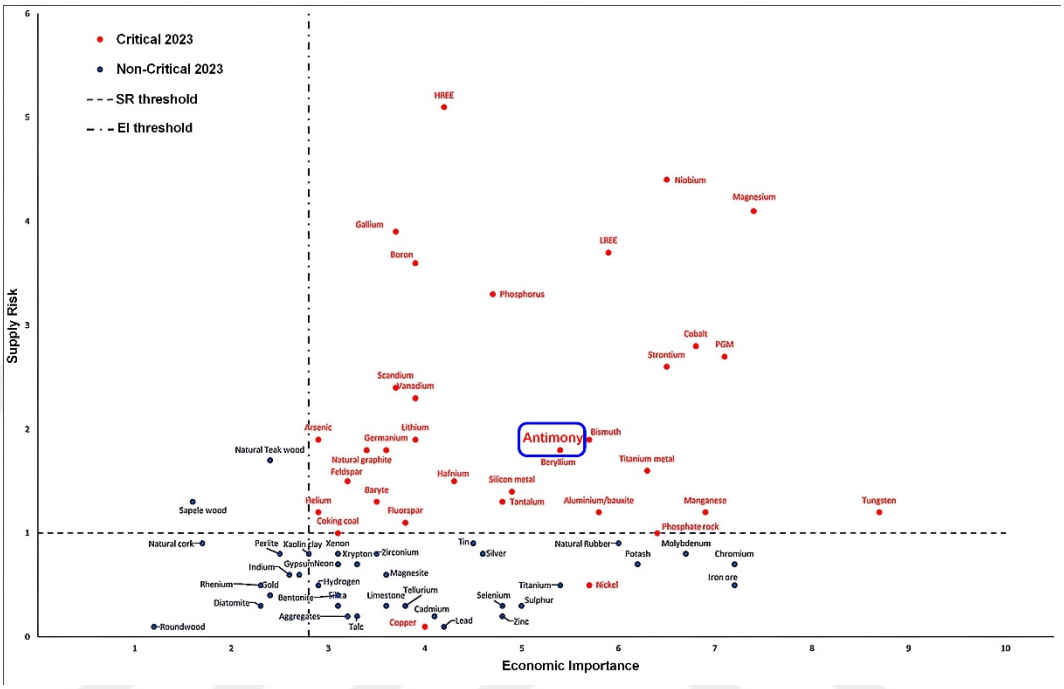

Figure 1.1. Critical raw materials determined by EU (2023)

Although China is the largest supplier of antimony, the report published by the EU (2023) indicates that Türkiye is the major supplier of antimony with a rate of 63% for EU countries, whereas the rest of the antimony supply was provided by Bolivia (26%) and China (6%) as shown in Figure 1.2.

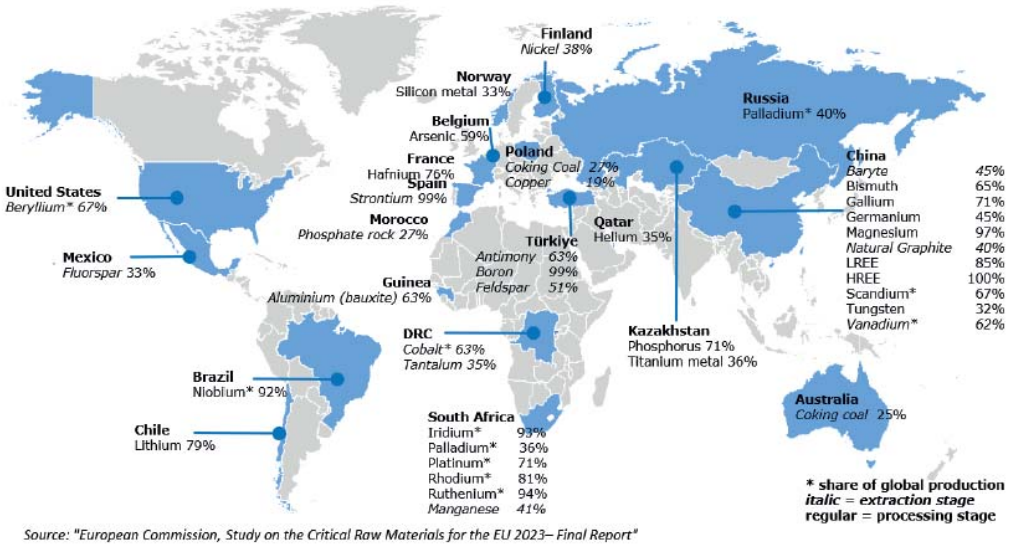

Figure 1.2. The major supplier of critical raw materials

Sb with superior properties has many uses in the industry, such as in the hardening of metals, protection against corrosion and fire, paper, plastic, and paint. For example, Lead-acid accumulators (the kind commonly used in automobiles) contain lead–alloyed antimony by 4-6%, and antimony's resistance to corrosion is the reason why the so-called "lead" battery terminals are made of lead-antimony alloy. Very high-purity antimony metal (99.99%+ pure) is used by the semiconductor industry as the main component for infrared detectors, diodes, and other devices and applications in silicon sheets in the form of compounds such as InSb, GaSb, and SbTe (Zhang et al., 2020).

Moreover, Sb in the form of antimony trioxide (Sb_2O_3) is a widely used flame retardant across many different industries such as; adhesives (to decrease the fire risk), paints (to prevent flames and smoke from the layer during a fire), paper (to reduce the fire risk and allow the paper products to withstand fire for long periods), plastic (to increase the durability of the product in case of fire), rubber and textile floor coverings (as a fire retardant additive). The main markets for flame-retardants include electronics, plastics, and fabrics used in the construction of children's clothing, airplane and automobile seat covers, and bedding. In the semiconductor industry, silicon wafers containing very high-purity antimony metal are used to create infrared detectors, diodes, and other electronic components. Antimony is also present in anti-friction bearings, type metal for mechanical typesetting, solder, and decorative castings made of pewter and Britannia metal. Antimony is incorporated into graphite bearings to improve heat tolerance. Nuclear reactors use beryllium and antimony as neutron sources during startup. Finely ground metallic antimony is referred to as "antimony black" and is used in bronze metals and plaster molds. In the presence of oxygen, antimony sulfide will burn. In the production of ammunition primers, detonators, smoke-screen generators, visual range-finding shells, tracer bullets, and the striking surface of safety matches, it serves as a crucial combustion-supporting element. Additionally, it is utilized to give fireworks their "glitter" effect. Antimony is used in the rubber business as a vulcanizing agent. In addition, antimony is used to make glass and ceramics. Sodium antimonate is employed as a glass bubble remover as well as a flame retardant. Currently, secondary production accounts for 20% of global antimony production and is mostly accomplished through the recycling of lead-acid vehicle batteries. To a much lesser extent, antimony-containing waste products from the manufacturing of copper, lead, and gold are also valued Because copper, lead, and gold processors must deal with lower-quality ores and stricter environmental regulations, making it more challenging to simply discard or stockpile antimony-containing residues, these secondary sources of antimony are anticipated to become more significant (Dupont and Binnemans, 2017). Accordingly, recycling of the metal in spent lead acid storage batteries of the type of metal and Babbitt is the main conservation technique employed in the antimony business. Additionally, intermediate smelting products such as slags, drosses, flue dusts, and residues produced at copper and lead smelters are recovered for antimonial lead and antimony metal. For antimonial lead applications, secondary antimony is far more plentiful than it is from original sources. In less significant applications, antimony oxides are employed as white paint

pigments in paints, whereas antimony trisulfide and pentasulfide provide black, vermillion, yellow, and orange pigments. Antimony trisulfide, a component of camouflage paint, reflects infrared light. The composition of safety matches and the brake linings of automobiles both use antimony trisulfide. Antimony pentasulfide is a vulcanizing agent that is employed in the manufacturing of red rubber. Catalysts, insecticides, weapons, and pharmaceuticals all use antimony compounds. Sb_2O_3 is also evaluated in additional applications such as glass production, alloys, brake pads, lithium–sodium batteries, and battery production (Anderson, 2001; Mostashari and Baie 2008; Öztürk et al., 2016; Beutl et al., 2018). Figure 1.3 shows the usage area of antimony in the EU.

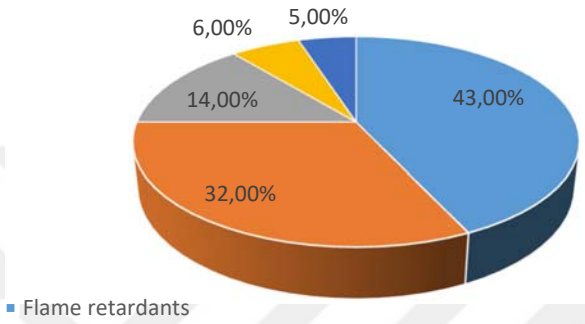

Figure 1.3. The general usage area of antimony in the EU

Sb is rarely found in its native form due to its strong affinities with other elements, including sulfur, copper, lead, gold, arsenic, and silver (Boyle and Jonasson, 1984). There are more than 100 antimony-bearing minerals present in the nature, but the most common one is stibnite (Sb_2S_3) mineral. Table 1.2 gives some examples of antimony-bearing minerals.

Table 1.2. Some examples of Sb-bearing minerals

Mineral		Chemical Formula	Sb (wt%)
Sulfides	Stibnite	Sb_2S_3	71.7
	Tetrahedrite	Cu_6Sb2S_6	29.8
	Jamesonite	$Pb_4FeSb6S_{14}$	35.4
	Zinckenite	$PbSb_2S_4$	42.1
Oxides	Senarmontite (cubic)	Sb_2O_3	83.5
	Valentinite (rhombohedral)	Sb_2O_3	83.5
	Cervantite (orthorhombic)	$Sb_2O_4/Sb_2O_3 \cdot Sb_2O_5$	79.2
	Stibiconite (antimony hydroxides)	$Sb_2O_4 \cdot H_2O$	74.8
Mixed	Kermesite	$2Sb_2S_3 \cdot Sb_2O_3$	83.5

1.1. The Aim of the Research

The abundance of Sb in the earth's crust is in a range from 0.2 to 0.5 ppm, which makes it a scarce element. Table 1.3 lists the reserves and production rate of antimony mining (2022 and 2023 years) in worldwide.

It is seen that antimony mine production in China accounts for 49% of global antimony mine production. However, Zhong et al. (2018) predicted that known antimony reserves will be depleted by 2050 because of the rates of ore production. Anderson (2019) indicated that the demand for Sb in lead-acid batteries will decrease, but the use of Sb in flame-retardants will increase in the plastics industry. Therefore, it is inevitable that metallurgical slags will evaluated as secondary Sb resources, except for primary ores and end-of-life products (lead-acid batteries). Also, the use of these slags as raw Sb sources decreases the potential pollution of the environment (Guo et al., 2014). Although there are many studies on the production of Sb from an antimony ore in the literature, studies focused on the recovery of Sb remaining in the slag after the pyrometallurgical process by using hydrometallurgical methods are limited. These studies focus on the recovery of Sb found in anode slime resulting from pyrometallurgical processes involving metals such as lead, copper, and tin (Binz and Friedrich, 2015; Han et al., 2017; Tan et al., 2018; Han et al., 2020; Palden et al., 2021).

Additionally, there is a study focusing on the characterization of crude products containing high levels of As and Pb obtained from an antimony smelting plant, which contains about 82–82.5% Sb (Ling et al., 2021). The removal of As in the crude product is achieved through HNO_3 leaching (Ling et al., 2022). No study has previously reported the extraction of antimony along with rare earth elements from similar resources. In this thesis, the recovery of antimony from a smelter slag and the extraction of rare earth elements have been investigated. This study is the first to report these findings. The use of a different residue source in this thesis, especially with a material composition different from the studies in the literature in terms of chemical content, is expected to positively contribute to the uniqueness of the study. It is planned to develop a process for Sb and Rare Earth Elements (REEs) recovery from a smelter slag generated during the processing of antimony ore in the plant, which is located in Adana, Türkiye. Preliminary studies indicated that the slag used in this study could be further evaluated as raw materials for REEs due to its content. Therefore, the work planned to be carried out in the thesis consists of four (4) work stages.

(1) Raw material characterization and grinding,

(2) Preliminary leaching test to determine the range of leaching parameters,

(3) Extraction of Sb and REEs from the slag in the presence of HCl acid under atmospheric conditions,

(4) Recovery of Sb from the PLS via hydrolysis test.

Table 1.3. Antimony mine production and reserves in the world (Survey, 2024).

Country	Mine Production (ton)		Reserves (ton)
	2022	2023	
United States	-	-	60,000
Australia	2,290	2,300	140,000
Bolivia	3,000	3,000	310,000
Burma	4,600	4,600	140,000
Canada	2	2	78,000
China	40,000	40,000	640,000
Guatemala	24	24	NA
Iran	500	500	NA
Kazakhstan	300	300	NA
Kyrgyzstan	40	40	260,000
Laos	220	220	NA
Mexico	700	700	18,000
Pakistan	79	80	26,000
Russia	4,300	4,300	350,000
Tajikistan	21,000	21,000	50,000
Türkiye	5,800	6,000	99,000
Vietnam	250	250	NA
World total	**83,100**	**83,000**	**>2.000,000**

2. PRELIMINARY WORK

The production of Sb from primary ores is a well-known process and is described in detail in previous studies (Zhao, 1988; Anderson, 2012). However, the recovery of Sb from end-of-life products and metallurgical slag should be investigated in detail to gain knowledge of Sb recovery.

Currently, there are many studies carried out using pyrometallurgical or hydrometallurgical processes on the recovery of Sb from different industrial wastes lead-acid battery (Liu et al., 2014; Binz and Friedrich, 2015; Alev, 2019), metal oxide varistors (Gutknecht et al., 2017; Karlsson et al., 2018), smelter slag (Anderson, 2001), arsenic filter cake(Zhang et al., 2012), Sb containing concentrates [copper concentrate (Awe and Sandström, 2010, Awe et al., 2013)], copper electro-refining stream (Díaz et al., 2023), antimony-rich oxidizing slag (Zhang et al., 2015), Sb-bearing dust (Zhong et al., 2018), etc. Dupont et al. (2016) reviewed in detail the recovery of Sb from end-of-life and industrial process residues. In another work, the trends, applications, and strategies in the Sb recovery were systematically reviewed by researchers (Dembele, 2022).

Figure 2.1 shows the recovery of Sb from the Sb-containing feedstock. This process comprises two main processes as follows: (i) leaching and (ii) purification. There are three options namely electrodeposition, hydrolysis, and cementation in the purification stage.

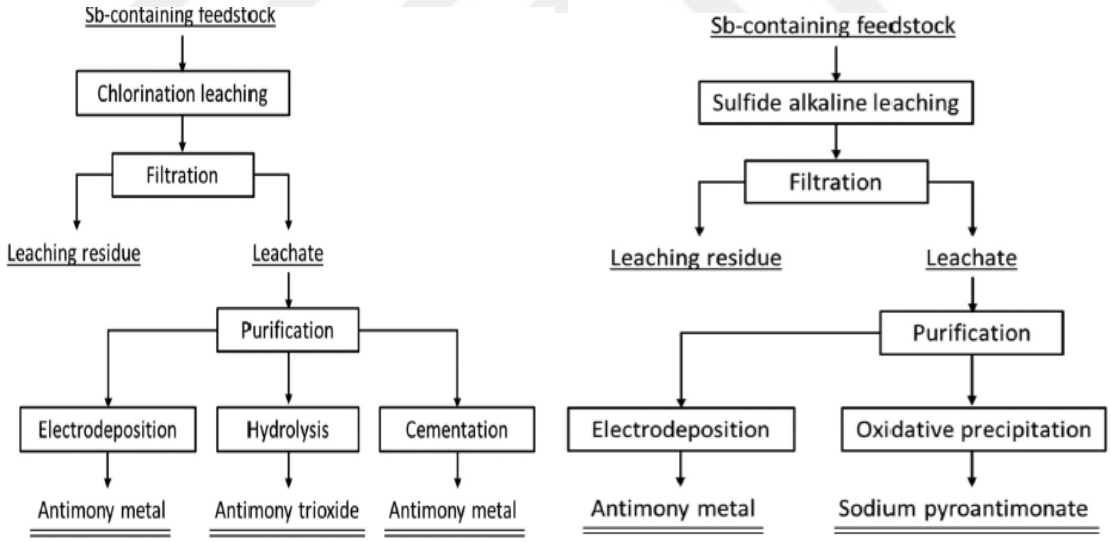

Figure 2.1. Hydrometallurgical processes for Sb recovery (Ling et al., 2022)

It is possible to process complex antimony ores with this method. Based on the mineralogical composition of raw material, acid or alkaline leaching can be applied. For example, the selective dissolution of Sb with an extraction rate of 96.64% from a stibnite ore was possible in the alkaline (Na_2S – NaOH) medium (Yang et al., 2017; Ye et al., 2019). The recovery of Sb and Bi from tin anode slime was investigated using soda roasting followed by alkaline leaching processes (Han et al., 2020). However, it was stated that the leaching behavior of Sb from Sb-bearing ores was

investigated based on pH-dependent release characteristics (Hu et al., 2016). Also, different leaching agents, including $FeCl_3$ (Ye et al., 2019), HCl with ozone (Rodríguez et al., 2016), and HCl-NaCl (Tian et al., 2016), can be used to provide an acidic medium to extract Sb from different raw materials. In another study, Sb with an extraction rate of 98.53% from ore was dissolved under the following conditions: a temperature of 50℃, an 8:1 of liquid-to-solids ratio, and a time of 1 h. There was no need to use oxidants for the leaching of Sb (Ling et al., 2022). However, the addition of tartaric acid prevents the precipitation of Sb dissolved during the HCl leaching (Groenewald, 1964; Moldan, 1966). NaCl was further used to prevent Sb hydrolysis. Previous research suggested the use of ultrasonic treatment during the leaching. The required reaction time for the leaching of Sb with high extraction rates by conducting ultrasonic power was three times lower compared to that of the regular leaching procedure (Zhang et al., 2015). Slurry electrolysis (a combination of leaching, purification, and electrolysis) was recommended to extract Sb from high As and Au-containing stibnite ore (Zhang et al., 2019). In another work, a potential-controlled chlorination leaching process was suggested to increase the extraction of Sb. The solution potential increased from 260 to 450 mV with the addition of Cl_2 and Sb, which was dissolved with an extraction rate of >99% (Cao et al., 2010). Sudova et al. (2024) suggested the use of deep eutectic solvents (a mixture of choline chloride and ethylene glycol) in the presence of iodine as an oxidant for the extraction of Sb from mining residues and all of Sb was dissolved at a temperature of 100 °C for 4 h.

Previous researchers stated that the presence of Fe ions in the solution may create problems in terms of the precipitate's purity, as the precipitation rate of Sb and Fe reached 99% with the addition of NH_4OH. The separation mechanism of Sb from an Sb-Fe mixed solution was systemically investigated by the hydrolysis technique (Ye et al., 2019). Hashimoto et al. (2003) determined the chemical equilibrium conditions of the Sb(III)-HCl-H_2O system and subsequently obtained various morphological properties of Sb compounds by precipitation with the addition of NaOH. Different Sb precipitates were obtained based on pH value, as shown in Figs. 2.2 and 2.3.

Sb_2O_3 particles were prepared with the addition of NH_4OH into $SbCl_3$ solution in the pH range of 8.5 – 9 (Hu et al., 2007). Some researchers have recommended for use of water to conduct the hydrolysis process for Sb, but their aging period was too long and the required aging time to obtain Sb precipitate was found to be 7 days with a recovery of 97% (Meng et al., 2015).

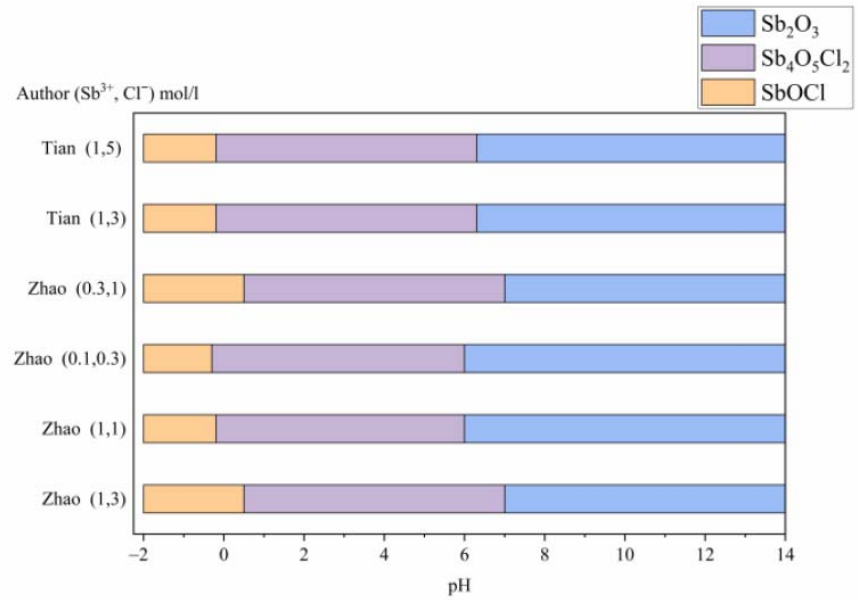

Figure 2.2. Theoretically distribution of Sb species as a function of pH (Gutierrez et al., 2023)

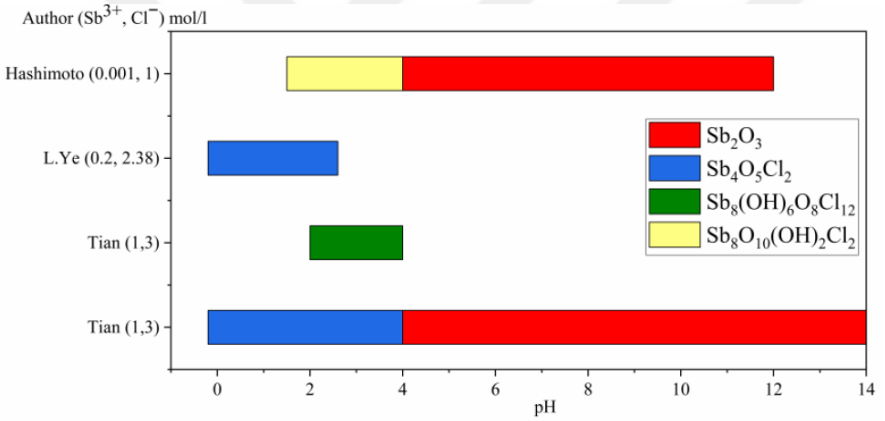

Figure 2.3. Distribution of Sb species as a function of pH based on the experimental studies (Gutierrez et al., 2023)

3. MATERIAL AND METHOD

3.1. Material

The slag sample was provided by Anadolu Antimon Factory, located in Adana, Türkiye. These slag samples are the byproducts of the antimony extraction process, where the ore containing antimony minerals is collected from various regions in Türkiye. The modal mineralogical composition of the ore (taken from Van Province), determined by Mineral Liberation Analysis (MLA), is shown in Figure 3.1.

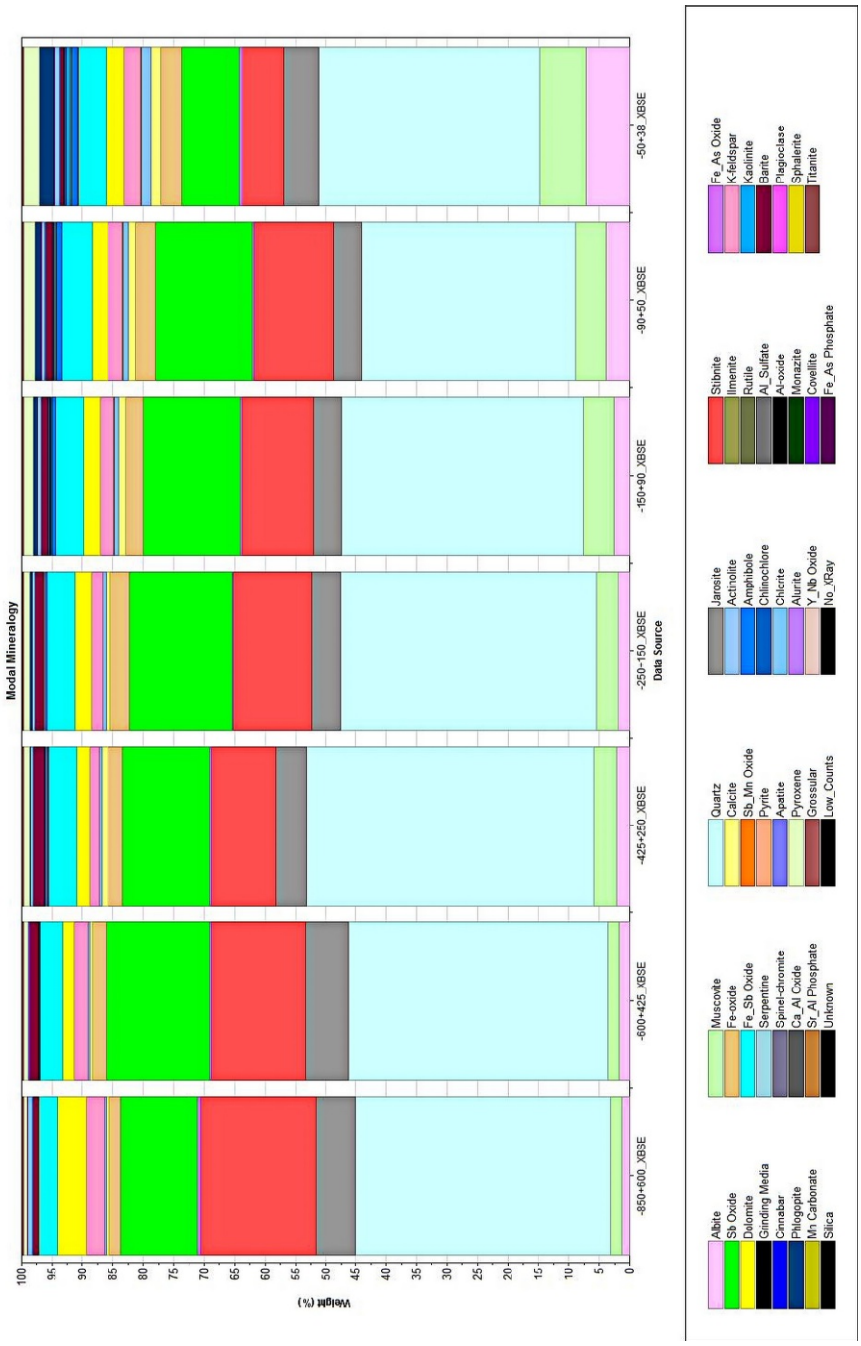

Figure 3.1. The mineralogical composition of the ore used in the pyrometallurgical process

MLA analysis shows that the ore used in this plant is mainly composed of quartz, stibnite, and Sb-oxide minerals. The following minerals, including jarosite, muscovite, and other minerals were detected in the minor phase (Figure 3.2).

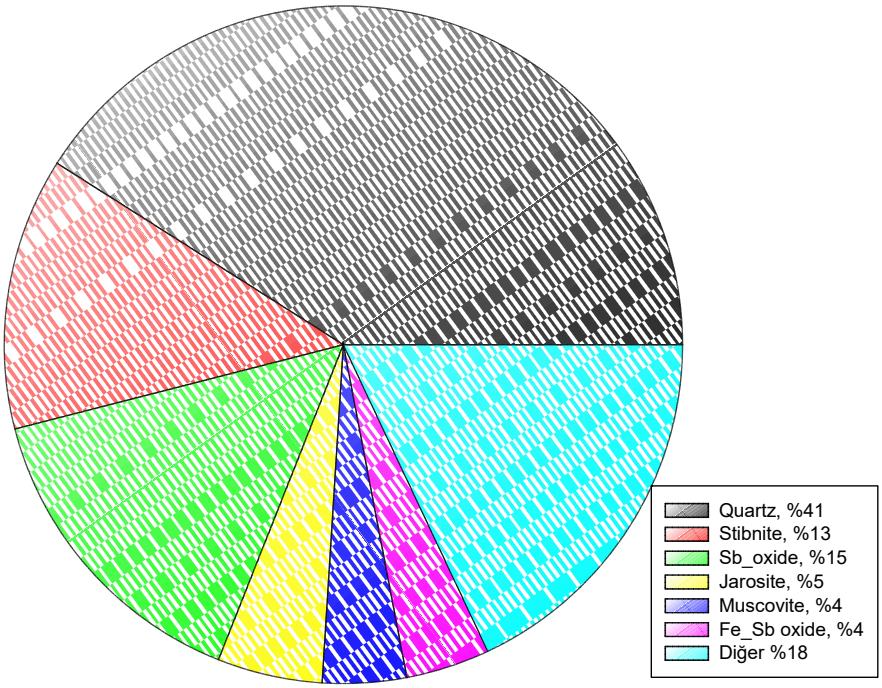

Figure 3.2. The mineral composition of the ore

Pyro-metallurgical process is carried out to produce antimony-based products with high purities from these ores. A flow-sheet conducted in this process can be seen in Figure 3.3.

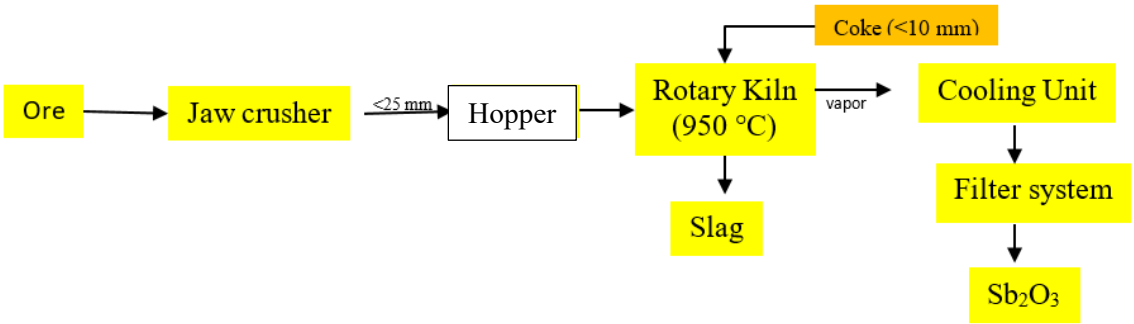

Figure 3.3. Processing of Sb_2O_3 from the ore in the plant

As clearly seen in Figure 3.3, the ore was crushed below 25 mm with the use of a jaw-crusher. The crushed ore was mixed with coke coal (-10 mm), and these mixtures were heated in the rotary

furnace at a temperature of 950 – 1150 °C. During the reduction process, antimony (Sb) is released into the atmosphere as gas forms from the ore and leaves the rotary furnace. Upon exposure to air, the Sb gas is oxidized and forms antimony oxide particles, which are subsequently captured in a filtration system. Equations 3.1 and 3.2 represent the chemical reactions involved in this process.

$$Sb_2S_3 + C + {}^{11}/_{2}\, O_2 \rightarrow 2Sb \uparrow + CO_2 \uparrow + 3SO_3 \uparrow \quad (3.1)$$

$$2Sb + {}^{3}/_{2}\, O_2 \rightarrow Sb_2O_3 \quad (3.2)$$

As a result of the pyrometallurgical process, the slag remaining in the rotary furnace was stored in suitable areas as waste material (Figure 3.4).

Figure 3.4. The view of the stockpile of the plant.

Approximately 3 tons of slag were collected from various pre-identified locations within the stockpile with the aid of an excavator (Figure 3.5). These locations were chosen based on random sampling points. Subsequently, the collected material was subjected to cone and quartering techniques to obtain a final sample (400 kg).

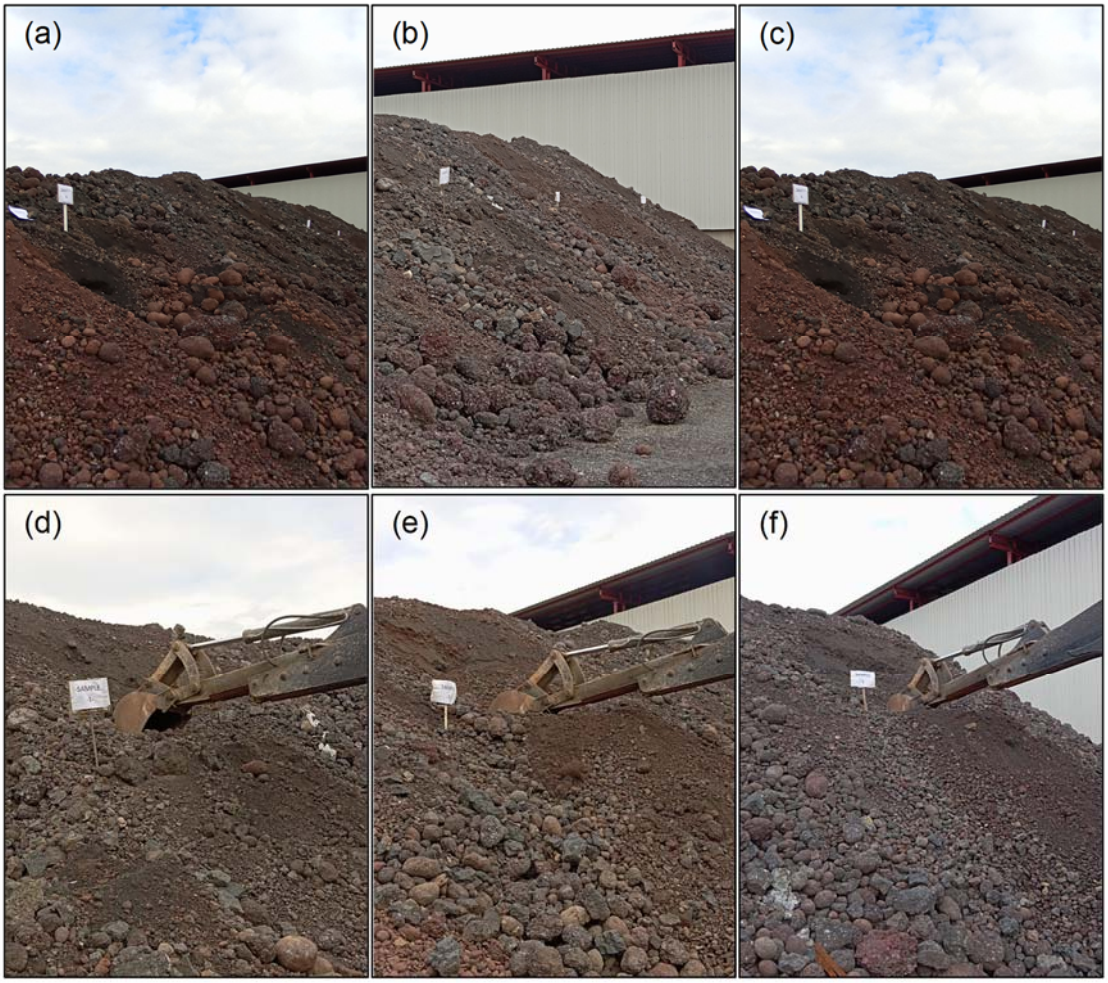

Figure 3.5. The photographs showing the sampling of the slag from the stockpile

The chemical composition of the representative sample (except for Si) was determined by an Atomic Absorption Spectrometer (AAS, Perkin Elmer 900H) after its digestion in a microwave digestor (CEM, Mars 6) with a mixture of HF+HCl+HNO_3+H_2O (1.5 mL+1.5 mL+1.5 mL+1 mL) at 200 °C for 30 min, followed by boric acid neutralization at 200 °C for 30 min. Inductively Coupled Plasma - Optical Emission Spectrometry (ICP-OES, Perkin Elmer 7000DV) was employed to confirm the accuracy of the AAS results. X-ray Fluorescence (XRF, Panalytical MiniPal) analysis was performed on the slag for compositional analysis. XRF analysis (Thermo Scientific) at Anadolu Antimony Factory further checked the contents of antimony (Sb) and arsenic (As) in the slag. The results of these analyses, including average values for each element, are presented in Tables 3.1 and 3.2. Table 3.1 details the chemical composition of the slag determined by AAS and XRF, while its rare earth elements (REEs) and other elements concentrations given in Table 3.2 were measured by ICP-MS (Perkin Elmer, NEXION 2000 P).

Table 3.1. The chemical composition of the slag used for experimental work in this thesis (%)

Element	Al	Ca	Fe	K	Mg	Mn	Na
Amount (wt, %)	2.10	1.32	2.12	0.55	0.51	0.05	<0.05
Element	Cu	Sb	Ni	P	Si	Ti	Cr
Amount (wt, %)	0.03	4.13	0.04	<0.01	33.39	0.09	0.03
Element	S	Loss on ignition: 2.60%					
Amount (wt, %)	0.51						

Table 3.2. The concentration of REEs and other elements in the slag

Element	Ce	Dy	Er	Eu	Gd	Ho	La
Amount (g/t)	31.11	3.91	1.10	0.44	4.46	1.24	78.52
Element	Lu	Nd	Tb	Th	Tm	U	Co
Amount (g/t)	0.45	33.78	0.96	2.43	0.34	24.30	11.65
Element	Y	Yb	Lu	Pt	As	Cd	Pb
Amount (g/t)	25.80	0.866	0.112	5.32	441	13	93.8
Element	Sc	Sm	Pr	Rb	Li	Sr	V
Amount	3.41	2.56	6.17	84.55	39.60	47.60	33.70
Element	W	Zn	Zr	Ni	Ba	Be	Bi
Amount (g/t)	0.162	942	23.50	348	43.5	1.50	0.031
Element	Cr	Ga	Ge	Mo			
Amount (g/t)	356	6.15	0.14	11.95			

The slag sample was also analyzed for their gold (Au) and silver (Ag) content due to their potential (Ubaldini et al., 2000; Pohl, 2011; Zhang et al., 2019). The Au and Ag concentrations in the slag were determined in four different laboratories and are listed in Table 3.3.

Table 3.3. The concentration of Au and Ag determined in four different laboratories in the slag

Element	MTA		ALS	Private Lab.		CUMERLAB
Ag (g/t)	21.20	23.70	26.20	25.65	24.01	--
Au (g/t)	3.60	3.70	3.61	3.951	4.065	3.58

The chemicals (HCl, HNO_3, H_2SO_4, NaOH, NH_4OH, and $C_4H_6O_6$) used in this thesis are of analytical grade and were used without any purification.

3.2. Method

The experimental study process, as shown in Figure 3.6, comprises different stages, including characterization and grinding, preliminary leaching tests, HCl leaching, and hydrolysis. These stages are explained below.

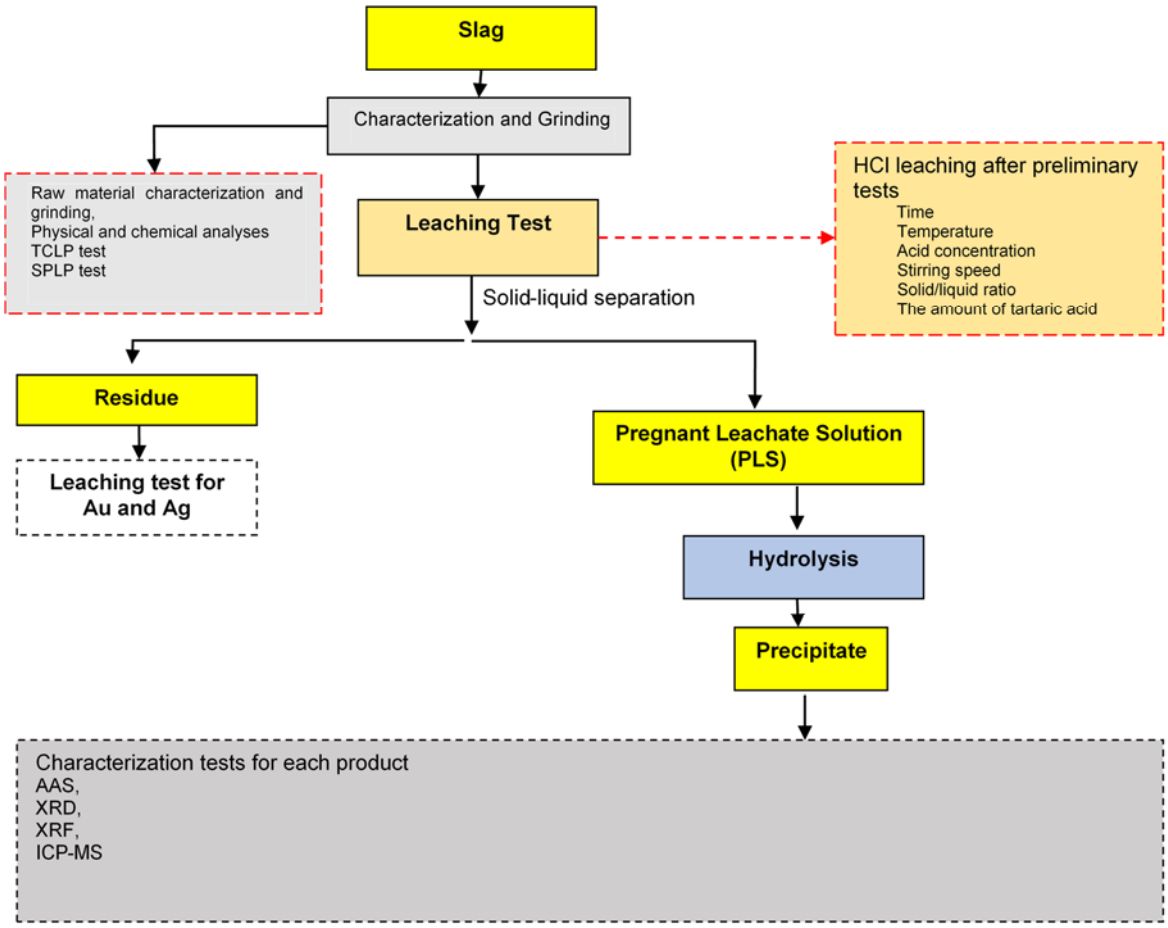

Figure 3.6. The experimental process conducted in this study

Although the leaching tests for Au and Ag from the residue was shown in Figure 3.6, any experiments was not investigated; the residue obtained in this thesis was stored for future studies.

3.2.1. Raw Material Characterization

Prior to conducting the specified leaching operations, the following characterization tests were carried out to determine the harmful potential of the slag to the environment:

- Appearance/odor
- pH
- Moisture content
- Organic matter content

- Inorganic content analysis

Toxic Characteristic Leaching Procedure (TCLP): The slag was mixed with a solution of acetic acid in a ratio of 1/20 (slag/solution). The pH of the solution was 4.93. The solution was stirred for 18 h at ambient temperature. After 18 h, the mixture was filtered by Whatman paper, and the concentration of Sb in the solution was measured by AAS. The purpose of this procedure is to determine the amount of Sb that can be leached from the slag under these conditions (EPA, 1994).

Synthetic Precipitation Leaching Conditions (SPLP): The leaching conditions conducted herein are the same procedures as the aforementioned above stage (TCLP) except for the pH of the solution and acid ratio. The pH of the solution was 4.20. A mixture of nitric acid:sulfuric acid with a ratio of 2:3 was used (EPA, 1994).

Radioactivity of the Slag: The radioactivity properties of the slag and residue were determined using a radiation detector.

Other Instrumental Analyses

The mineralogical composition of the slag was determined using a PANalytical EMPYREAN X-Ray diffractometer (XRD) equipped with Cu Kα radiation (λ= 1,54049 Å) in the 2θ range of 10–85° with a 0.02 step size, and the obtained diffraction pattern was evaluated using a PDXL software program for mineral identification. The surface morphology of the slag was evaluated using a scanning electron microscope (SEM, FEI Quanta 650 Field Emission). In addition, the presence of Au and Ag in the slag was proved by SEM. The particle size distribution of the slag using a Malvern Mastersizer (Hydro 2000 MU) was determined. The surface property of the slag was further determined using X-Ray Photoelectron Spectroscopy (XPS, Thermo Scientific K-Alpha).

3.2.2. Grinding

In this stage, the slag was crushed using a lab-scale jaw crusher and ground in a ball mill for different times (1 h and 2 h). Therefore, the effects of particle size on the leaching behavior of the slag were investigated.

3.2.3. Preliminary Leaching Test

A series of preliminary leaching tests were carried out in a 500 mL glass jacketed reactor (equipped with a glass condenser) to determine the range of experimental parameters for the leaching of Sb from the slag. The equipment used for leaching test can be seen in Figure 3.7.

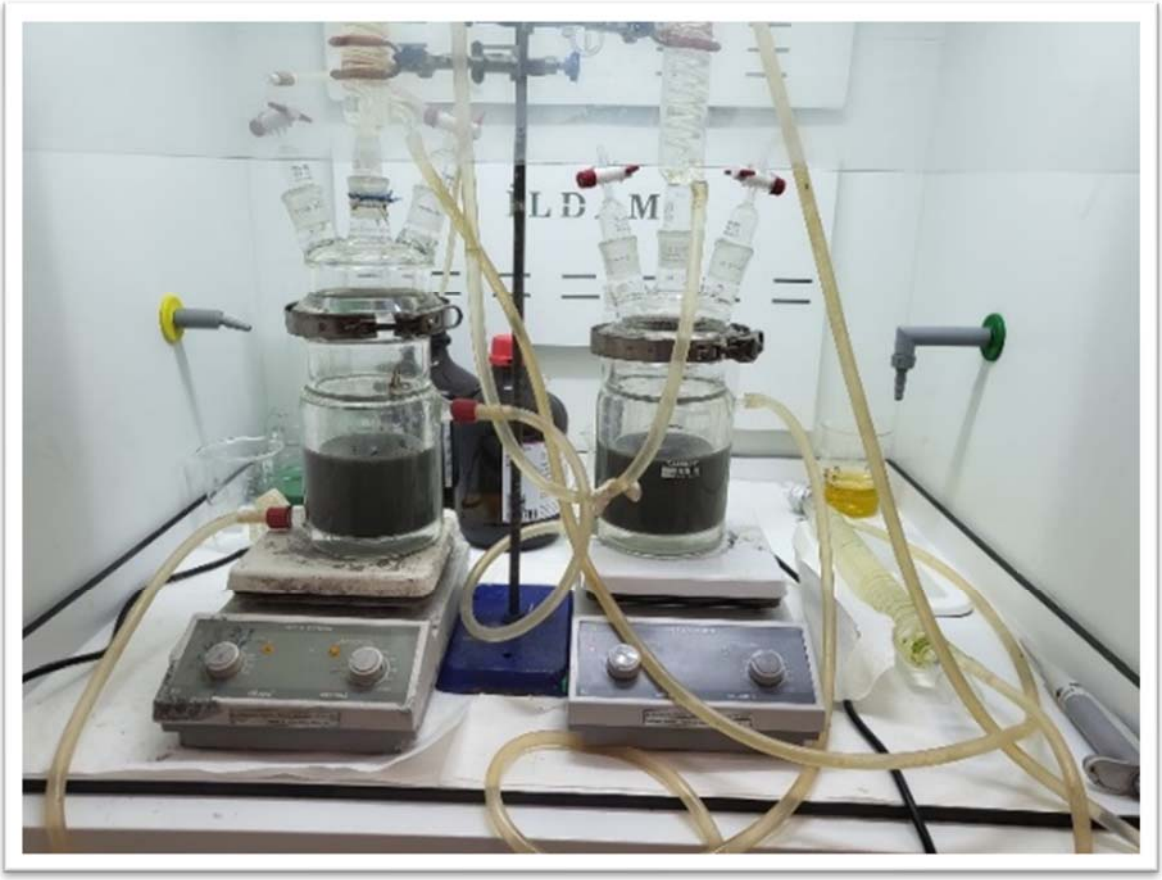

Figure 3.7. The equipment used in the leaching test

Different parameters, including particle size, acid type (H_2SO_4, HNO_3, and HCl), acid concentration, leaching time, and stirring speed, were investigated. Previous studies indicate that the leaching of Sb should be carried out at high temperatures to obtain satisfactory results. Considering these findings, reaction temperature and solid-to-liquid ratio were kept as 60℃ and 1:5, respectively. The reaction temperature was provided by a circulation water bath (JSR-22T) and it was measured by a laser thermometer. In each leaching test, 200 mL of the solution was used. The slurry was stirred by a magnetic stirrer (MTOPS MS300HS). At the end of the reaction time, the stirring was stopped, and the slurry was centrifuged (ELEKTRO-MAG M415 M) and filtered using Whatman NO 1 filter paper. The concentration of Sb in the pregnant leach solution (PLS) was analyzed by AAS. The following Equation was used to determine the extraction rate of Sb from the slag. The leaching residue was washed many times and dried at 105℃ in an oven (Memmert) for characterization tests.

$$ER\ (\%) = \frac{A \times B}{C \times D} \times 100 \qquad (3.1)$$

Where ER is the extraction rate (%), A is the concentration of element (mg/L), B is the final volume of the PLS, C is the initial concentration of the slag (mg/kg), D is the amount of slag used in the leaching (kg)

3.2.4. HCl Leaching Test

Considering preliminary leaching test results, HCl acid was selected as a leaching agent for this study. The effects of parameters on the leaching of Sb, REEs, and other elements identified as impurities from the slag were determined. The parameters with their levels are listed in Table 3.4.

Table 3.4. The parameters investigated in the leaching test

Parameters	Value
Particle size (d_{50})	<25 µm
Stirring speed (rpm)	300
Acid concentration (M)	1, 2, 3, 4, 5, 6, 7, 8, and 9
Amount of tartaric acid (g/L)	0, 1, 3, 5, and 6
Solid-to-liquid ratio (g/mL)	1/8, 1/10, 1/12, and 1/15
Time (min)	45, 75, 90, 180, 240, 360, 480, 600, 900, and 1200
Temperature (°C)	Room temperature, 40, 60, and 75

It was decided to conduct leaching experiments based on the OFAT (One Factor at a Time) approach. The concentration of Sb and other impurities (Al, K, Ca, Mg, Mn, and Si) from the slag was determined by AAS, while the amounts of REEs in the PLS after each leaching test were determined by ICP-MS (Perkin Elmer NEXION 2000 P). The extraction rate of all measured elements was calculated using the Equation given above (Equation 3.1).

3.2.5. Chemical Kinetics

A series of leaching experiments under the best conditions at different temperatures (20, 40, 60, and 75℃) were carried out for different times. During the leaching, the sampling procedure was conducted in a certain time to observe the leaching behavior of the Sb. The obtained results for Sb leaching were evaluated using the shrinking core model, which is one of the most used approach to understand the leaching mechanism. Four different models with their equations are listed in Table 3.5.

Table 3.5. Different chemical kinetic models and equations used in this thesis

Model	Equation
Diffusion from product layer	$1 - 2/3\alpha + (1-\alpha)^{2/3} = k \times t$
Liquid boundary layer diffusion controlled model (Jander equation)	$1 - (1-\alpha)^{2/3} = k \times t$
Chemical reaction (surface) controlled model	$1 - (1-\alpha)^{\frac{1}{3}} = k \times t$
Both chemical and diffusion controlled	$1 - 2(1-\alpha)^{\frac{1}{3}} + (1-\alpha)^{2/3} = k \times t$

The reaction rate constant was calculated, and the activation energy (E_a) was determined based on the best-shrinking core model.

3.2.6. Additional Leaching Tests for REEs

Additional leaching tests were conducted for different times under optimum conditions to determine the effect of tartaric acid amount on the leaching behavior of La from the slag.

3.2.7. Hydrolysis

After the leaching tests, the PLS was prepared for the hydrolysis test. It was aimed to precipitate Sb with high precipitation rates with no Fe precipitation. Many parameters, including metal concentration, pH, and Cl concentration, played a crucial role in the hydrolysis process (Speight, 2018; Ye et al., 2019). Furthermore, it was stated by previous researchers that the color of the obtained product may vary based on the alkaline types (Jo and Yoon, 1989). NH_4OH, NaOH, and Na_2CO_3). As such, the Sb_2O_3 product obtained with the use of water was white, while yellowish Sb_2O_3 was obtained in the presence of NH_4OH. Herein, two different bases (NaOH and NH_4OH) were used. The molarity of NaOH and NH_4OH were prepared in 5 M in liquid form. The hydrolysis tests were carried out based on the Taguchi approach (L32, 2^1 4^3). The experimental parameters with their levels are listed in Table 3.6.

Table 3.6. Hydrolysis experiments parameters with their levels

Parameters	**Level**
Alkaline types	NH_4OH and NaOH
Stirring speed (rpm)	100, 200, 300, and 400
Temperature (°C)	50, 60, 70, and 80
pH	1.5, 2, 2.5, and 3

Table 3.7 gives the experimental conditions for the hydrolysis test. In each hydrolysis test, the PLS with a volume of 100 mL was used. The pH of the PLS increased to the desired levels with the addition of two different alkaline (NH_4OH and NaOH). When the pH of the PLS reached the desired levels, the stirring was kept for an additional 30 min at the desired temperature. When the required time was over, solid-to-liquid separation was carried out using a centrifuger followed by Whatman 1 paper.

Table 3.7. The experimental conditions in the hydrolysis test

Exp. No	Alkaline type	Stirring speed	Temperature	pH	Exp. No	Alkaline type	Stirring speed	Temperature	pH
1	NH_4OH	100	50	1.5	17	NaOH	100	50	3
2	NH_4OH	100	60	2	18	NaOH	100	60	2.5
3	NH_4OH	100	70	2.5	19	NaOH	100	70	2
4	NH_4OH	100	80	3	20	NaOH	100	80	1.5
5	NH_4OH	200	50	1.5	21	NaOH	200	50	3
6	NH_4OH	200	60	2	22	NaOH	200	60	2.5
7	NH_4OH	200	70	2.5	23	NaOH	200	70	2
8	NH_4OH	200	80	3	24	NaOH	200	80	1.5
9	NH_4OH	300	50	2	25	NaOH	300	50	2.5
10	NH_4OH	300	60	1.5	26	NaOH	300	60	3
11	NH_4OH	300	70	3	27	NaOH	300	70	1.5
12	NH_4OH	300	80	2.5	28	NaOH	300	80	2
13	NH_4OH	400	50	2	29	NaOH	400	50	2.5
14	NH_4OH	400	60	1.5	30	NaOH	400	60	3
15	NH_4OH	400	70	3	31	NaOH	400	70	1.5
16	NH_4OH	400	80	2.5	32	NaOH	400	80	2

The concentrations of Sb and Fe in the solution after the hydrolysis were measured by AAS. The hydrolysis ratio of Sb was calculated using the following Equation 3.2. The obtained precipitate was washed with hot water and dried at 105 ºC for 1 h in an oven. An additional washing procedure was carried out with the addition of alkaline to remove chloride from the precipitate and therefore Sb-oxide can be obtained. The same drying procedure was conducted.

$$PR = 100 - (\frac{c \times v}{c_1 \times v_1} \times 100) \quad (3.2)$$

Where, PR is the precipitation rate (%), c is the final concentration of the element after the hydrolysis (mg/L), v is the final volume of the solution after the hydrolysis (mL), c_1 is the initial concentration of an element in the PLS before the hydrolysis (mg/L), v_1 is the initial volume of the PLS (mL)

The XRD patterns of the selected products were analyzed and the pattern were identified by Highscore software. Also, the polymorph properties of the selected products were examined by SEM. Additional hydrolysis tests were carried out for the optimization of the process according to the results obtained based on the Taguchi approach (Table 3.8).

Table 3.8. The experimental conditions of additional hydrolysis test

Exp. No	**Alkaline type**	**Stirring speed (rpm)**	**Temperature (°C)**	**pH**
HE-1	NH_4OH	100	50	1.5
HE-2	NH_4OH	100	50	1.25
HE-3	NH_4OH	100	50	1.00
HE-4	NaOH	100	50	1.5
HE-5	NaOH	100	50	1.25
HE-6	NaOH	100	50	1.00

4. RESULTS AND DISCUSSIONS

4.1. Characterization of the Slag

Firstly, a series of analyses were conducted to determine some physicochemical properties of the slag used in this thesis. Physico-chemical analyses including color, pH, moisture, dried matter, loss on ignition and inorganic phase analysis (XRD), Toxic Characteristic Leaching Procedure (TCLP), Synthetic Precipitation Leaching Conditions (SPLP), Ecological Toxicity Test, Acute Toxicity Test (fish test), and Radioactivity test were conducted. The obtained results for the physicochemical properties of the slag are summarized in Table 4.1.

Table 4.1. Physicochemical properties of the slag

Parameter	Result	Analysis Method
Color	Grey/No odor	-
pH	5.8	TS EN 15933
Moisture	<0.1	TS 9546 EN 12880
Dry matter	>99.9	TS 9548 EN 12880
Loss on ignition (% weight)	<0.1	TS EN 12879

Many methods can be used to determine the toxicity properties of the slag generated in pyrometallurgical processes, and TCLP and SPLP methods are recommended (Fallis, 1992; EPA, 1994). The behavior of organic acid (acetic acid) with a low molecular weight on the slag was determined in the TCLP method (de Andrade Lima and Bernardez, 2011). In contrast, acid rain's effect on the slag in the stockpile was simulated in the SPLP procedure (Nikfar et al., 2020). The difference between those methods was the chemicals used. Acetic acid was used in the TCLP, whereas a mixture of nitric-sulphuric acid was used in the SPLP. Table 4.2 shows the amount of Sb dissolved from the slag.

Table 4.2. The amount of Sb dissolved from the slag and its extraction rate

Method: TCLP		
Element	**Amount of dissolved Sb (mg/L)**	**Extraction rate (%)**
Sb	10.82±0.01	0.05
Method: SPLP		
Element	**Amount of dissolved Sb (mg/L)**	**Extraction rate (%)**
Sb	13.06±0.01	0.06

The dissolved amount of Sb was 10.82 mg/l, corresponding to an extraction rate of 0.05%. Although the amount of dissolved Sb was relatively lower than that of a previous study (Guo et al.,

2014), it was thought that this value was higher than acceptable levels in drinking water. The amount of Sb dissolved in a mixture of HNO_3:H_2SO_4 acid was found to be 13.06 mg/L

Prior to conducting the leaching process, the radioactivity of the slag was measured using a radiation detector (Gamma Easy). The average radiation value of the slag was measured to be 0.13 µSv/h, which was lower than that of the standard level (0.30 µSv/h) for life.

4.1.1. Mineralogical Composition of the Slag

It was determined that the dominant mineral in the slag sample is quartz (SiO_2) and it contains a relatively low amount of stibiconite ($Sb_3O_6(OH)$) mineral (Figure 4.1). Detailed mineralogical analysis conducted using the Rietveld method revealed the presence of microline ($KAlSi_3O_8$), magnetite (Fe_3O_4, <%5), and hedenbergite ($CaFeSi_2O_6$) minerals within the slag.

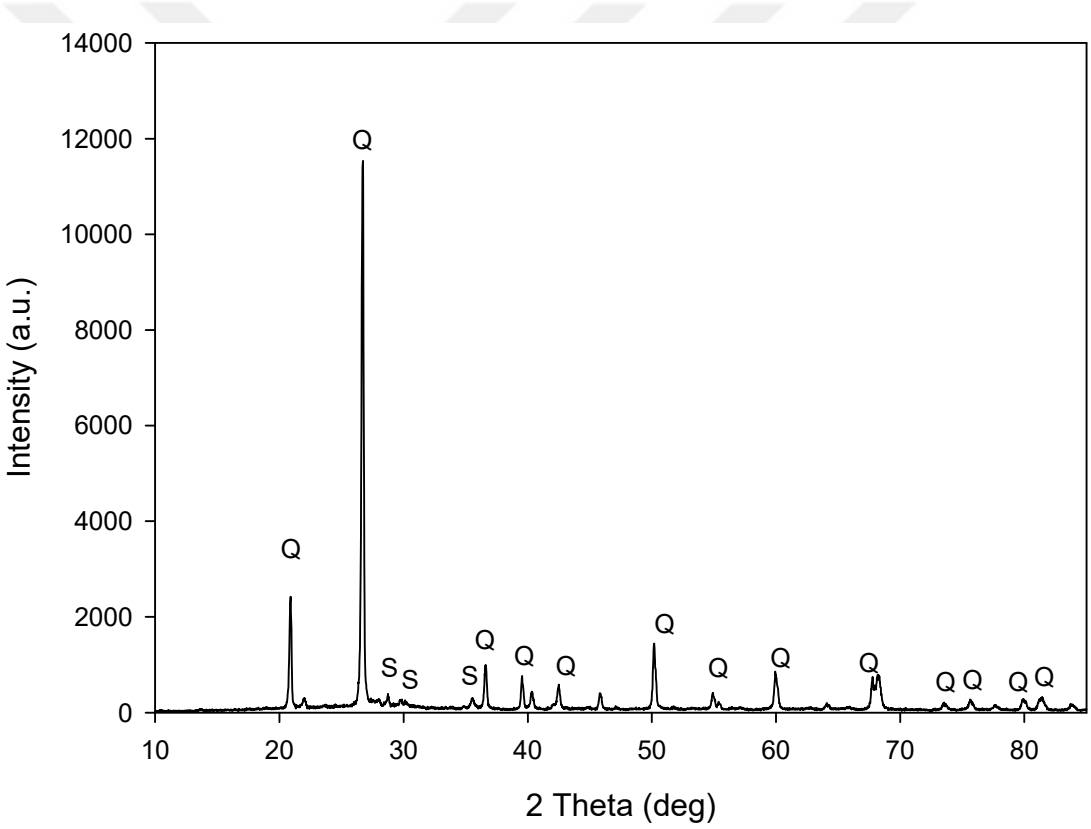

Figure 4.1. XRD pattern of the slag used in this thesis (Q: Quartz (Card No: 01-086-1628, S: Stibiconite, Card No: 96-101-1146)

SEM analyses were carried out to evaluate the properties of the slag. Figure 4.2 shows the SEM images and EDX analyses taken from polished slag. It was determined that the slag has an inherently shapeless and amorphous structure. From an elemental content perspective, it was also observed that the Sb element under study forms compounds with different elements (S, O) and/or element groups (Fe, Al, Si, Na, Ca), has a very small particle size distribution, and cannot be obtained by conventional methods. The main element of the slag, consistent with XRD analysis, was

determined to be quartz (SiO_2) through SEM images. Elements such as Ag and Th could be detected via BSE images, and their presence was confirmed by EDX analysis.

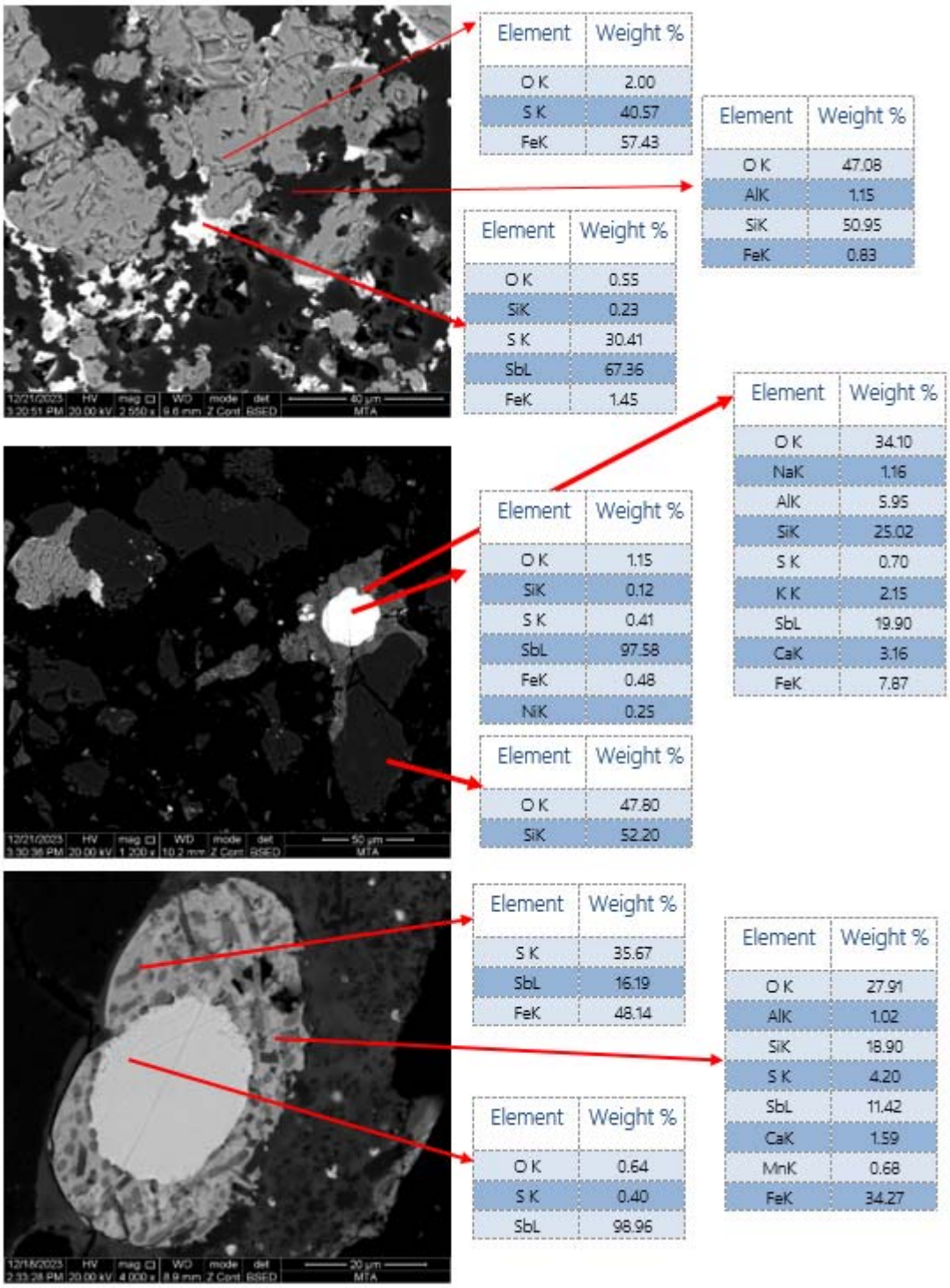

Figure 4.2. SEM images of the slag used in this thesis

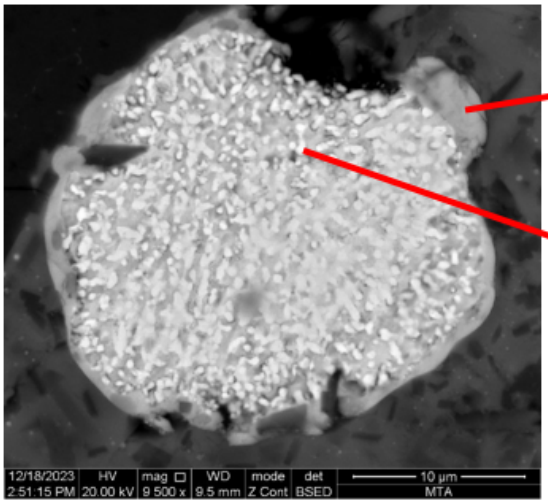

Element	Weight %
O K	0.61
S K	1.59
AgL	0.66
ThM	0.22
SbL	87.69
NiK	9.23

Element	Weight %
O K	2.78
AlK	0.57
SiK	2.29
S K	25.79
SbL	63.20
FeK	5.36

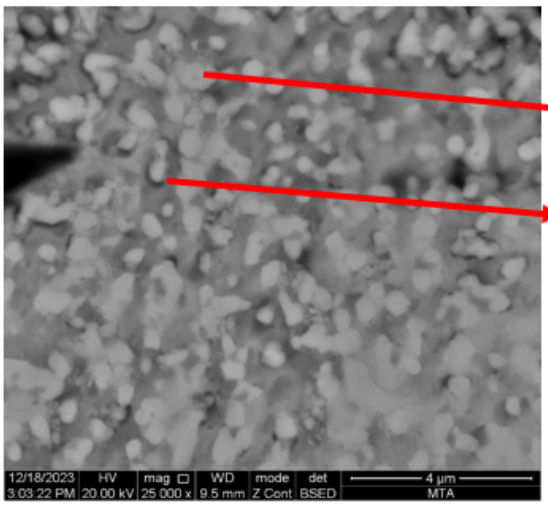

Element	Weight %
F K	0.91
SiK	0.34
S K	1.18
AgL	0.67
SbL	84.75
FeK	1.05
NiK	8.43
ThL	2.66

Element	Weight %
O K	1.24
SiK	0.55
S K	1.25
AgL	0.68
SbL	85.84
FeK	0.79
NiK	7.16
ThL	2.49

Figure 4.2. SEM images of the slag used in this thesis (continued)

Figure 4.3 demonstrates the SEM images of the slag without the use of polishing and coating processes. Although the detection of the Au element was possible through spatially performed EDX analysis, the main peaks of Sb and Au were of the same peak intensity in the analysis conducted with the EDX detector, thereby preventing a clear interpretation regarding the presence of Au. Therefore, SEM image of the occurrence of Au in the slag could not be recieved.

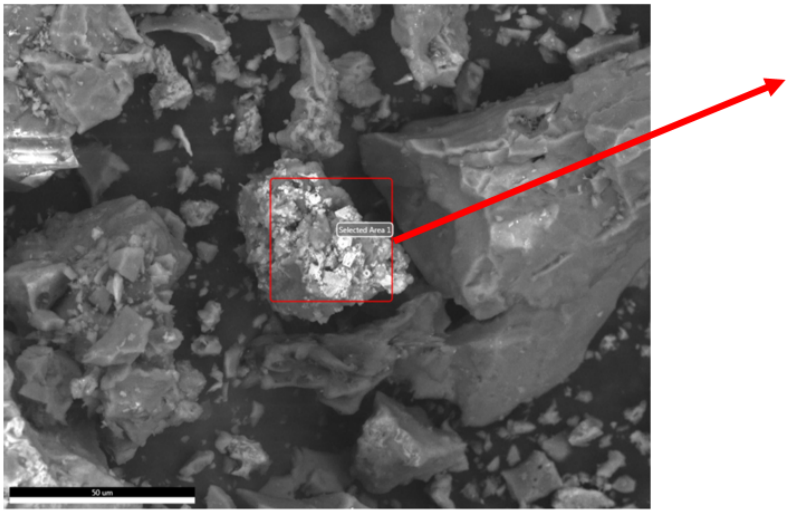

Element	Weight %
C K	4.68
O K	52.68
MgK	0.75
AlK	0.49
SiK	25.99
AgL	0.01
CaK	8.25
FeK	4.61
AuL	2.53

Figure 4.3. SEM images of the slag no-coated with carbon

Figure 4.4 presents the XPS spectra of the slag. The presence of Na, Fe, Sb, Ca, K, and Si elements on the surface of the sample was detected in the general survey (Figure 4.4.a). The presence of C observed in the analysis is attributed to carbon contamination. Due to the overlapping of the O1s elemental spectrum with the $Sb_3d_{5/2}$ orbital during analysis, it was recommended to use the $Sb_3d_{3/2}$ spectrum for deconvolution analysis (Schwoeble et al., 2011). As a result of the analysis, the presence of an oxide peak attributed to the $Sb_3d_{3/2}$ orbital within the O1s peak was identified (Figure 4.4.b).

The elemental spectrum shown in blue represents the lower limit of the integral obtained after background correction, while the yellow peaks represent the deconvoluted peaks resulting from the analysis. Thus, the O1s and $Sb_3d_{5/2}$ orbitals yielded three peaks, one of which (approximately 9.4 eV apart from $Sb_3d_{3/2}$) is attributed to Sb oxide, while the other two belong to the O element. The low amount of S element detected on the sample surface did not allow any inferences regarding an interaction between S and Sb (Figure 4.4.d). Three different Sb oxides are known: Sb_2O_3 (Sb^{3+}), Sb_2O_4 (Sb^{4+}), and Sb_2O_5 (Sb^{5+}) (Moulder et al., 1992; Wagner et al., 2003). The representation of the $Sb_3d_{3/2}$ spectrum with only one peak indicates that the Sb element present in the slag sample used in the study is in the form of Sb_2O_3 No evidence of metallic Sb or other Sb oxide minerals was obtained on the slag.

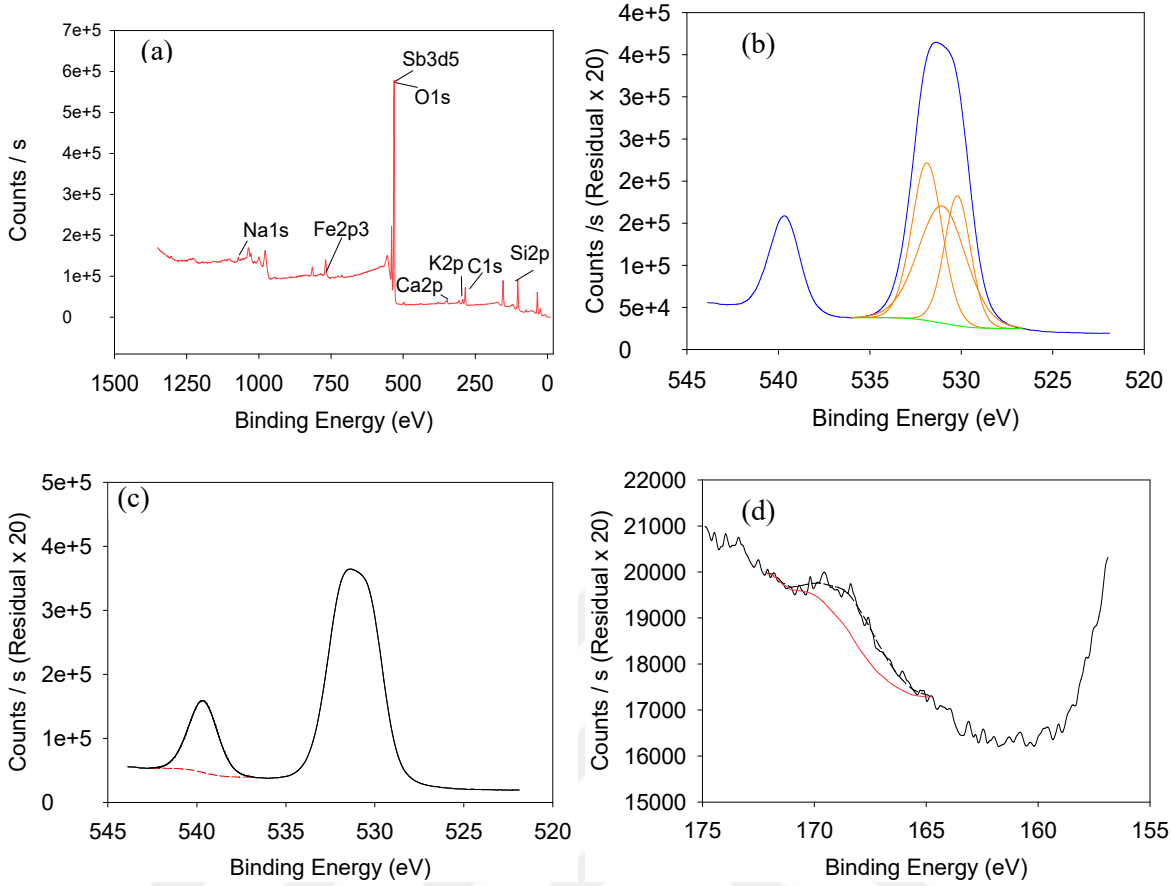

Figure 4.4. XPS analyses of the slag

4.2. Results of Preliminary Leaching Tests

The ore collected from a Smelter plant and brought to the laboratory was crushed by a jaw crusher and ground in a ball mill for two different times. The particle size distributions of the ground slag are shown in Figure 4.5. The average particle sizes (d_{50}) of the slag prepared for the leaching test were found to be 24.5 µm and 51.55 µm, respectively. It is understood from Figure 4.2 that the uniformity of the product is good.

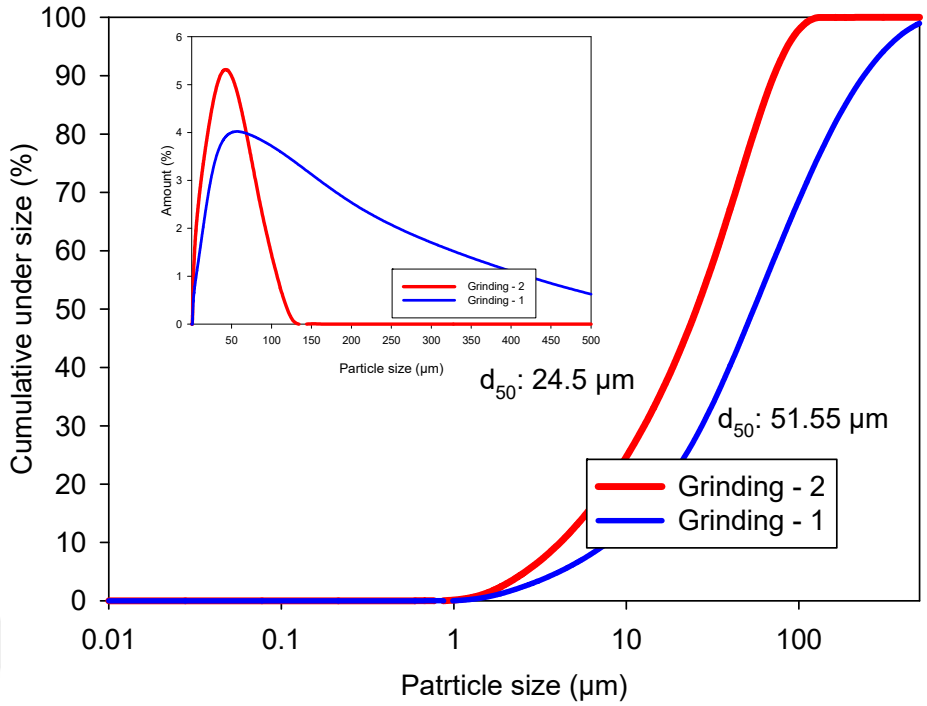

Figure 4.5. Particle size of the slag after grinding in different times

The E-pH diagram in Figure 4.6 shows Sb-based species in acidic solutions at 25 °C. Using this diagram, the phase conversion of Sb can be predicted during the leaching. It is seen that an acidic and positive-potential atmosphere are necessary for the leaching of Sb. Although HCl was suggested as the best leaching agent for Sb, herein HNO_3 and H_2SO_4 were used for comparison.

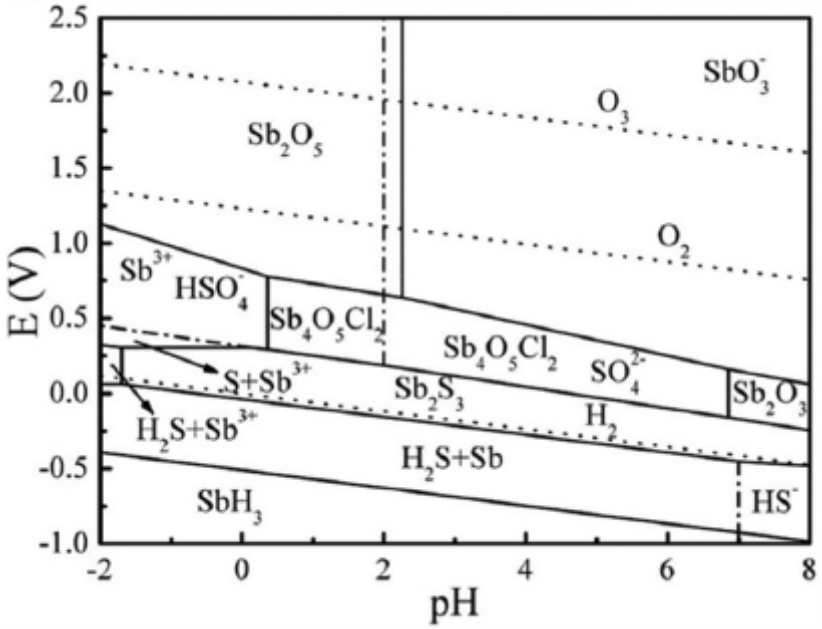

Figure 4.6. E-pH diagram at 25°C, (a) Sb-Cl-H_2O system with 0.1 M Sb^{3+} (Tian et al., 2016)

The effects of particle size on the extraction of Sb from the slag were investigated under the following conditions: a reaction temperature of 60 °C, a time of 45 min, a solid-to-liquid ratio of 5/1, and a stirring speed of 300 rpm. Figure 4.7 shows the preliminary experimental findings for the leaching of Sb from the slag. It was determined that a decrease in the particle size led to an increase in the extraction rate of Sb as shown in Figure 4.7(a). The extraction rate of Sb from the slag increased in parallel with the increase of HCl. The Sb with an extraction rate of 45% was achieved from the slag with a particle size of <25 µm in the presence of 6 M HCl, whereas the extraction rate of Sb was found to be around 35% from the slag with a particle size of 52 µm under the same conditions.

As expected, the Sb extraction rate increased over an extended time (Figure 4.7(b)). For example, an increase in the reaction time from 45 min to 180 min led to obtain high Sb extraction rates, which are 59% and 45% for the slag with a particle size of 24.5 µm and 51.55 µm, respectively.

Figure 4.7(c-d) shows the effect of acid types and stirring speed on the extraction of Sb from the slag ground for two different times. In these tests, the following parameters were kept constant: acid concentration of 6 M, time of 180 min, solid-to-liquid ratio of 1/5, and temperature of 60 ºC. The extraction rate of Sb in the presence of HCl was found to be >50%, which was higher than other inorganic acids (H_2SO_4 and HNO_3). In the leaching process, mixing the slurry at a controlled rate enhances the interaction between the leaching agent and the solid, thereby prolonging their contact time. This augmentation in the hydrodynamic behavior of the leaching system leads to a reduction in the thickness of the liquid boundary layer, consequently bolstering leaching efficiency.

As shown in Figure 4.7.d, the positive influence of increased agitation speed on Sb dissolution was determined. The intensified interaction between particles and the leaching agent is evident, corresponding to higher stirring speeds. However, experiments conducted at speeds exceeding 300 rpm revealed a limited increase in Sb dissolution efficiency. It can be inferred that the augmentation in extraction efficiency, attributed to vortex formation dependent on stirring speed, is achieved by elevating it from 150 rpm to 300 rpm. Similar findings were seen in the literature. Aktaş and Çetiner (2020) demonstrated that a speed of 200 rpm is adequate for vortex formation and subsequent Sb dissolution, with no discernible change in efficiency observed at higher speeds.

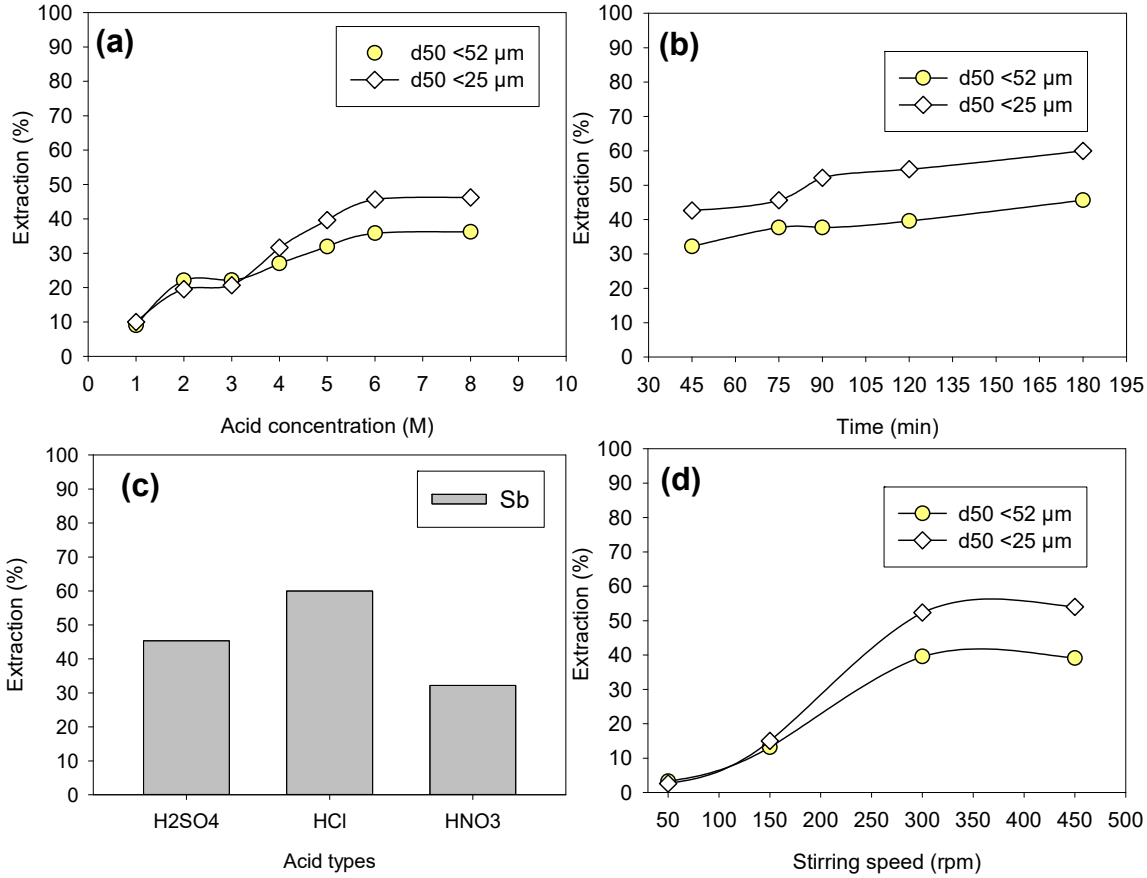

Figure 4.7. The experimental findings obtained from preliminary leaching tests

Figure 4.8 shows the Eh-log[Cl^-] diagram of the Sb-Cl-H_2O system at ambient temperature (Sillen 1971). It is seen that an increase of the Cl^- ions in the leaching system triggered the increase in the extraction rate of Sb from the slag, compared to that of other leaching agents (see Figure 4.7(c)). These findings are proved by previous study (Çetiner, 2022), which indicates that Sb (III) species may form chloro-complexes, and its solubility increases within increasing Cl^- ions activity. Therefore, it was decided to use HCl as the leaching agent for this study. In addition, the slag was prepared with a size of <25 µm in a ball mill for use in the subsequent leaching tests.

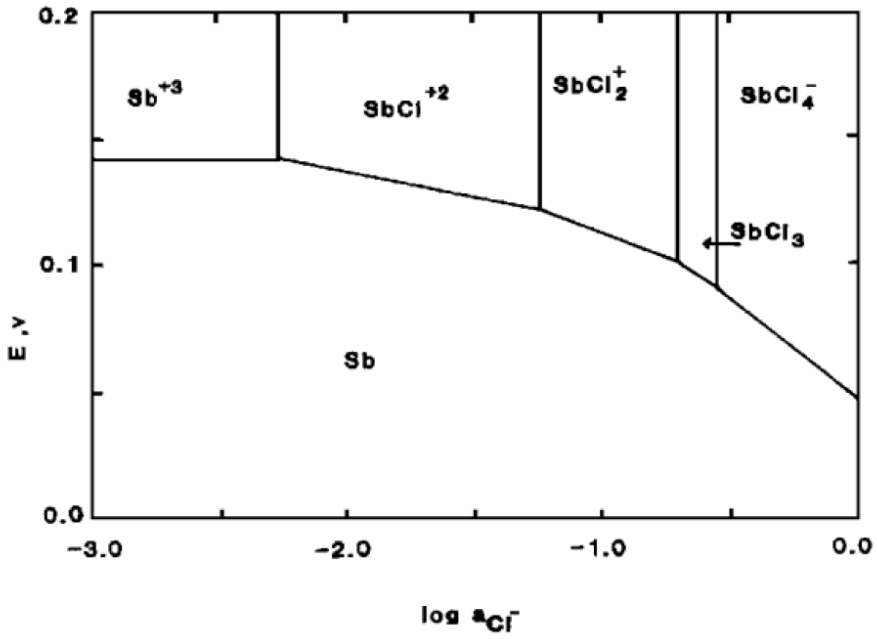

Figure 4.8. Eh – log [Cl^-] diagram of Sb – Cl – H_2O system

4.3. HCl Leaching Test

Hu et al. (2007) suggested that leaching experiments should be carried out to extract Sb from raw materials at higher reaction temperatures. The following equation represents the possible leaching reaction.

$$Sb_3O_6(OH) + 13HCl \rightarrow 3SbCl_{3(aq)} + 7H_2O + 4Cl \quad (4.1)$$

In these tests, the effects of the acid concentration, tartaric acid amount, solid-to-liquid ratio, reaction temperature, and time on the extraction of Sb from the slag were investigated. Furthermore, the leaching behaviors of the impurities and REEs were examined.

4.3.1. Effect of Acid Concentration

First, the effects of the acid concentration (1, 2, 3, 4, 5, 6, 7, 8, and 9 M) on the extraction of Sb from the slag (<25 μm) were determined in the presence of HCl. The strength of the acid concentration plays a crucial role in the leaching process. Other parameters, which were constant, were a reaction time of 45 min, reaction temperature of 60 ºC, solid-to-liquid ratio of 1/5, and stirring speed of 300 rpm. Figure 4.9 shows photographs of the PLS after the leaching tests. An increase in the acid concentration caused the PLS to become yellowish from colorless. These changes in PLS color indicate the dissolution of Sb and other elements.

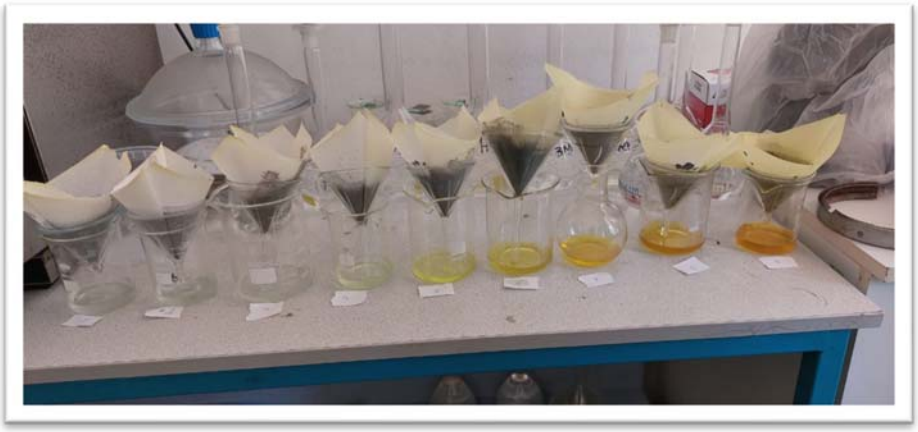

Figure 4.9. The changes in the PLS color depending on the acid concentration

The extraction rates of Sb and other elements (Al, K, Ca, Mg, Mn, and Si) from the slag are shown in Figure 4.10. Sb and Fe extraction rates showed a linearly increasing trend with increasing acid concentration. However, the extraction rate of Fe was more than two times higher (69%) than that of Sb (32%) in the presence of the highest HCl concentration (9 M), as shown in Figure 4.10(a). Previous studies have indicated that the HCl concentration should be high for the extraction of Sb; otherwise, dissolved Sb may be hydrolyzed depending on time, and therefore, the extraction rate of Sb from the slag started to decrease (Chae et al., 2020).

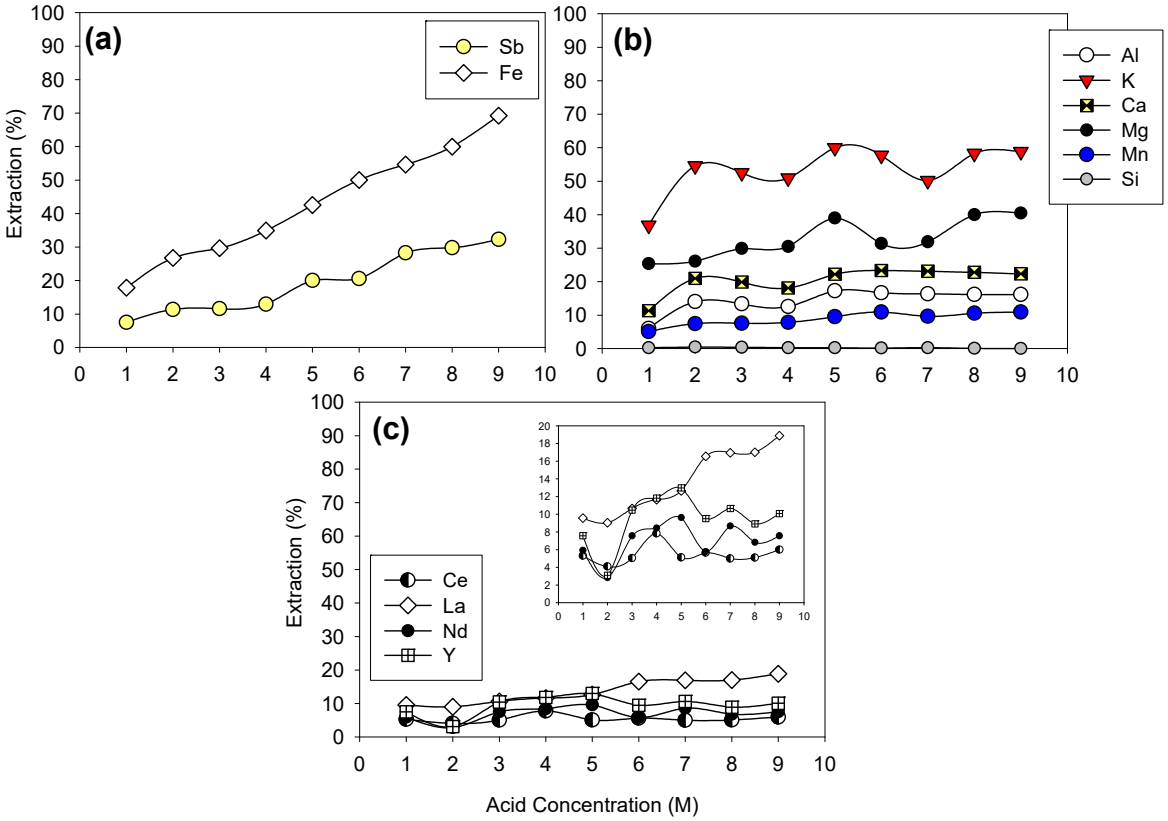

Figure 4.10. The effects of acid concentration on the extraction rate of (a) Sb and Fe, (b) impurities, and (c) REEs from the slag

Based on the experimental findings, leaching tests were performed for the subsequent stages in the presence of 6 and 8 M HCl. Moreover, the extraction rates of other impurities were lower than 30% (Figure 4.10(b)), except for the extraction rate of K. Figure 4.10(c) shows that the leaching behaviors of REEs were quite below (<10%) even at the highest HCl concentration, except for La, for which the extraction rate was 18%.

4.3.2. Effect of Tartaric Acid Amounts

As mentioned above, Sb ions may be hydrolyzed, decreasing the extraction rate of Sb (Groenewald, 1964; Moldan, 1966). Therefore, the experimental findings were significantly influenced. Previous studies have indicated that adding tartaric acid makes Sb ions more stable in PLS during leaching (Küçükoğlu et al., 2022). With the addition of tartaric acid, Sb ions form the Sb-tartrate complex, which has a more negative potential than hydrogen ions and prevents the hydrolysis of Sb from the PLS. For this purpose, the effects of tartaric acid (0, 1, 2, 3, 5, and 6 g/L) on the extraction of Sb from the slag were determined in the presence of 6 and 8 M HCl. The experimental parameters that were kept constant were as follows: reaction time of 45 min; reaction temperature of 60 ºC; solid-to-liquid ratio of 1/5, and stirring speed of 300 rpm. The use of tartaric acid has a positive effect on the Sb extraction rate, as listed in Table 4.3.

Table 4.3. The effect of tartaric acid on the extraction rate of Sb

Tartaric acid (g/L)	Extraction rate of Sb (%) HCl: 6 M	Extraction rate of Sb (%) HCl: 8 M
0	20.58	29.77
1	19.29	32.10
3	24.08	30.67
5	23.96	31.61
6	26.63	32.75

Figure 4.11 and Figure 4.12 show the effect of tartaric acid on the extraction rates of Sb together with other elements and REEs from the slag. When the experimental findings were evaluated, it was observed that there was no effect on the extraction rate, except for La extraction. The increase in the extraction rate of La from the slag was due to the increase in the tartaric acid content. However, the increase in the extraction rates of other REEs (Ce, Y, and Nd) is negligible. In addition, the HCl concentration should be 8 M to extract La at high extraction rates in the presence of tartaric acid (6 g/L). Although there was no effect on the extraction rate of Sb in the presence of tartaric acid, tartaric acid was used at a concentration of 1 g/L in the subsequent leaching tests to minimize the possible hydrolysis of Sb ions. Additional leaching tests were performed to determine the effects of tartaric acid on the extraction rate of REEs in the subsequent stages.

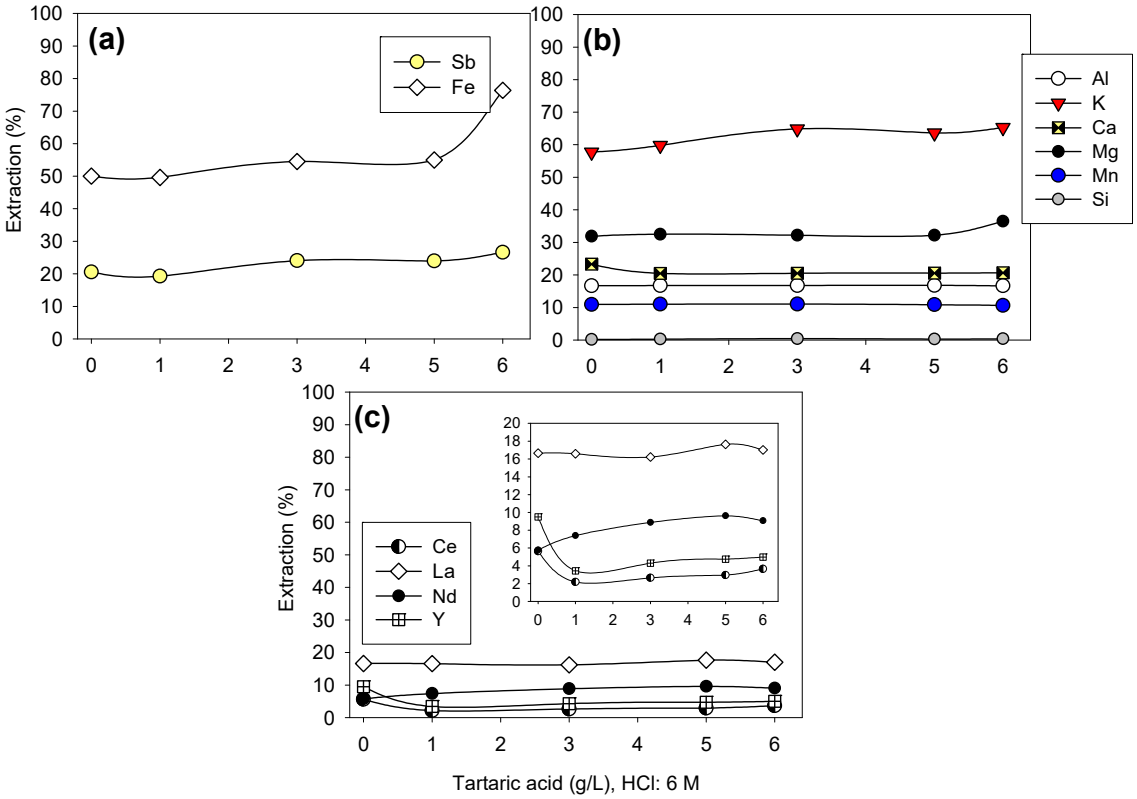

Figure 4.11. The effects of tartaric acid on the extraction rate of (a) Sb and Fe, (b) impurities, and (c) REEs from the slag in the presence of 6 M HCl

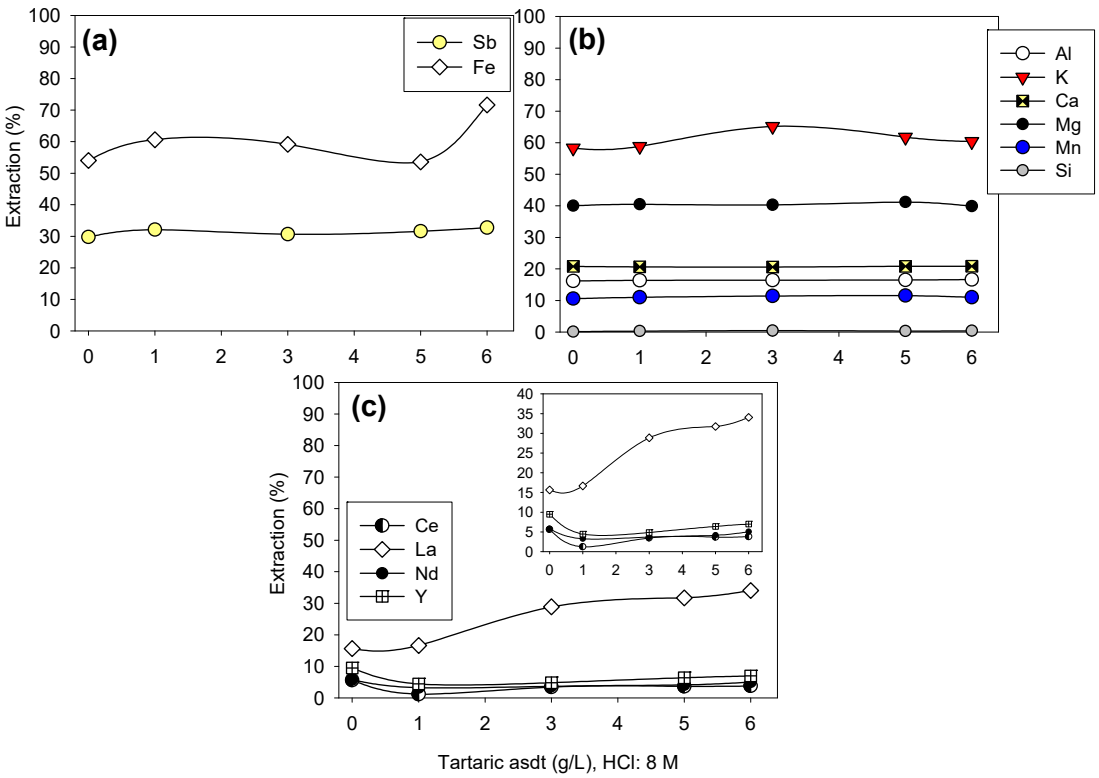

Figure 4.12. The effects of tartaric acid on the extraction rate of (a) Sb and Fe, (b) impurities, and (c) REEs from the slag in the presence of 8 M HCl

4.3.3. Effect of Solid-to-Liquid Ratio

Figure 4.13 shows the effect of the solid/liquid ratio on the leaching efficiency. The experimental parameters were maintained at constant levels, including a reaction temperature of 60 °C, time of 45 min, HCl concentration of 8 M, and stirring speed of 300 rpm. The solid/liquid ratio plays a crucial role, with a decrease in the sample quantity per solvent concentration accelerating the dissolution process. As the solid/liquid ratio decreased from 1/5 to 1/20 under consistent experimental conditions, the extraction rate of Sb increased from 32% to approximately 45%. Notably, the extraction rate of Fe from the slag surpassed that of Sb, with nearly all Fe content passing into the solution under 1/20 solid/liquid ratio conditions (extraction rate >99%). Similarly, except for Mn and Si, the extraction rate of other impurities reaches 100% within decreasing solid/liquid ratios. As anticipated, a decrease in the solid/liquid ratio accelerated the extraction rate of La. However, no discernible differences in the extraction rates were observed for Ce, Nd, and Y.

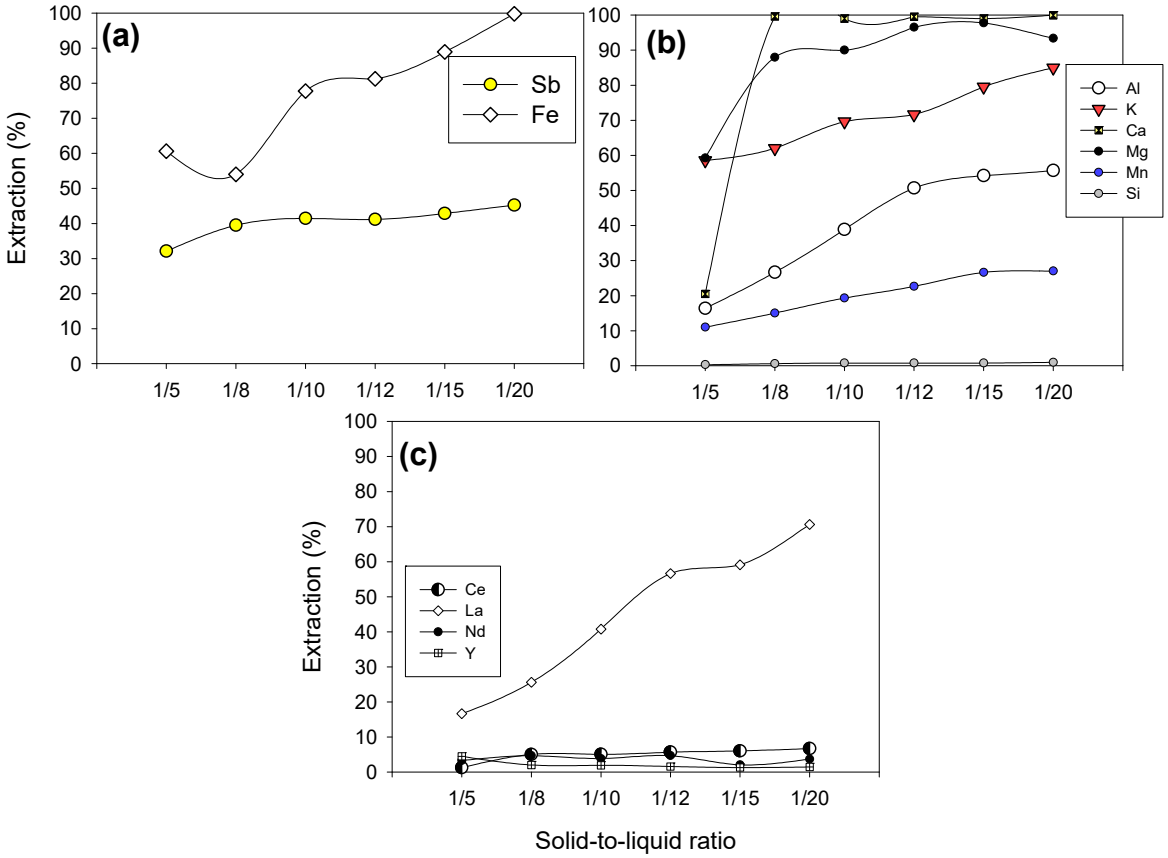

Figure 4.13. The effects of solid-to-liquid ratio on the extraction rate of (a) Sb and Fe, (b) impurities, and (c) REEs from the slag

4.3.4. Effects of Reaction Time and Temperature

To investigate the effects of reaction time and temperature, a series of experiments were carried out at room temperature, 40 °C, 60 °C, and 75 °C for varying durations (45, 60, 90, 120, 150, and 180 min). Figures 4.14 – 4.17 show the extraction rates of Sb and Fe as a function of time. Other

parameters kept constant at this stage included an HCl concentration of 8 M, solid/liquid ratio of 1/10, tartaric acid amount of 1 g/L, and stirring speed of 300 rpm. Experiments conducted at room temperature yielded very low extraction rates of Sb and Fe from the slag (<30%). Despite increasing the reaction time from 45 to 180 min, no positive effect on the extraction rate was observed at room temperature. These findings are consistent with those of Guo et al. (2017), who reported limited extraction rates even with increased acid concentration and stirring speed at room temperature (Sb extraction rate <30%). It has been reported that a higher reaction temperature is required for highly efficient Sb extraction. For instance, experiments conducted at 40°C with a reaction time of 45 min yielded an Sb extraction rate of approximately 40%. In contrast, an increase in the reaction time, the extraction rate of Sb dissolution efficiency tended to increase from 40% to approximately 80%. Similarly, in these experiments, an increase in the dissolution efficiency of other impurities over time was observed. However, limited dissolution values were observed for REEs in the same experiment.

When the temperature was increased from 40 °C to 60 °C, almost all of the Fe contained in the slag had passed into the solution by the end of 180 min. An increase in the temperature led to an Sb extraction rate of approximately 80% after 180 min. Palden et al. (2021) also indicated that a temperature of at least 50 °C is necessary for the extraction rate of Sb from the slag. Therefore, the Sb dissolution behaviors observed in this study are consistent with those reported in the literature. Some studies have examined both Sb and Fe leaching behaviors. The results obtained in these studies differ from those of the present study in terms of the extraction rate of Fe. Although high Sb dissolution values were achieved at high temperatures in the presence of HCl, they ensured very low levels of Fe passage into the solution. For example, during the dissolution of stibnite ore with HCl, the Sb dissolution efficiency was >80%, depending on the leaching conditions, whereas the Fe dissolution efficiency was less than 10% (Tian et al., 2016). This difference is thought to be due to the Fe content of raw material.

As expected, as the temperature increased, Sb began to pass into the solution at the targeted levels, while the rates of undesirable impurities passing into the solution also increased, and almost all of the K, Ca, and Mg contained in the slag were dissolved. When the reaction temperature was 60°C, the La dissolution efficiency of the slag was approximately 50% after 180 min. However, no positive increase in Ce, Nd, and Y extraction rates was observed over time.

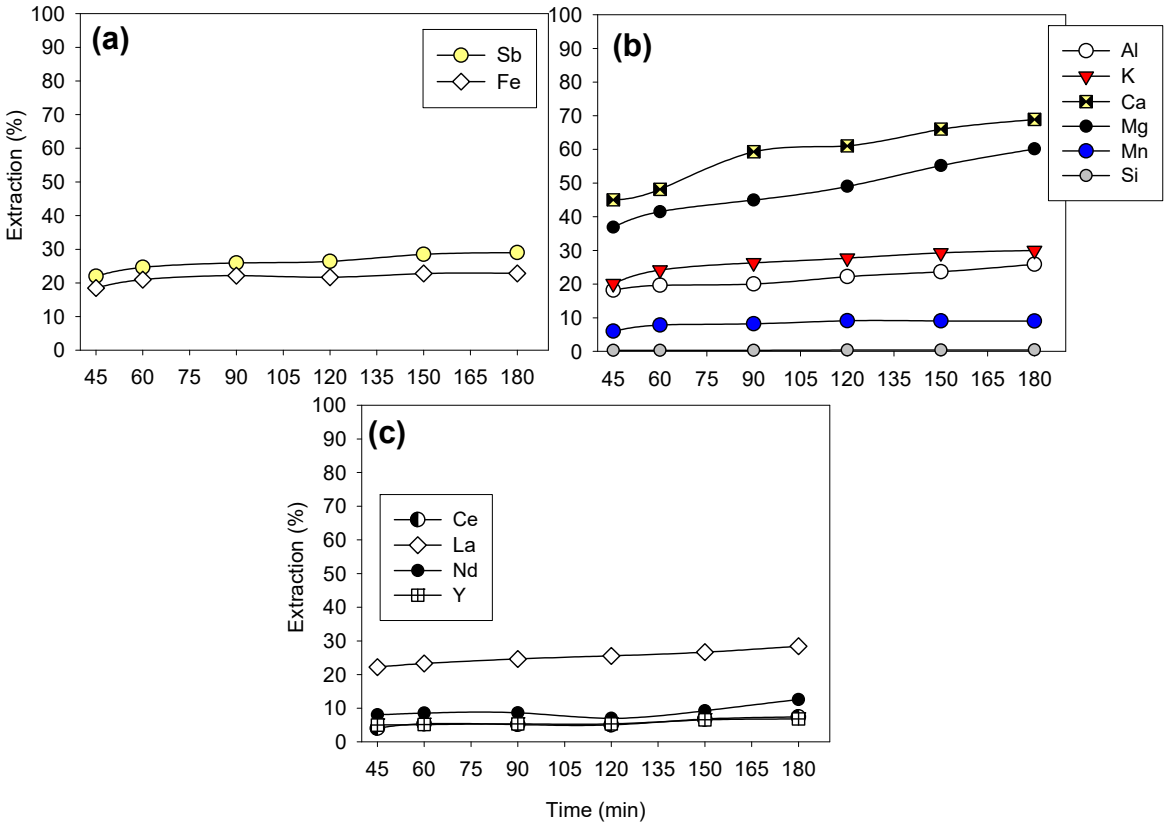

Figure 4.14. The effects of reaction time on the extraction rate of (a) Sb and Fe, (b) impurities, and (c) REEs from the slag at ambient temperature

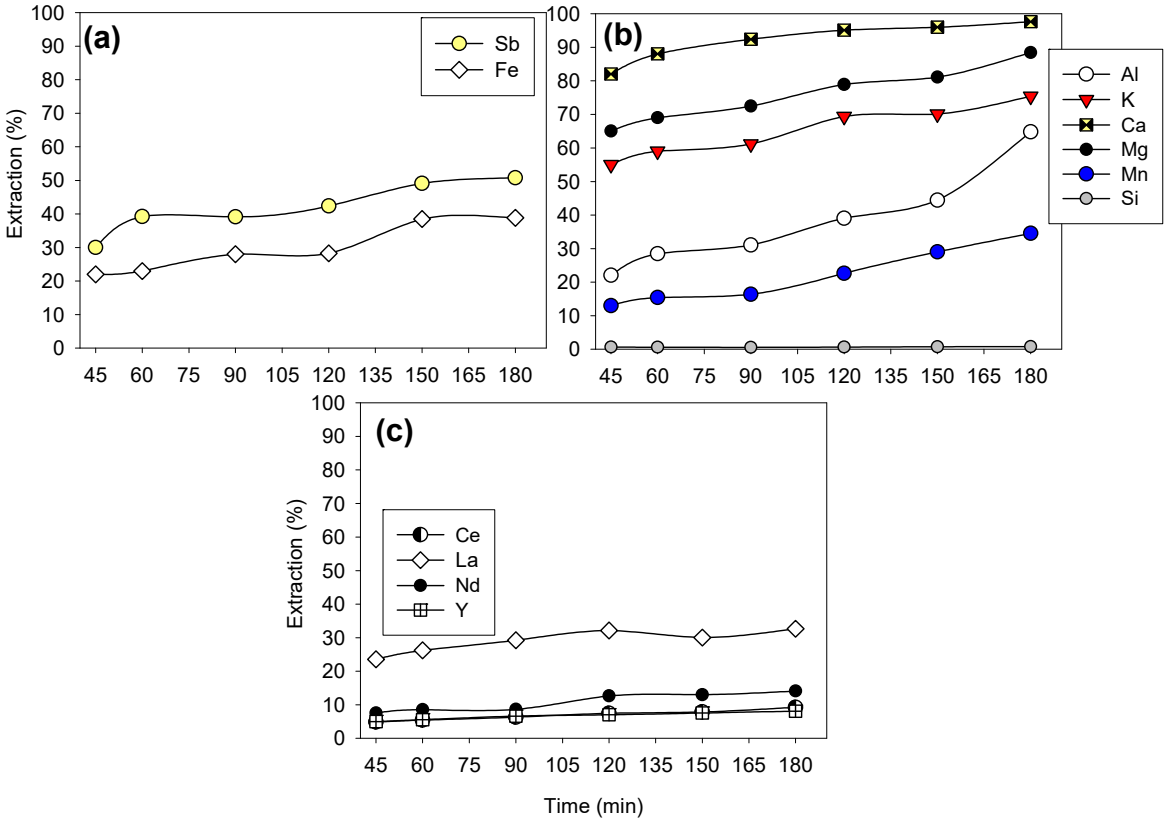

Figure 4.15. The effects of reaction time on the extraction rate of (a) Sb and Fe, (b) impurities, and (c) REEs from the slag at a temperature of 40 °C

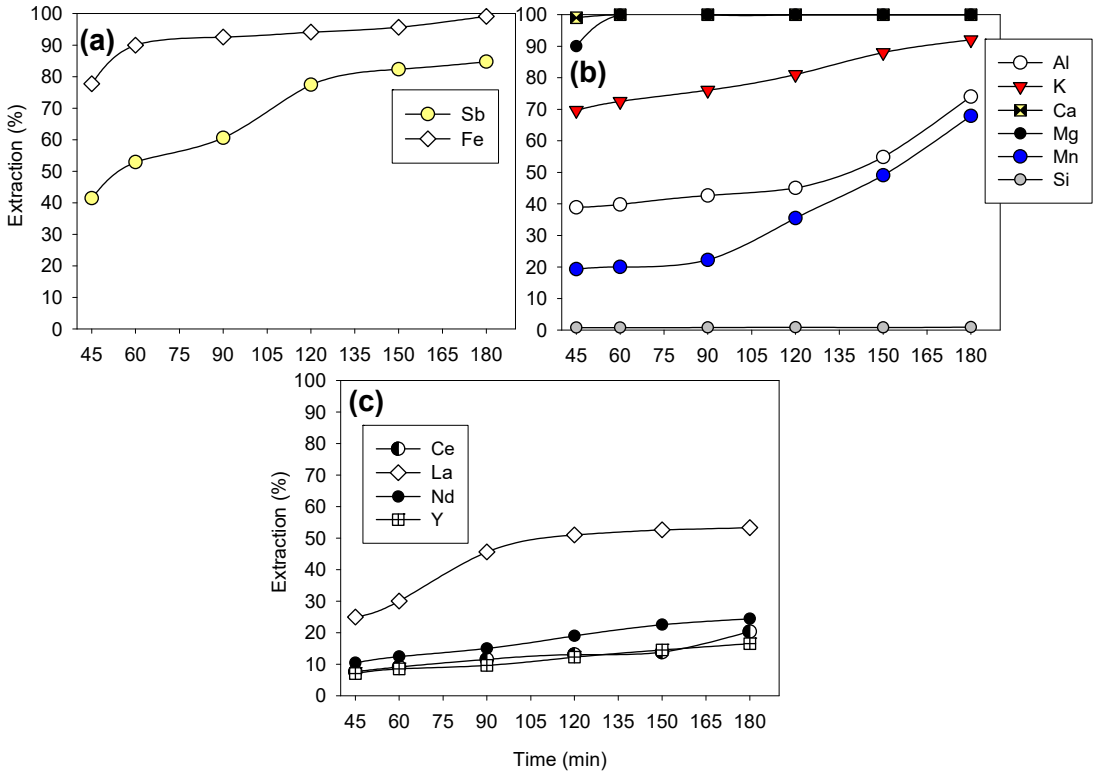

Figure 4.16. The effects of reaction time on the extraction rate of (a) Sb and Fe, (b) impurities, and (c) REEs from the slag at a temperature of 60 °C

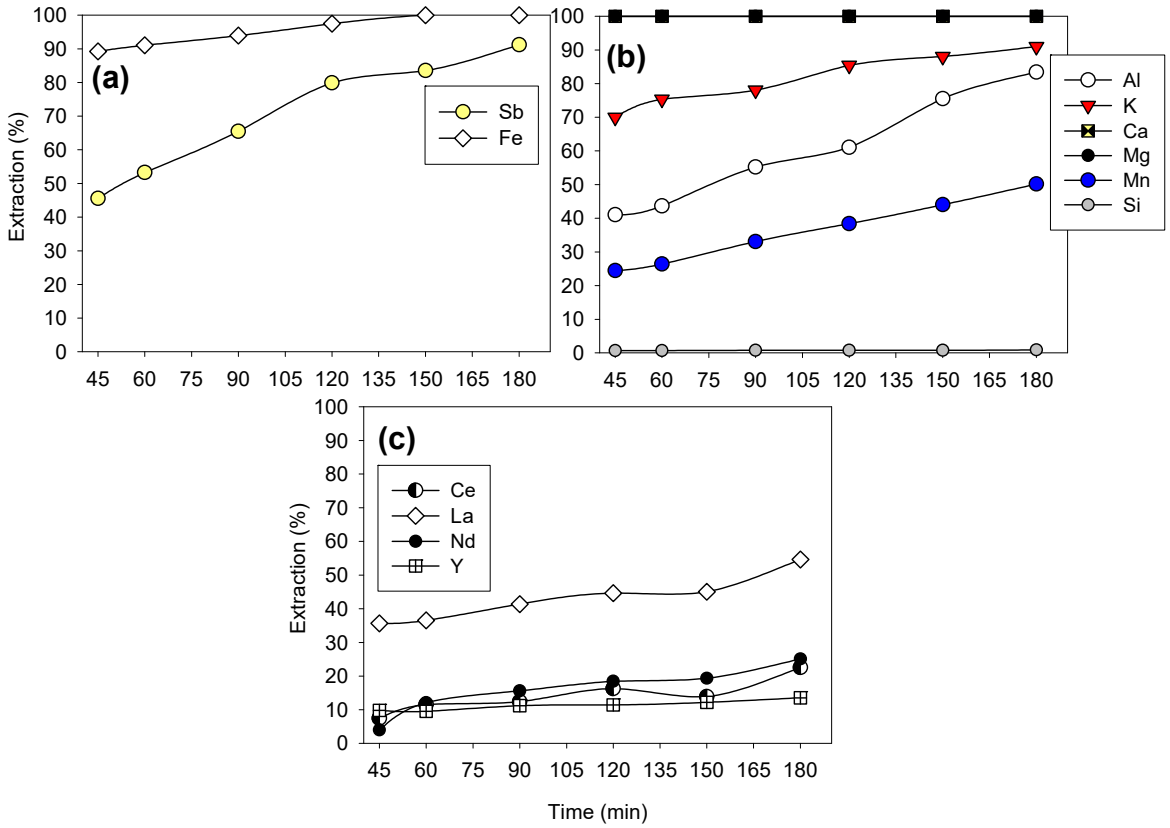

Figure 4.17. The effects of reaction time on the extraction rate of (a) Sb and Fe, (b) impurities, and (c) REEs from the slag at a temperature of 75 °C

4.4. Chemical Kinetics

Based on the experimental results, the leaching parameters required for achieving high efficiency in extracting Sb from the slag under atmospheric conditions are determined as follows:

- HCl concentration: 8 M,
- Solid/liquid ratio: 1/10,
- Stirring speed: 300 rpm,
- Amount of tartaric acid : 1 g/L,
- Reaction temperature: 75 °C,
- Reaction time: 180 minutes.

At this stage, the leaching experiments were conducted at different temperatures (room temperature, 40°C, 60°C, and 75°C) and durations to elucidate the extraction behavior of Sb during the leaching process. Experimental results obtained depending on time are shown in Figure 4.18.

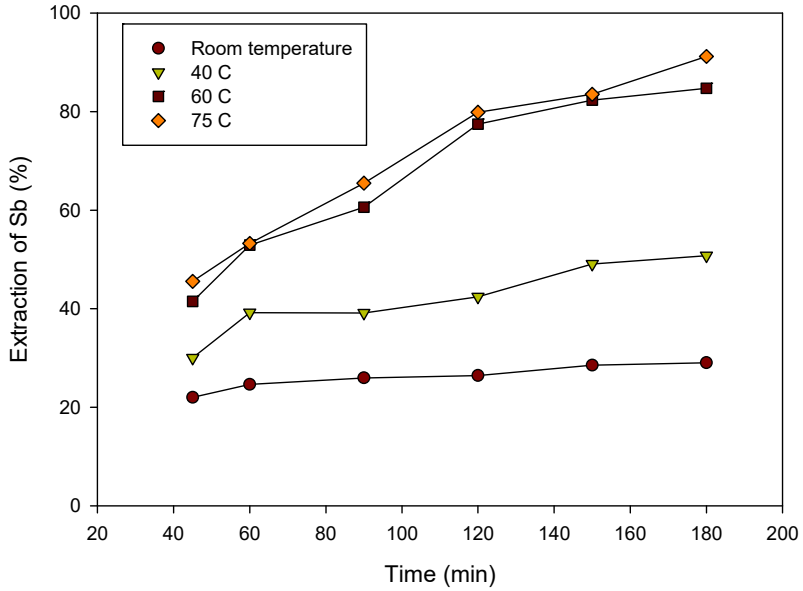

Figure 4.18. The extraction rate of Sb from the slag at different temperatures

Leaching processes generally occur at the solid/liquid interface. The stages occurring during the leaching process are represented schematically in Figure 4.19. The stages occurring in this process are listed below:

(i) Diffusion of the solvent along the liquid boundary layer,

(ii) Diffusion of the solvent along the product layer,

(iii) Adsorption of the solvent on the surface of solid particles,

(iv) Surface reaction and desorption of products,

(v) Diffusion of products along the product layer, and

(vi) Diffusion of products along the liquid boundary layer.

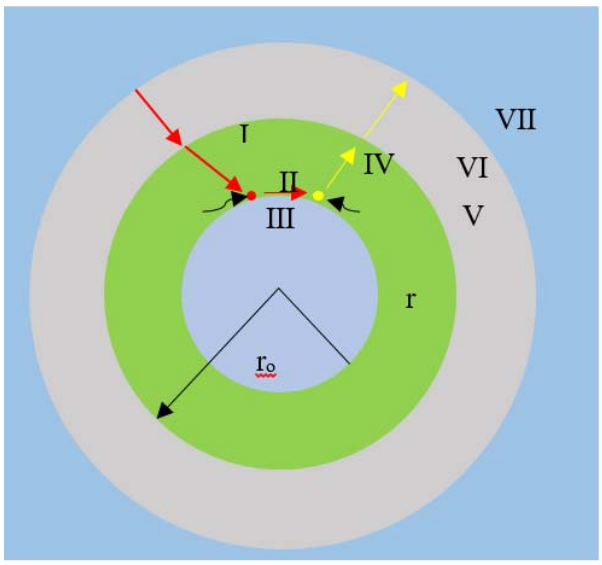

Figure 4.19. Stages occurred during the leaching process (ro = the initial radius of the slag, r = the radius of the residue) (Havlík, 2007)

The occurrence of the stages mentioned above in the leaching process depends on the physical and chemical properties of the solid particle targeted for dissolution, the type of solvent used, and the experimental conditions (Brahim et al., 2022). Therefore, mathematical modeling is an effective method used to determine the types of reactions and investigate leaching behaviors. The shrinking core model is one of the most commonly used mathematical models. With this method, values such as reaction type and reaction rate constant can be determined, and activation energy values for the dissolution reaction can also be calculated according to the most suitable chemical kinetic model. Thus, the most suitable kinetic model for the dissolution mechanism of Sb can be identified. In this thesis, experimental results were evaluated using four different models (provided in Table 3.5); namely, (1) ash layer diffusion-controlled (diffusion from product layer), (2) film diffusion-controlled, (3) surface reaction-controlled (chemical), and (4) both chemical and diffusion-controlled. Using the equations given in Table 3.5, the extraction rate of Sb from the slag depending on time, is converted into values that can be used in different kinetic models to explain the leaching behavior of the Sb. Table 4.4 lists the values for each kinetics model.

Table 4.4. The conversion of the extraction rate of Sb to evaluate the leaching mechanism

Temperature (°C)	Time (min)	The amount of Sb Dissolved (%)	Kinetics model			
			Chemical (Surface) Reaction controlled	Film diffusion controlled	Diffusion from product layer	Both chemical and diffusion-controlled
Room temperature (20°C)	**45**	22.01	0.080	0.153	0.006	0.287
	60	24.64	0.090	0.172	0.008	0.321
	90	25.95	0.095	0.182	0.009	0.337
	120	26.42	0.097	0.185	0.009	0.343
	150	28.51	0.106	0.200	0.010	0.370
	180	29.02	0.108	0.204	0.011	0.376
40 °C	**45**	30.01	0.112	0.212	0.012	0.388
	60	39.20	0.153	0.282	0.021	0.502
	90	39.14	0.153	0.282	0.021	0.501
	120	42.40	0.168	0.308	0.025	0.540
	150	49.11	0.202	0.363	0.035	0.620
	180	50.78	0.210	0.377	0.038	0.639
60 °C	**45**	41.46	0.163	0.300	0.024	0.529
	60	52.92	0.222	0.395	0.042	0.664
	90	60.61	0.267	0.463	0.059	0.749
	120	77.45	0.391	0.630	0.113	0.919
	150	82.35	0.439	0.685	0.136	0.962
	180	84.75	0.466	0.715	0.150	0.980
75 °C	**45**	45.56	0.183	0.333	0.030	0.578
	60	53.27	0.224	0.398	0.043	0.668
	90	65.50	0.299	0.508	0.071	0.802
	120	79.90	0.414	0.657	0.124	0.941
	150	83.54	0.452	0.700	0.143	0.971
	180	91.19	0.555	0.802	0.194	1.022

It was possible to evaluate the extraction mechanism of Sb as a function of temperature, as depicted in Figure 4.20. In determining which of the four chemical kinetic models best explains the mechanism of Sb dissolution from the slag, particular attention has been paid to the R-squared (R^2) value. As observed, the R^2 value for each model is more significant than 0.90. The proximity of the R^2 values to 1 indicates that the experiments can be explained by these models. Considering the R^2 values obtained at each temperature, it has been concluded that the ash layer diffusion method is the best model for modeling the extraction of Sb from the slag.

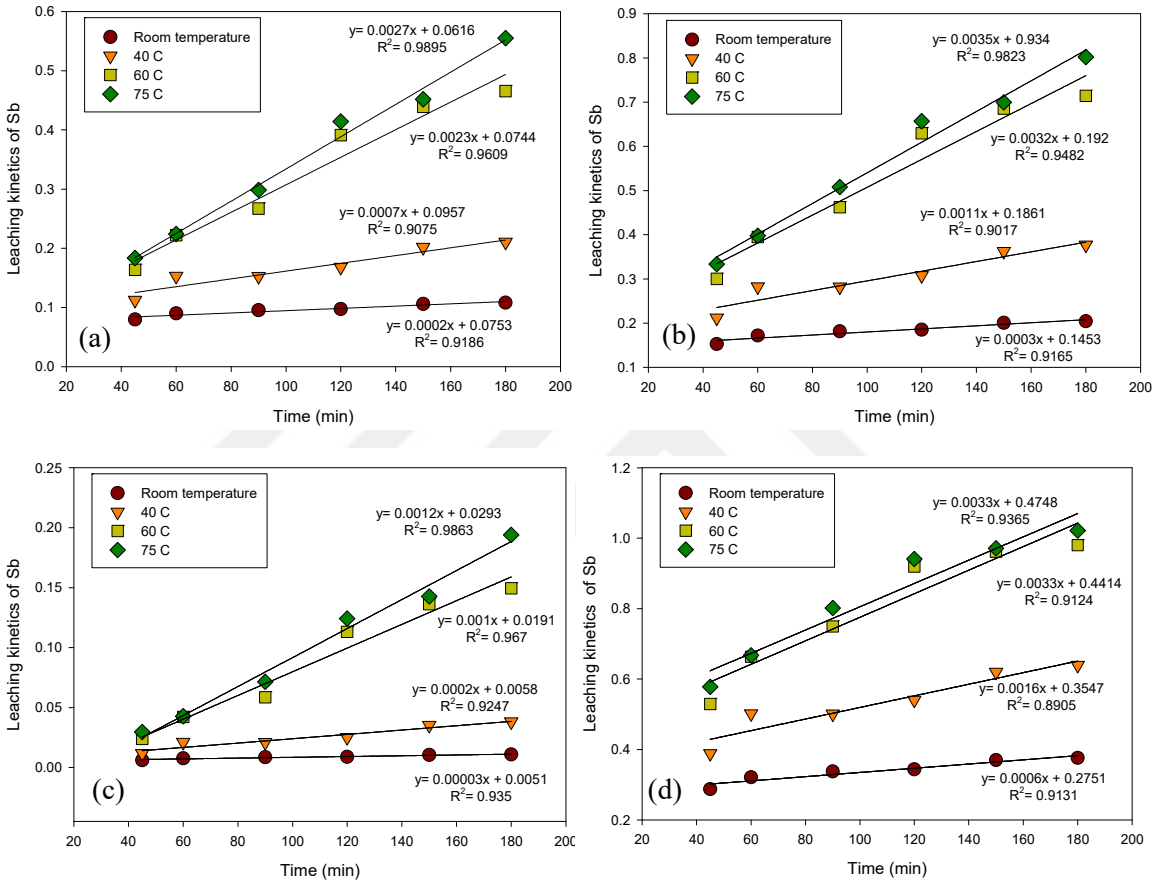

Figure 4.20. Sb dissolution kinetics depending on time at different temperatures (a) Chemical reaction (surface) controlled model, (b) Film diffusion model (Jander equation), (c) Diffusion from product layer, and (d) Both chemical and diffusion controlled model

The reaction rate constant values were calculated from the slope values of these models (Figure 4.20.b). Table 4.5 lists that the reaction rate constant values in a range of between 6.01×10^{-5} min^{-1} and 107.84×10^{-5} min^{-1}, depending on the temperature. The Arrhenius curve was plotted using these reaction rate constants as shown in Figure 4.21.

Table 4.5. The reaction rate constants for the ash layer diffusion model

Temperature (°C)	Temperature (1/T, K) x 10^{-3}	Reaction rate constant (min^{-1})	ln K
20	3.412969	6.01×10^{-5}	-9.71943
40	3.194888	21.15×10^{-5}	-8.46117
60	3.003003	83.08×10^{-5}	-7.09317
75	2.873563	107.84×10^{-5}	-6.83228

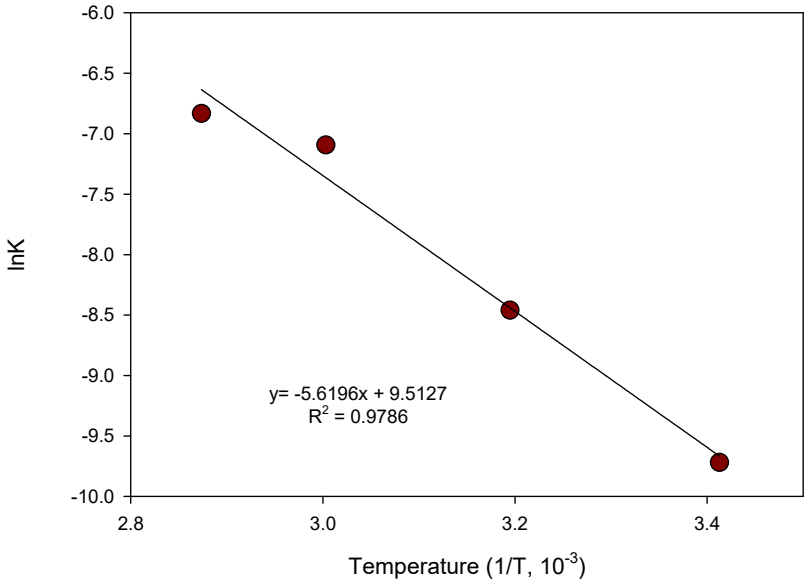

Figure 4.21. Arrhenius curve for the extraction of Sb from the slag

The activation energy (E_a) can be calculated using the following Equation (4.2). The conducted leaching reactions are classified based on their Ea values. For example, if E_a <20 kJ/mol, the reaction was governed by a diffusion-controlled mechanism. Conversely, if E_a>42 kJ/mol, it indicates an exponential relationship between the rate constant and temperature, the leaching mechanism can be explained by a chemically controlled mechanism (Ait Brahim, Ait Hak et al. 2022). The E_a was calculated to be 46.75 kJ/mol, which indicates that the chemically controlled mechanism governed the leaching of Sb from the slag.

$$k = A_o e^{\frac{-E_a}{RT}} \quad (4.2)$$

4.5. Additional Leaching Experiments for REEs

It was determined that the addition of tartaric acid not only prevented the hydrolysis of dissolved Sb ions but also posivitely contributed to the extraction of La from the slag. In previous stages, the extraction rate of La from the slag was around 50% under optimum leaching conditions (see Figure 4.18). Therefore, it was decided to conduct leaching experiments in extended times. The

parameters that are kept constant in these experiments were as follows: HCl concentration: 8 M, solid/liquid ratio: 1/10, stirring speed: 300 rpm, tartaric acid concentration: 1 g/L, and reaction temperature: 60 °C. The experimental results can be seen in Figure 4.22. It was determined that a leaching time of 20 h is required for the complete extraction of La contained in the slag. The extraction rates of other REEs (Ce, Y, and Nd) under the same conditions are in the range of 25 – 40 %.

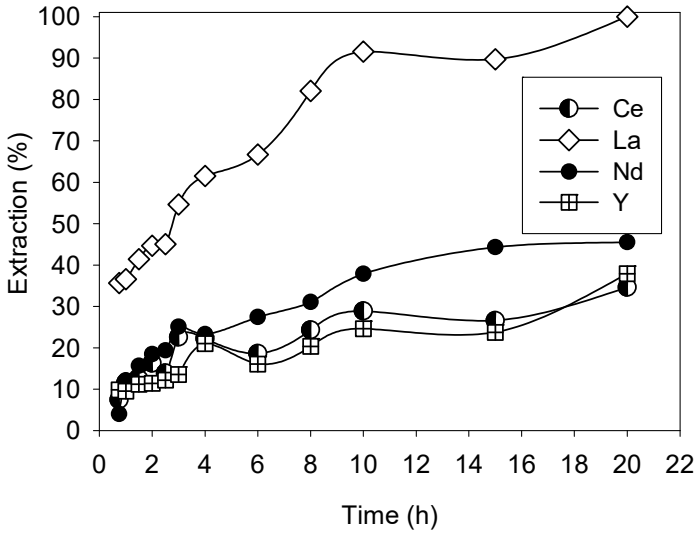

Figure 4.22. The leaching behaviors of REEs under optimum conditions in extended leaching times (tartaric acid amount : 1 g/L)

Figure 4.23 shows that additional leaching experiments at a temperature of 60 and 75 °C were conducted to determine the effect of tartaric acid amount on the extraction of REEs from the slag, respectively. An increase in the amount of tartaric acid makes the extraction of La with high rates in shorter times. While the experiments conducted with 1 g/L tartaric acid determined a leaching time of 20 h for the complete extraction of La, increasing the tartaric acid concentration from 1 g/L to 6 g/L reduced the time required for high-efficiency dissolution of La to 180 min. These findings are consistent with previous studies (Zhang et al., 2016), which reveal that the required time for the extraction of La from the soil decreased with the increase of tartaric acid concentration in the leaching system.

Under these applied conditions, the extraction rate of Sb from the slag was determined to be 91.19%. While the extraction rate of La was approximately 97%, the extraction rates of other REEs (Y, Ce, Nd) were found to be ≤50%. The extraction rates of other elements in the slag, which were not considered in this thesis due to their low concentrations, are also detailed in Table 4.6.

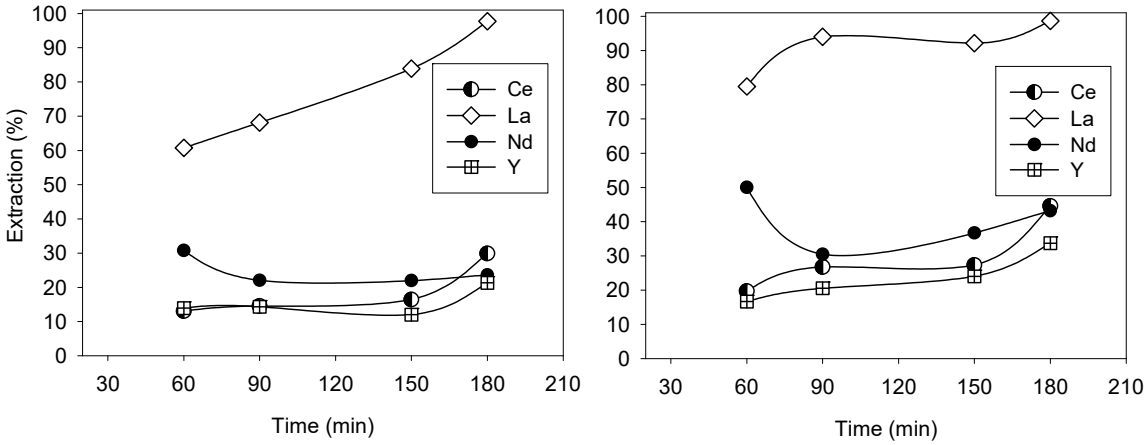

Figure 4.23. Leaching behaviors of REEs from the slag under optimum conditions in extended leaching times (tartaric acid amount: 6 g/L)

Table 4.6. The extraction rate of all elements present in the slag under optimum conditions

Element	Leaching Residue (g/t)	Slag (g/t)	Extraction rate (%)	Element	Leaching Residue (g/t)	Slag (g/t)	Extraction rate (%)
La	2.89	78.62	97.13	**Tm**	0.082	0.138	35.25
Y	20.2	25.8	38.93	**Yb**	0.529	0.866	33.43
Ce	19.65	**31.11**	50.73	**Pr**	2.15	3.46	32.28
Nd	21.55	33.78	50.24	**W**	0.105	0.162	29.37
As	53.7	441	90.50	**Lu**	0.073	0.112	28.97
Nb	0.939	4.36	83.20	**Zn**	664	942	23.19
Ni	83.6	348	81.26	**Th**	2.17	2.99	20.91
In	0.007	0.021	74.00	**Ba**	111	140	13.60
Cr	151	356	66.92	**Tl**	37.6	47	12.82
Cd	1.47	3.45	66.77	**Ga**	4.94	6.15	12.47
Eu	0.549	1.155	62.92	**Zr**	19.6	23.5	9.11
Co	5.79	11.65	61.23	**Ge**	0.12	0.14	6.59
Pb	49.6	93.8	58.75	**Hf**	0.554	0.637	5.22
U	12.85	24.3	58.75	**Rb**	75.1	84.6	3.26
Dy	2.05	3.58	55.34	**V**	30.7	33.7	0.73
Sr	27.3	47.6	55.26	**Mo**	10.9	11.95	0.60
Er	0.632	1.1	55.19	**Sc**	3.51	3.81	__
Ho	0.291	0.504	54.96	**Li**	36.7	39.6	__
Gd	2.32	4.01	54.87	**Be**	1.46	1.5	__
Tb	0.382	0.644	53.73	**Cs**	23	22.2	____

4.6. Hydrolysis Test

This technique is used for the recovery of Sb from the PLS. In this process, Sb ions are hydrolyzed with different precipitators (water or alkaline) at a specific temperature. The possible chemical reactions during the hydrolysis process are explained in Equations 4.2-4.5.

$$4SbCl_3 + 5H_2O \rightarrow Sb_4O_5Cl_2 \downarrow + 10HCl \quad (4.2)$$
$$Sb_4O_5Cl_2 + 2NH_4OH \rightarrow 2Sb_2O_3 + 2NH_4Cl + H_2O \quad (4.3)$$
$$Sb_4O_5Cl_2 + 2NaOH \rightarrow 2Sb_2O_3 + 2NaCl + H_2O \quad (4.4)$$
$$Sb_4O_5Cl_2 + 2Na_2CO_3 \rightarrow 2Sb_2O_3 + 4NaCl + CO_2 \quad (4.5)$$

As seen in Equation 4.2, HCl formed in line with the production of $Sb_4O_5Cl_2$ particles, and therefore the pH of the solution increased slowly (Tian et al., 2016). Uysal (2019) indicates that the concentration of Cl^- and OH^- ions determines the stability of $SbCl_3$ system. A mixture of Sb-products was obtained based on Sb^{3+} and Cl^- concentrations (Hashimoto et al., 2003). Depending on the equilibrium changes, Sb ions may form a precipitate or the precipitate obtained may dissolve again. Different Sb compounds ($Sb_4O_5Cl_2$, Sb_2O_3, and SbOCl) were formed based on the process (Han-ying, 1984; Liu et al., 2010). It was known that $SbCl_3$ undergoes hydrolysis in water to form SbOCl (Equation 4.2). With the addition of bases, $Sb_4O_5Cl_2$ is formed in the presence of tartaric and HCl acids. The theoretical prediction for the hydrolysis product depending on the pH was illustrated by previous studies (Du, 2012), as shown in Figure 4.24.

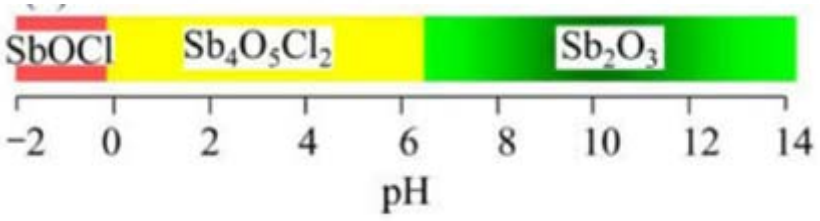

Figure 4.24. Sb hydrolysis products based on pH

It is known that other impurities (Al, K, Mg, Na, Mn) present in the PLS did not decrease the purity of the precipitate obtained after the hydrolysis because all impurities are in ion form in the PLS, except for Fe ions that start to precipitate in these pH range (0 – 4). The precipitation behaviors of these metals depending on the pH value can be seen in Figure 4.25. REEs (La, Y, Ce, and Nd) stayed in soluble form in the range of pH 0 – 4 (Figure 4.26).

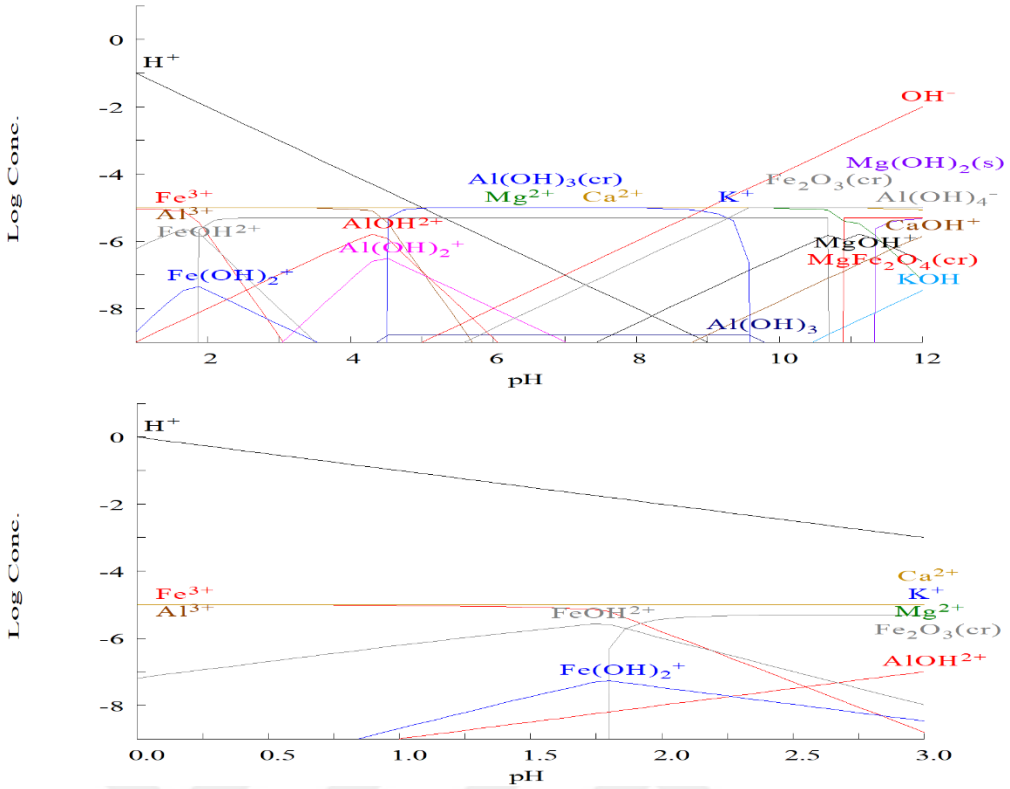

Figure 4.25. Precipitation behaviors of impurities in a range of different pH: (a) 0 – 12 and (b) 0 - 3

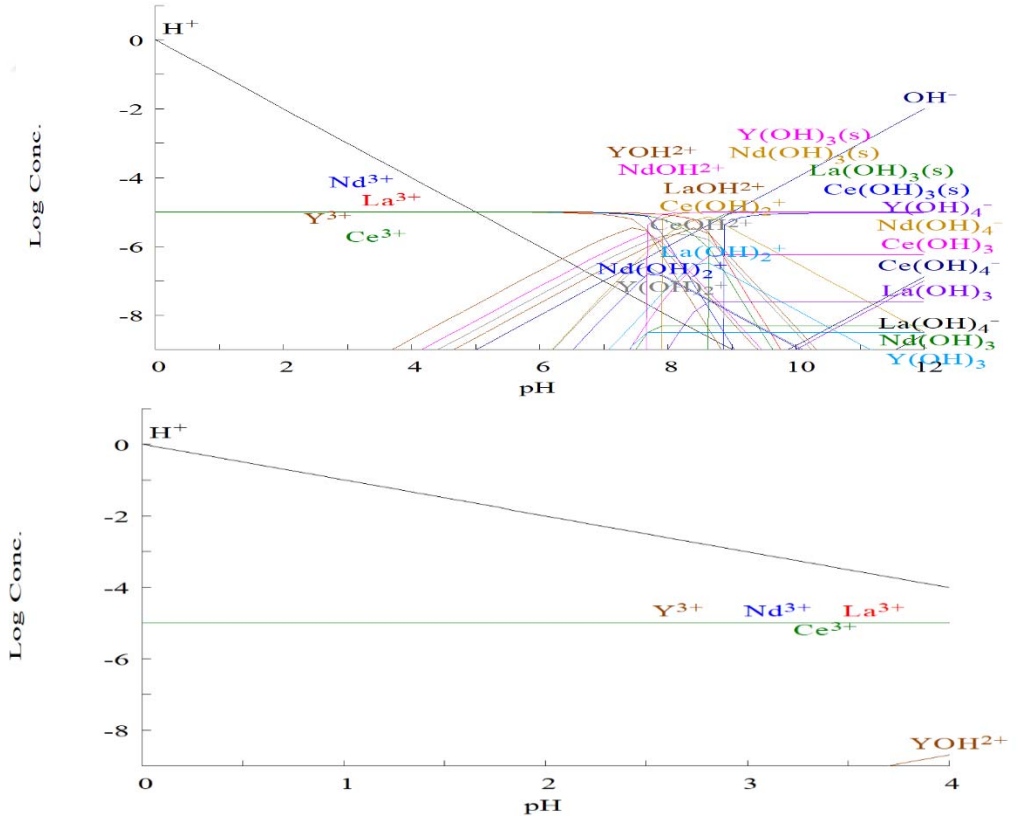

Figure 4.26. Precipitation behavior of REEs in a range of different pH: (a) 0 – 12 and (b) 0 – 3

Uysal (2019) explained the formation of Sb depending on pH value in detail, but the hydrolysis mechanism of Sb is not fully understood. Considering previous studies, a series of experiments were conducted. The results obtained from the hydrolysis test are listed in Table 4.7. Sb ions from the PLS were hydrolyzed with a precipitation rate of 47.78 – 99.38% depending on the experimental conditions, while the precipitation rate of Fe from the PLS was in a range of 2.14% - 98.83%. To evaluate these experimental results easily, Figure 4.27 was plotted. The photographs taken during the hydrolysis test can be seen in Figure 4.27.

Table 4.7. Experimental results obtained in the hydrolysis test

Exp. No	**Precipitation rate of Sb (%)**	**Precipitation rate of Fe (%)**	**Exp. No**	**Precipitation rate of Sb (%)**	**Precipitation rate of Fe (%)**
1	90.38	25.12	17	99.38	98.83
2	80.62	63.69	18	92.48	85.91
3	93.09	87.05	19	79.76	62.08
4	94.00	91.00	20	81.36	29.65
5	53.86	13.54	21	88.03	79.52
6	66.02	36.32	22	82.02	66.31
7	73.87	51.03	23	79.03	55.11
8	85.00	91.00	24	65.51	38.21
9	50.91	8.02	25	71.51	55.35
10	47.78	2.14	26	84.82	80.36
11	89.09	79.55	27	60.76	35.21
12	71.64	46.87	28	72.60	57.14
13	55.75	17.09	29	89.31	82.46
14	55.92	17.41	30	90.86	88.27
15	89.91	81.10	31	59.55	26.70
16	75.45	53.99	32	68.35	42.72

Figure 4.27. Some photographs taken during the hydrolysis test

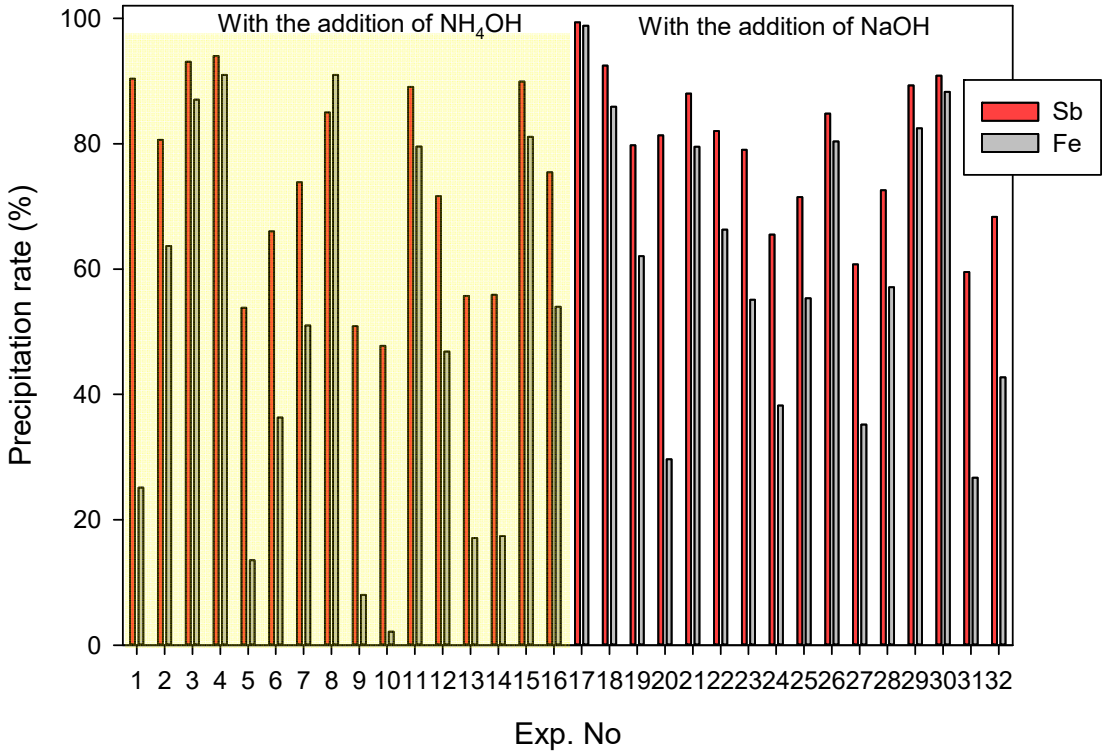

Figure 4.28. The obtained experimental results in the hydrolysis test.

Different options can be selected in the Taguchi approach to evaluate the experimental results. These are: “larger to better”, “smaller is better, and “nominal is the best”. Herein, it was aimed at increasing the precipitation rate of Sb while minimizing the precipitation rate of Fe from the PLS. Therefore, the “larger-to-better” option was selected to evaluate the precipitation rate of Sb, and the “smaller-is-better” option was used for the precipitation of Fe. Figure 4.29 shows the values

of S/N ratio calculated based on S/N analysis. The effects of hydrolysis conditions can be easily determined from these S/N graphs.

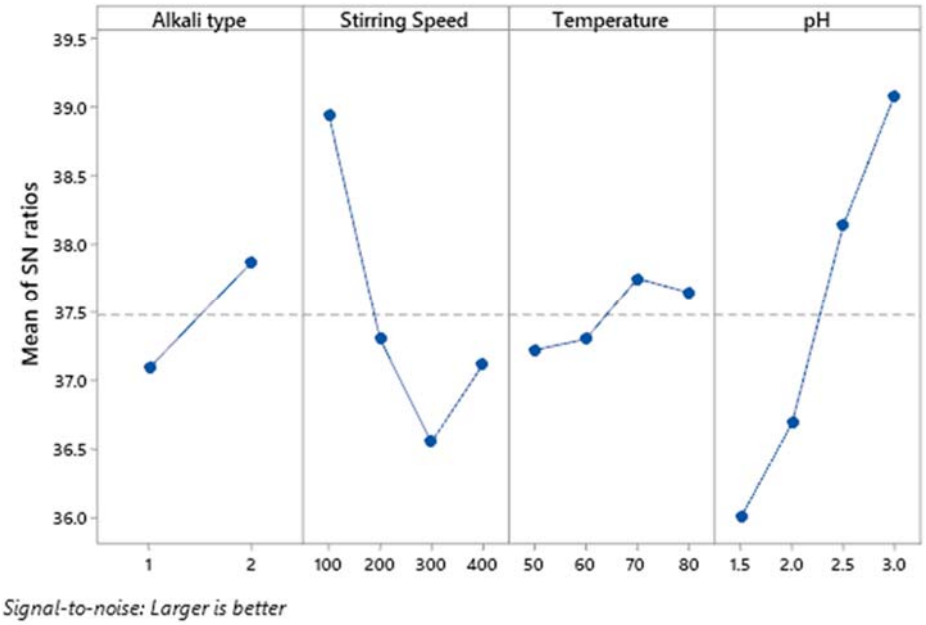

Figure 4.29. S/N values of the experimental parameters for the precipitation of Sb from the PLS

As such, the influences of precipitation conditions (from the highest to the lowest effect) on the precipitation rate of Sb was ordered as follows: pH > stirring speed > alkali type > reaction temperature. To obtain Sb-precipitate with high recoveries, the hydrolysis test should be carried out using NaOH in a temperature of 70 °C at the solution pH of 3 in the PLS that had been stirred at 100 rpm. The S/N values for the precipitation of Fe indicate that an increase in the solution pH up to 3 with the addition of NaOH resulted in the precipitation of Fe together with Sb (Figure 4.30).

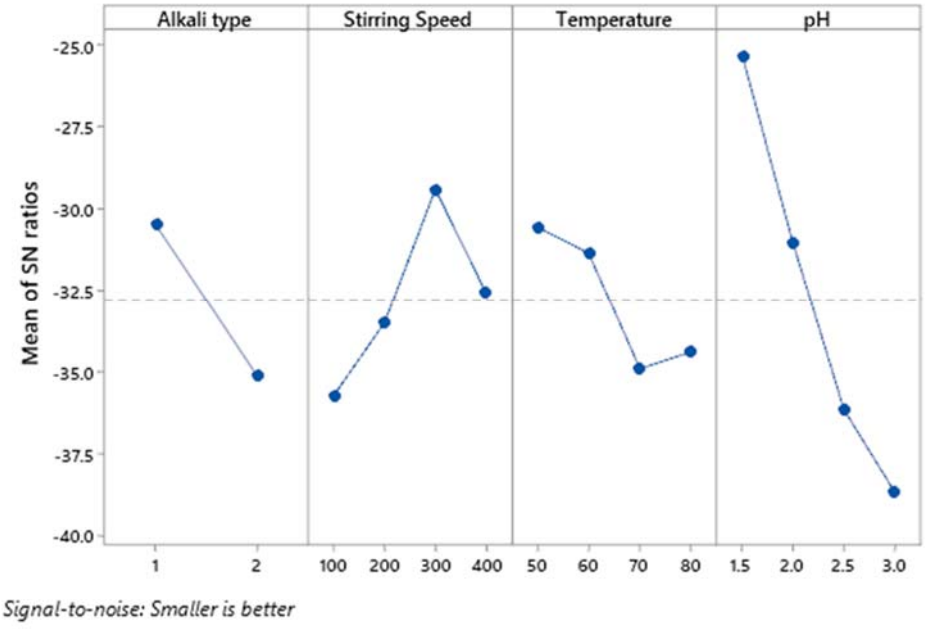

Figure 4.30. S/N values of the experimental parameters for the precipitation of Fe from the PLS

The ANOVA analysis given in Table 4.9 showed that the solution pH and stirring speed strongly affect the precipitation rate of Sb. The R-squared value for the model was 85.39%. The effect of alkaline types and temperature was negligible for Sb precipitation. However, the precipitation rate of Fe was highly dependent on all production parameters. The R-squared value for the model was 91.40%.

Table 4.8. ANOVA results

For the precipitation of Sb from the PLS					
Source	**DF**	**Adj SS**	**Adj MS**	**F-Value**	**P-Value**
Alkaline type	1	264.81	264.81	5.97	0.023
Stirring Speed	3	1852.45	617.48	13.93	0.000
Temperature	3	56.26	18.75	0.42	0.738
pH	3	3267.04	1089.01	24.56	0.000
Error	21	930.99	44.33		
Total	31	6371.54			
Model Summary: S: 6.65, R-squared: 85.39%,					
For the precipitation of Fe from the PLS					
Source	DF	Adj SS	Adj MS	F-Value	P-Value
Alkaline type	1	1497.6	1497.56	15.05	0.001
Stirring Speed	3	2165.4	721.79	7.26	0.002
Temperature	3	640.0	213.32	2.14	0.125
pH	3	17911.7	5970.57	60.01	0.000
Error	21	2089.2	99.49		
Total	31	24303.8			
Model Summary: S:9.97, R-squared: 91.40%					

The precipitates were washed with water or alkaline and dried at 105 °C for 2 h in an oven. The crystallographic properties of the selected precipitates were imaged by SEM, as shown in Figure 4.32. The obtained precipitates had amorphous structures. EDX analysis proved the precipitation of Fe together with Sb. The precipitate contained in range of 13.13% - 21.45% Fe, depending on the precipitation conditions. For example, the precipitate (obtained under the Exp. No:3 conditions) mainly comprised 55.05% Sb, 23.51% O, and 21.45% Fe.

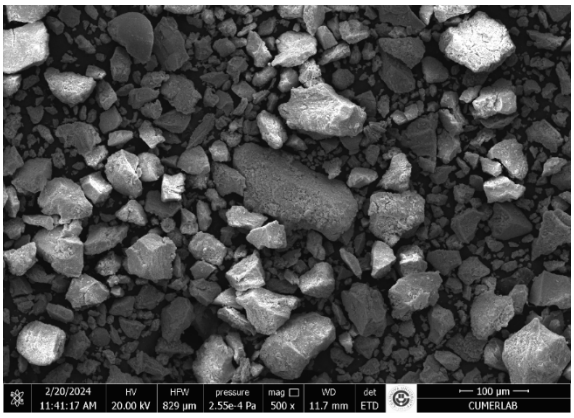

Exp No: 32

O: %20.54, Sb: 61.08%, and Fe: %18.38

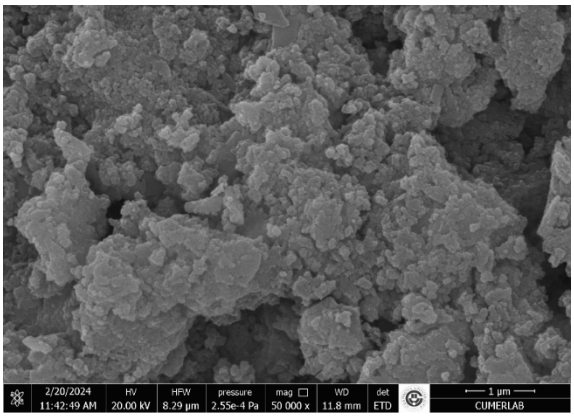

Exp. No: 3

O: 23.51%, Sb: 55.05%, and Fe: 21.45%

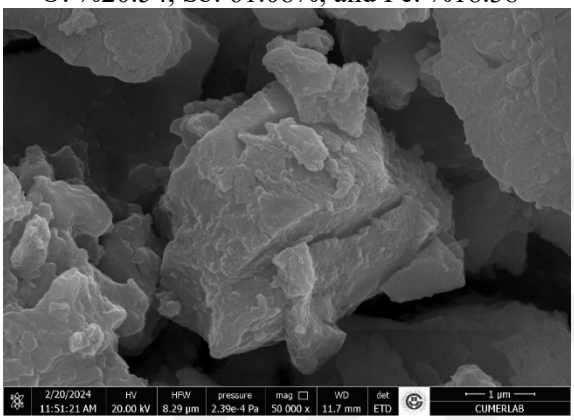

Exp. No: 8

O: 25.45%, Sb: 47.48%, and Fe: 26.36%

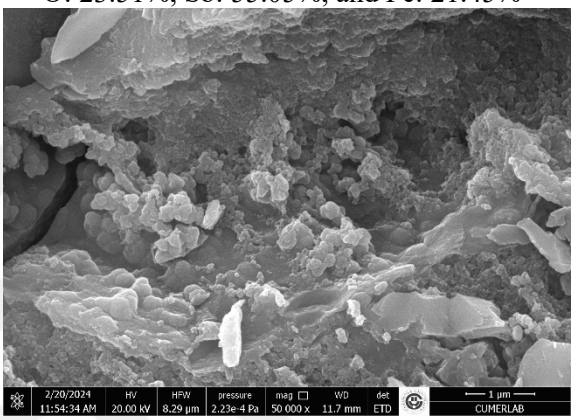

Exp. No: 24

O: 21.57%, Sb: 65.11%, and Fe: 13.13%

Figure 4.31. SEM images of the selected precipitates and their chemical compositions determined by EDX

It was aimed at decreasing the Fe content in the precipitate. The contour diagrams show the effects of pH and stirring speed on the precipitation rate of Sb and Fe from the PLS, respectively (Figure 4.31). The precipitation rates of Sb and Fe from the PLS increased with the increase of the pH. The contour diagrams indicate that the stirring speed strongly influenced the precipitation rate of Sb and Fe. During the hydrolysis test, if the PLS was stirred at higher speeds the precipitation rate for both elements started to decrease. For example, the precipitation rates of Sb and Fe were found to be around 75% and 20% when the solution pH was 1.7 and the stirring speed was <150 rpm. It was decided to conduct additional hydrolysis tests at a solution pH of ≤ 1.50. The obtained results are given in Table 4.9.

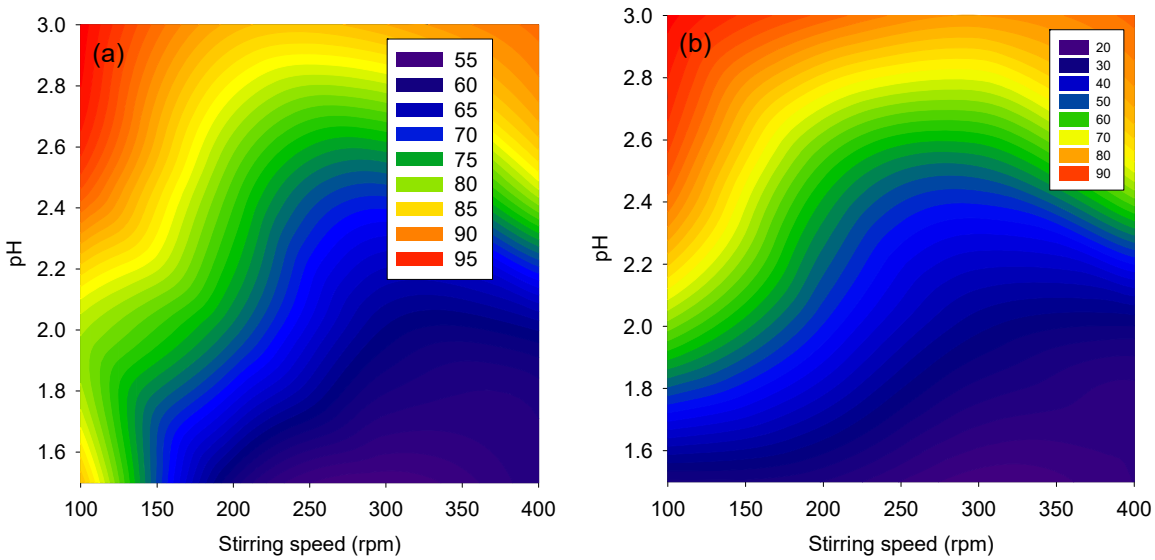

Figure 4.32. Contour diagrams that show the effects on pH and stirring speed on the hydrolysis of Sb and Fe from the PLS (a) the precipitation rate of Sb and (b) the precipitation rate of Fe

Table 4.9. The obtained experimental results from the additional hydrolysis test

Exp. No	**Final Volume (mL)**	**Precipitation rate of Sb (%)**	**Precipitation rate of Fe (%)**	**pH**
HE-1*	145	85.65	7.96	1.50
HE-2*	153	No precipitate		1.25
HE-3*	155	No precipitate		1.00
HE-4*	203	82.77	22.74	1.50
HE-5*	203	26.75	7.94	1.25
HE-6*	206	25.98	2.99	1.00

*NH_4OH was used in the HE-1, HE-2, and HE-3, while NaOH was used in the HE-4, HE-5, and HE-6.

The precipitation rate of Sb was higher than that of 80% at a solution pH of 1.0 under the Exp. No HE-1. However, a decrease in the precipitation rate of Sb was determined when the solution pH reached 1.25 or 1 using NaOH (HE-5 and HE-6). Furthermore, there were no precipitates obtained at the same pH values with the addition of NH4OH (Figure 4.33). Depending on conditions, the precipitates with different colors were obtained (Figure 4.34).

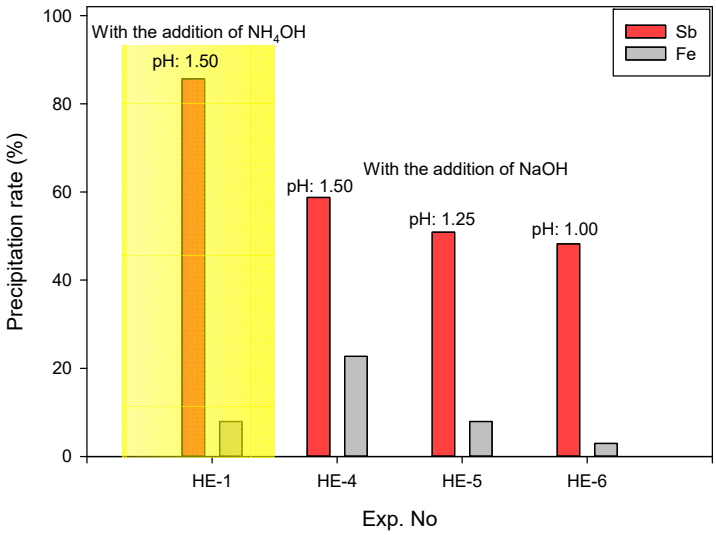

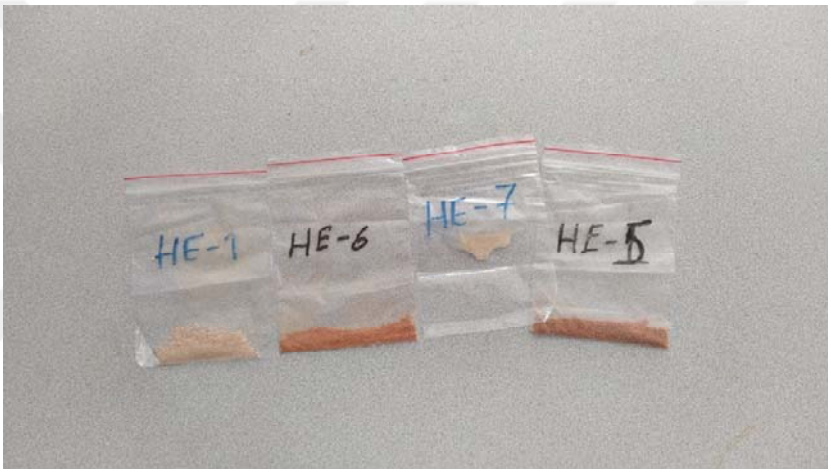

Figure 4.33. (a) The precipitation rate of Sb and Fe from the PLS in the additional hydrolysis test (b) Photographs of the obtained precipitates

It was understood from the SEM analyses given in Figure 4.34 that the washing procedure must be carried out when the hydrolysis test ended up. The EDX analysis was performed on the selected precipitates. The presence of Cl in the precipitate was observed in a range of 42.97% - 65.02%, which was easily removed by the washing process. Table 4.10 lists the final solution pH after the washing procedure. Figure 4.35 shows the SEM images of the washed precipitates that contain no chlorine ions.

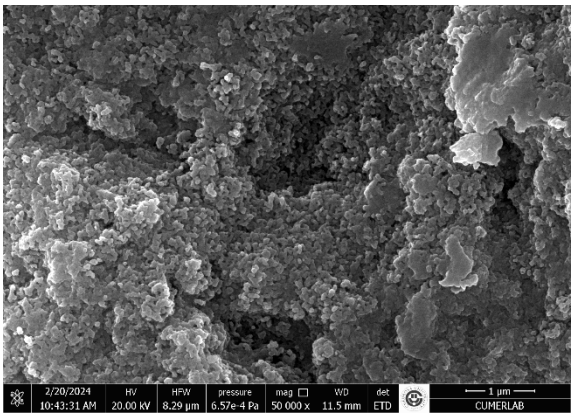

Exp. No: HE-5

O: 10.95%, Sb: 36.09%, Cl: 42.97%, and Fe: 9.93%

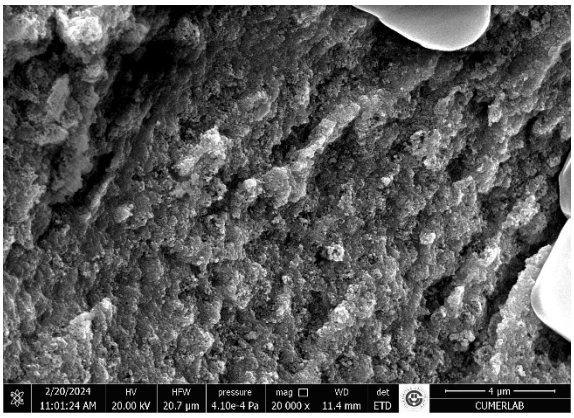

Exp. No: HE-6

O: 15.28%, Sb: 16.81%, Cl: 65.02%, and Fe: 2.89%

Exp. No: HE-1

O: 10.23%, Sb: 47.13%, Cl: 40.13%, and Fe: 2.51%

Figure 4.34. SEM images of the selected precipitates obtained in the additional hydrolysis test and their chemical compositions determined by EDX prior to conducting the washing procedure

Table 4.10. Measured pH values after washing procedures

Products obtained under the following Exp No.	**Final pH**	**Washing type**
HE-1	8.70	With NH_4OH
HE-5	8.83	With NaOH
HE-1	3.02	With water
HE-5	2.58	With water

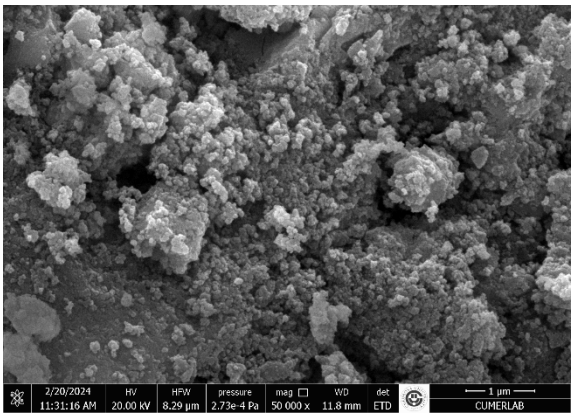

Exp. No:52 (washed with water)
O: 19.63, Sb: 67.39%, and 12.98%

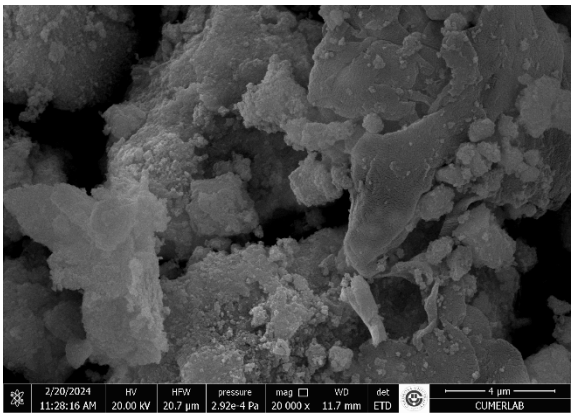

Exp. No: HE-61 (washed with NaOH)
O: 17.76%, Sb: 66.68%, and Fe: 15.57%

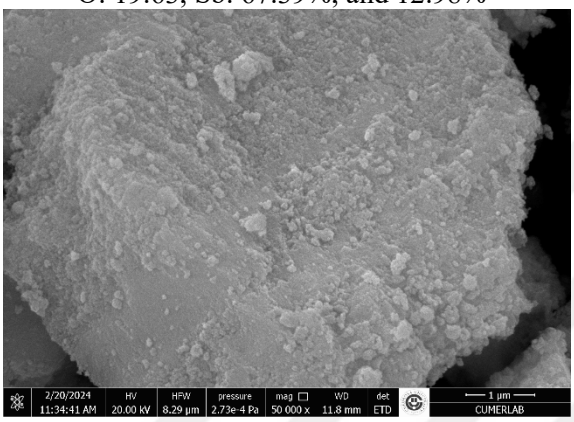

Exp. No: HE-51 (washed with NaOH)
O: 18.52%, Sb: 70.57%, and Fe: 10.9%

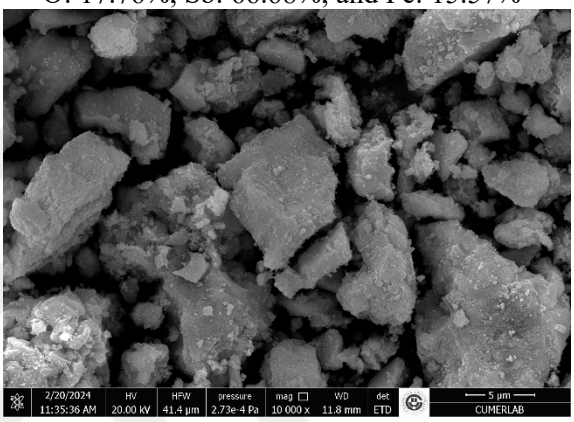

Exp No: HE-1 (washed with NH_4OH)
O: 16:23%, Sb: 81.43%, and Fe:2.34%

Figure 4.35. SEM images of the selected precipitates obtained in the additional hydrolysis test and their chemical compositions determined by EDX after the washing procedure

The precipitate, which was obtained under Exp No HE-1 conditions, contained 81.43% Sb, 16.23% O, and 2.34% Fe. Considering all results, it was decided to use NH_4OH rather than NaOH to prepare Sb-precipitate with desired purities as the precipitation rate of Fe was higher when NaOH was used. The precipitates were identified as antimony oxide minerals in XRD analysis. However, the XRD patterns of the selected products given in Figure 4.36 indicated that the amorphization of the product was high due to the low peak intensities. Similar results obtained by Diaz et al (2013), show no crystalline structure were observed under any pH and temperature conditions.

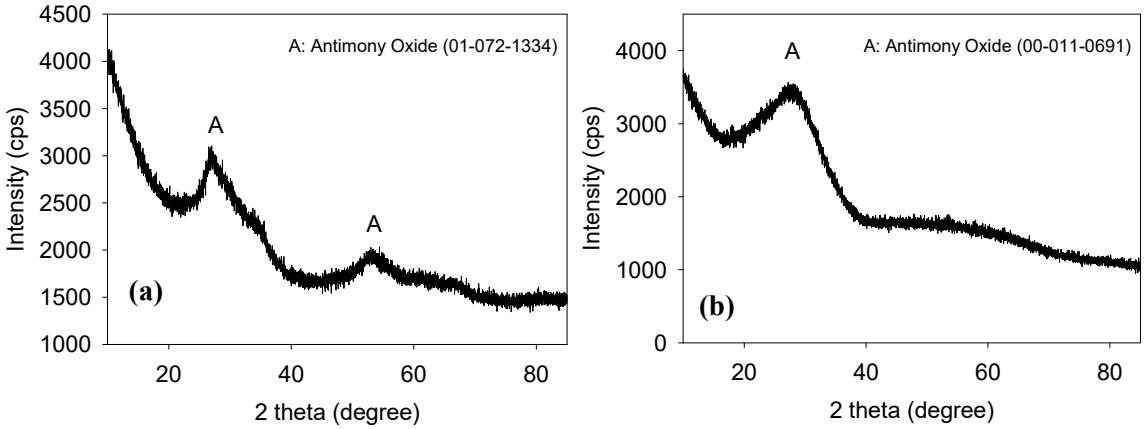

Figure 4.36. XRD pattern of the selected product (a) HE-1 and (b) HE-5

5. CONCLUSIONS

In this thesis, it was aimed to investigate the recovery of Sb from a smelter slag (4.13% Sb) generated in a smelting furnace using HCl leaching and hydrolysis processes. The slag used in this thesis was provided by Anadolu Antimony Factory located in Adana, Türkiye. The characterization of the slag was determined using various techniques, including physico-chemical properties (pH, moisture, odor, organic matter content, inorganic content), TCLP, SPLP, and radioactivity measurement. Different instrumental analyses, such as XRD, XPS, and SEM, were conducted on the slag and the selected precipitates.

The ore was mainly composed of quartz mineral along with minor minerals: stibiconite $Sb_3O_6(OH)$, Microline ($KAlSi_3O_8$), magnetite (Fe_3O_4, <%5), and hedenbergite ($CaFeSi_2O_6$). XPS analysis indicates that Sb in the slag was in oxide form. Preliminary leaching tests were carried out to determine the parameters and their levels for subsequent stages. Considering these results, it was determined that Sb (III) species may form chloro-complexes and its solubility increases within increasing Cl- ions activity. Therefore, it was decided to use HCl as the leaching agent for this study instead of other inorganic acids. The effects of leaching parameters on the extraction rates of Sb, impurities, and REEs were investigated using the OFAT approach. These parameters were acid concentration (1, 2, 3, 4, 5, 6, 7, 8, and 9 M), amount of tartaric acid (0, 1, 3, 5, and 6 g/L), solid-to-liquid ratio (1/8, 1/10, 1/12, and 1/15), time (45, 75, 90, 180, 240, 360, 480, 600, 900, and 1200 min), and temperature (room temp, 40, 60, and 75 °C). The best conditions for the leaching process were determined as follows: HCl concentration: 8 M, solid-to-liquid ratio: 1/10, Stirring speed: 300 rpm, amount of tartaric acid : 1 g/L, Reaction temperature: 75 °C and reaction time: 180 min. The leaching mechanism of the slag was evaluated by different shrinking core models including; inner-diffusion-controlled model, liquid boundary layer diffusion controlled model (Jander equation), chemical reaction controlled model, and both chemical and diffusion controlled model. The Ea was calculated to be 46.75 kJ/mol, which indicates that the leaching of Sb from the slag was governed by the chemically controlled mechanism.

Moreover, the use of tartaric acid had a significant influence on the leaching of La from the slag. An increase in the amount of tartaric acid makes the extraction of La with high rates in shorter times. For example; experiments conducted with 1 g/L tartaric acid required a leaching time of 20 h for the complete extraction of La, while increasing the tartaric acid concentration from 1 g/L to 6 g/L reduced the time required for high-efficiency dissolution of La to 180 min from 20 h. Under the best leaching conditions, the extraction rate of Sb from the slag was determined to be 91.19%. While the extraction rate of La was approximately 97%, the extraction rates of other REEs (Y, Ce, Nd) were measured to be ≤50%.

The hydrolysis tests were conducted based on the Taguchi approach (L32, 2^1 4^3). The effects of alkaline types (NH_4OH and NaOH), stirring speed (100, 200, 300, and 400 rpm),

temperature (50, 60, 70, and 80 °C), and pH (1.5, 2, 2.5, and 3) on the precipitation of Sb from the PLS were investigated. The presence of Fe in the PLS created pollution problems in the precipitate obtained after the hydrolysis. Sb ions from the PLS were hydrolyzed with a precipitation rate of 47.78 – 99.38% depending on the experimental conditions, while the precipitation rate of Fe from the PLS was in a range of 2.14% - 98.83%. The validiation of these models was proved by the ANOVA analysis. Additional hydrolysis tests were carried out at pH ≤1.5. Depending on the pH, the precipitates with different colors were obtained due to the precipitation of Fe together with Sb. NH4OH was suggested to use in the hydrolysis test to obtain preciptiate with higher purities. The final product was mainly composed of 16.23% O, 81,43% Sb, and 2.34% Fe. The product was identified as antimony oxide. For future studies, some studies are recommended below:

(i) Pressure leaching of Sb from the slag,

(ii) Electro-winning of Sb from the PLS,

(iii) Production of tripuhyite ($FeSbO_4$) mineral from the PLS,

(iv) Cementation of Sb from the PLS with the addition of different metal powders.

REFERENCES

Agency, U. E. P. 1994. Method 1312: Synthetic precipitation leaching procedure. Test methods for evaluating solid waste, physical/chemical methods.

Ait Brahim, J., Ait Hak S., Achiou, B., Boulif, R., Beniazza, R., and Benhida, R. 2022. Kinetics and mechanisms of leaching of rare earth elements from secondary resources. Minerals Engineering 177.

Schwoeble AJ,, Strohmeier, BR, and Piasecki, JD. 2010. Proc SPIE 7729 772916-1–772916-16

Aktaş, S. and B. N. Çetiner (2020). Investigation of alkaline leaching parameters on stibnite concentrate. Mining, Metallurgy & Exploration 37(5): 1729-1739.

Alev, G. (2019). Recovery of antimony generated in waste lead-acid battery. MSc.

Anderson, C. (2001). Hydrometallurgically treating antimony-bearing industrial wastes. JoM 53: 18-20.

Anderson, C. (2012). The metallurgy of antimony. Geochemistry 72: 3-8.

Anderson, C. (2019). Antimony production and commodites. Mineral Processing and Extractive Metallurgy Handbook. R. C. USA: Society for Mining, Metallurgy and Exploration, SME.

Awe, S. A. and Å. Sandström (2010). Selective leaching of arsenic and antimony from a tetrahedrite rich complex sulphide concentrate using alkaline sulphide solution. Minerals Engineering 23(15): 1227-1236.

Awe, S. A., J.-E. Sundkvist, N.-J. Bolin and Å. Sandström (2013). Process flowsheet development for recovering antimony from Sb-bearing copper concentrates. Minerals Engineering 49: 45-53.

Beutl, A., D. Henriques, V. Motalov, D. Cupid, T. Markus and H. Flandorfer (2018). A thermodynamic investigation of the Li–Sb system. Journal of Thermal Analysis and Calorimetry 131: 2673-2686.

Binz, F. and B. Friedrich (2015). Recovery of antimony trioxide flame retardants from lead refining residues by slag conditioning and fuming. Chemie Ingenieur Technik 87(11): 1569-1579.

Boyle, R. and I. Jonasson (1984). The geochemistry of antimony and its use as an indicator element in geochemical prospecting. Journal of Geochemical Exploration 20(3): 223-302.

Brahim, J. A., S. A. Hak, B. Achiou, R. Boulif, R. Beniazza and R. Benhida (2022). Kinetics and mechanisms of leaching of rare earth elements from secondary resources. Minerals Engineering 177: 107351.

Cao, H.-Z., J.-Z. Chen, H.-J. Yuan and G.-Q. Zheng (2010). Preparation of pure SbCl3 from lead anode slime bearing high antimony and low silver. Transactions of Nonferrous Metals Society of China 20(12): 2397-2403.

CD Wagner, AV Naumkin, A Kraut-Vass, JW Allison, CJ Powell, and JR Rumble, Jr., NIST X-ray Photoelectron Spectroscopy Database, Version 3.5, National Institute for Standards and Technology, Gaithersburg, MD, 2003. Available online at: http://srdata.nist.gov/xps/Default. aspx.

Çetiner, B. N. (2022). Extraction of antimony from its native suphide and oxide containing ores by microwave leaching, arsenic elemination and nano size antimony synthesis PhD, Marmara University.

Chae, S., K. Yoo, C. B. Tabelin and R. D. Alorro (2020). Hydrochloric Acid Leaching Behaviors of Copper and Antimony in Speiss Obtained from Top Submerged Lance Furnace. Metals 10(10).

Commission, E. (2023). 2023 of critical raw materials for the EU.

de Andrade Lima, L. and L. Bernardez (2011). Characterization of the lead smelter slag in Santo Amaro, Bahia, Brazil. Journal of hazardous materials 189(3): 692-699.

Dembele, S., A. Akcil, S. Panda (2022). Technological Trends, Emerging Applications and Metallurgical Strategies in Antimony Recovery from Stibnite. Minerals Engineering 175.

Díaz, E., J. A. Maldonado Calvo, J. M. Gallardo and A. Paúl (2023). Extraction of antimony from a hydrochloric acid side stream of copper electro-refining by hydrolysis. Hydrometallurgy 219.

Du, X. (2012). Research on the hydrolysis equilibrium of antimony trichloride in the Sb 3+–Cl−–H 2 O system. Trans. Nonferrous Metals Soc. China 41(5): 75-79.

Dupont, D., & Binnemans, K. (2017). Preventing antimony from becoming the next rare earth. *Recycling Technology*, 18-20.

Dupont, D., S. Arnout, P. T. Jones and K. Binnemans (2016). Antimony Recovery from End-of-Life Products and Industrial Process Residues: A Critical Review. Journal of Sustainable Metallurgy 2(1): 79-103.

Fallis, A. (1992). Toxicity characteristic leaching procedure, method 1311. J. Chem. Inf. Model. https://doi. org/10.1017/CBO9781107415324 4.

Government, A. (2024). Critical minerals at Geoscience Australia. Retrieved 6.05.2024, 2024, from https://www.ga.gov.au/scientific-topics/minerals/critical-minerals.

Groenewald, I. D. (1964). The polarographic determination of lead in antimony sulphide flotation concentrates. Analyst 89: 140-141.

Guo, X., K. Wang, M. He, Z. Liu, H. Yang and S. Li (2014). Antimony smelting process generating solid wastes and dust: characterization and leaching behaviors. J Environ Sci (China) 26(7): 1549-1556.

Guo, X.-y., Y.-t. Xin, H. Wang and Q.-h. Tian (2017). Leaching kinetics of antimony-bearing complex sulfides ore in hydrochloric acid solution with ozone. Transactions of Nonferrous Metals Society of China 27(9): 2073-2081.

Gutknecht, T., C. Forsgren and B.-M. Steenari (2017). Investigations into high temperature separation of antimony from metal oxide varistors. Journal of Cleaner Production 162: 474-483.

Han, J., C. Liang, W. Liu, W. Qin, F. Jiao and W. Li (2017). Pretreatment of tin anode slime using alkaline pressure oxidative leaching. Separation and Purification Technology 174: 389-395.

Han, J., Z. Ou, W. Liu, F. Jiao and W. Qin (2020). Recovery of antimony and bismuth from tin anode slime after soda roasting–alkaline leaching. Separation and Purification Technology 242.

Han, J., Z. Ou, W. Liu, F. Jiao and W. Qin (2020). Recovery of antimony and bismuth from tin anode slime after soda roasting–alkaline leaching. Separation and Purification Technology 242: 116789.

Han-ying, J. (1984). Physical chemistry of hydrometallurgy, Beijing: Metallurgical Industry Press.

Hashimoto, H., T. Nishimura and Y. Umetsu (2003). Hydrolysis of antimony (III)-hydrochloric acid solution at 25° C. Materials transactions 44(8): 1624-1629.

Havlík, T. (2007). Kinetics of heterogeneous reactions of leaching processes. TRANSLATIONS-VE RIECANSKY 13060.

Hu, X., X. Guo, M. He and S. Li (2016). pH-dependent release characteristics of antimony and arsenic from typical antimony-bearing ores. J Environ Sci (China) 44: 171-179.

Hu, Y., H. Zhang and H. Yang (2007). Direct synthesis of Sb2O3 nanoparticles via hydrolysis-precipitation method. Journal of Alloys and Compounds 428(1-2): 327-331.

JF Moulder, WF Stickle, PE Sobol, and KD Bomben, Handbook of X-ray Photoelectron Spectroscopy, Perkin- Elmer Corporation, Eden Prairie, MN, 1992.

Jo, K. H. and K. H. Yoon (1989). Preparation of sol-gel derived (Ba0. 2Pb0. 8) TiO3 powders. Materials research bulletin 24(1): 1-9.

Karlsson, T., C. Forsgren and B.-M. Steenari (2018). Recovery of antimony: a laboratory study on the thermal decomposition and carbothermal reduction of Sb (III), Bi (III), Zn (II) oxides, and antimony compounds from metal oxide varistors. Journal of Sustainable Metallurgy 4: 194-204.

Küçükoğlu, Ö., B. N. Çetiner, M. H. Morcalı and S. Aktaş (2022). Comparison of the Antimony Cementation from Chloride Media Using Various Cementators. Mining, Metallurgy & Exploration.

Liang, J., S. Zhang, C. Liao, L. Xiao and G. Wang (2016). Effects of tartaric acid, citric acid and malic acid removing lanthanum from polluted soils. Journal of Ecology and Rural Environment 32(1): 115-119.

Ling, H., A. Malfliet, B. Blanpain and M. Guo (2022). A review of the technologies for antimony recovery from refractory ores and metallurgical residues. Mineral Processing and Extractive Metallurgy Review 45(3): 200-224.

Ling, H., A. Malfliet, B. Blanpain and M. Guo (2022). Selective removal of arsenic from crude antimony trioxide by leaching with nitric acid. Separation and Purification Technology 281: 119976.

Ling, H., B. Blanpain, M. Guo and A. Malfliet (2021). Characterization of antimony-containing metallurgical residues for antimony recovery. Journal of Cleaner Production 327: 129491.

Liu, L., Z. Hu, Y. Cui, B. Li and X. Zhou (2010). A facile route to the fabrication of morphology-controlled Sb2O3 nanostructures. Solid state sciences 12(5): 882-886.

Liu, W., T. Yang, D. Zhang, L. Chen and Y. Liu (2014). A new pyrometallurgical process for producing antimony white from by-product of lead smelting. Jom 66: 1694-1700.

Meng, L., S.-G. Zhang, D.-A. Pan, B. Li, J.-J. Tian and A. A. Volinsky (2015). Antimony recovery from SbCl5 acid solution by hydrolysis and aging. Rare Metals 34(6): 436-439.

Miller, M. (1973). Antimony. 1973.: 45-50.

Moldan, I. R. Z. S. B. (1966). The determination of silver in sulphide minerals by absorption spectrophotometry. Analytiac Chimica Acta 37: 27-32.

Mostashari, S. and S. Baie (2008). Thermogravimetry studies of cotton fabric's flame-retardancy by means of synergism of lithium bromide and antimony trioxide. Journal of thermal analysis and calorimetry 94(1): 97-101.

Nikfar, S., A. Parsa, N. Bahaloo-Horeh and S. M. Mousavi (2020). Enhanced bioleaching of Cr and Ni from a chromium-rich electroplating sludge using the filtrated culture of Aspergillus niger. Journal of Cleaner Production 264.

Öztürk, E., S. Aksöz, Y. Altıntas, K. Keşlioğlu and N. Maraşlı (2016). Experimental measurements of some thermophysical properties of solid CdSb intermetallic in the Sn–Cd–Sb ternary alloy. Journal of Thermal Analysis and Calorimetry 126: 1059-1065.

Palden, T., L. Machiels, M. Regadío and K. Binnemans (2021). Antimony Recovery from Lead-Rich Dross of Lead Smelter and Conversion into Antimony Oxide Chloride (Sb4O5Cl2). ACS Sustainable Chemistry & Engineering 9(14): 5074-5084.

Pohl, W. L. (2011). Economic geology: principles and practice, John Wiley & Sons.

Rodríguez-Rodríguez, C., F. Nava-Alonso, A. Uribe-Salas and J. Viñals (2016). Pyrargyrite (Ag3SbS3): Silver and antimony dissolution by ozone oxidation in acid media. Hydrometallurgy 164: 15-23.

Sillen, L. G. (1971). Stability constants of metal-ion complexes. Special publication.

Speight, J. G. (2018). Reaction mechanisms in environmental engineering: analysis and prediction, Butterworth-Heinemann.

Sudová, M., M. Sisol, M. Kanuchova, M. Marcin and J. Kurty (2024). Environmentally Friendly Leaching of Antimony from Mining Residues Using Deep Eutectic Solvents: Optimization and Sustainable Extraction Strategies. Processes 12(3).

Survey, U. S. G. (2024). Mineral Commodity Sumaries 2024. USGS Science for a changing world.

Tan, C., L. Li, K. Li and D. Zhong (2018). Separation of As from high As-Sb dust using Fe2O3 as a fixative under O2-N2 atmosphere. Separation and Purification Technology 194: 81-88.

Tian, Q., H. Wang, Y. Xin, D. Li and X. Guo (2016). Ozonation leaching of a complex sulfidic antimony ore in hydrochloric acid solution. Hydrometallurgy 159: 126-131.

Ubaldini, S., F. Veglio, P. Fornari and C. Abbruzzese (2000). Process flow-sheet for gold and antimony recovery from stibnite. Hydrometallurgy 57(3): 187-199.

Uysal, A. (2019). Antimony recovery from various antimony solutions by cementation and process optimization. MSc, Marmara University.

Yang, T., S. Rao, W. Liu, D. Zhang and L. Chen (2017). A selective process for extracting antimony from refractory gold ore. Hydrometallurgy 169: 571-575.

Ye, L., Z. Ouyang, Y. Chen and Y. Chen (2019). Ferric chloride leaching of antimony from stibnite. Hydrometallurgy 186: 210-217.

Ye, L., Z. Ouyang, Y. Chen, H. Wang, L. Xiao and S. Liu (2019). Selective separation of antimony from a Sb-Fe mixed solution by hydrolysis and application in the hydrometallurgical process of antimony extraction. Separation and Purification Technology 228.

Zhang, B., Q. Li, W. Shen and X. Min (2012). Recovery of bismuth and antimony metals from pressure-leaching slag. Rare metals 31: 102-106.

Zhang, R. L., X. F. Zhang, S. Z. Tang and A. D. Huang (2015). Ultrasound-assisted HCl-NaCl leaching of lead-rich and antimony-rich oxidizing slag. Ultrason Sonochem 27: 187-191.

Zhang, X., S. Friedrich and B. Friedrich (2020). Separation behavior of arsenic and lead from antimony during vacuum distillation and zone refining. Journal of Materials Research and Technology 9(3): 4386-4398.

Zhang, Y., C. Wang, B. Ma, X. Jie and P. Xing (2019). Extracting antimony from high arsenic and gold-containing stibnite ore using slurry electrolysis. Hydrometallurgy 186: 284-291.

Zhao, T. (1988). The metallurgy of antimony. China, Central South University of Technology Press Changsha.

Zhong, D.-p., L. Li and C. Tan (2018). Recovery of antimony from antimony-bearing dusts through reduction roasting process under CO—CO2 mixture gas atmosphere after firstly oxidation roasted. Journal of Central South University 25(8): 1904-1913.

CURRICULUM VITAE

Ahmedaljaali Ibrahim Idrees IBRAHIM, holds an MSc in Mining Engineering from Çukurova University, Adana, Turkey (2021-2024) and a BSc in Mining Engineering from Omdurman Islamic University, Omdurman, Sudan (2012-2017). He has experience as a Mineral Processing Engineer at Ariab Mining Company in Sudan (2020-2021), where he developed and optimized gold separation processes, implemented a carbon absorption solution that increased gold yield by 20%, and conducted routine efficiency analyses. Previously, he worked as a Teaching Assistant in the Department of Mining Engineering at Omdurman Islamic University (2017-2019), assisting with lectures, mentoring students, and developing curricular materials. His papers have been published in several journals classified as Q1 and Q2, including studies on sodium-feldspar ore beneficiation, vanadium and nickel recovery from petroleum coke ash, and nickel characterization in chromite beneficiation tailings. Ahmedaljaali is fluent in Arabic, advanced in English, and has intermediate proficiency in Turkish.